Title

The impact of CRISPR Cas9 ribonucleoprotein delivery modality on intracellular uptake mechanism and gene editing outcomes

Author

Karp, Hannah

Publication Date

2024

Peer reviewed|Thesis/dissertation

The impact of CRISPR Cas9 ribonucleoprotein delivery modality on intracellular uptake mechanism and gene editing outcomes

By

Hannah Karp

A dissertation submitted in partial satisfaction of the

requirements for the degree of

Doctor of Philosophy

in

Chemistry

in the

Graduate Division

of the

University of California, Berkeley

Committee in charge:

Professor Jennifer Doudna, Chair
Professor Alanna Schepartz
Professor Dave Savage

Fall 2024

The impact of CRISPR Cas9 ribonucleoprotein delivery modality on intracellular uptake mechanism and gene editing outcomes

By

Hannah Karp

Abstract

The impact of CRISPR Cas9 ribonucleoprotein delivery modality on intracellular uptake mechanism and gene editing outcomes

By

Hannah Karp

Doctor of Philosophy in Chemistry (Chemical Biology)

University of California, Berkeley

Professor Jennifer Doudna, Chair

CRISPR genome editing tools continue to propel major advances in biological research and offer new therapeutic avenues to treat genetic diseases. For *in vivo* therapeutic or research applications, there is the additional hurdle of safe and effective delivery of CRISPR effectors intracellularly. For gene therapies, delivering CRISPR ribonucleoproteins (RNPs), rather than DNA or RNA, can result in comparably efficient genome modification while mitigating undesirable clinical outcomes, such as off-target editing and increased immunogenicity, that can arise from extended gene editor expression.

First, we discuss progress towards engineering next-generation CRISPR RNPs for mammalian genome engineering with broader and efficient genomic targeting capabilities, improved editing specificity, packability and nuclease activity, and outline key considerations and remaining critical challenges. Next, we compared two delivery strategies, electroporation and enveloped delivery vehicles (EDVs), to investigate the Cas9 dosage requirements for genome editing. Using fluorescence correlation spectroscopy (FCS), we determined that >1300 Cas9 RNPs per nucleus are typically required for productive genome editing. EDV-mediated editing was >30-fold more efficient than electroporation, and editing occurs at least two-fold faster for EDV delivery at comparable total Cas9 RNP doses. We hypothesize that differences in efficacy between these methods result in part from the increased duration of RNP nuclear residence resulting from EDV delivery. Our results directly compare RNP delivery strategies, showing that packaged delivery could dramatically reduce the amount of CRISPR-Cas9 RNPs required for experimental or clinical genome editing. Lastly, to identify prominent Cas9 RNP delivery bottlenecks and commonalities, we utilized spatiotemporally resolved proteomics to compare RNP delivery by electroporation, EDVs, and *in trans* cell penetrating peptides (PERC), in HEK293T and T-cells. This workflow uncovered cell-type differences in uptake for EDVs and PERC. Regardless of delivery strategy, Cas9 associates with endogenous RNA binding proteins and localizes to the nucleoli prior to degradation. This method enables flexible comparison of Cas9 RNP delivery strategies, and the impact of cell-type on uptake mechanism.

We conclude with an outlook on the future of CRISPR RNP delivery and contextualize key remaining challenges. Together, the projects presented in this dissertation contribute to the growing understanding of CRISPR RNP engineering and delivery strategies.

Acknowledgements

Pursuing my PhD has been the most meaningful and difficult task of my life. I certainly did not accomplish this effort in a vacuum; I was supported extensively throughout by my mentors, peers, friends, and family. My acknowledgements here barely scratch the surface and writing this I have been filled with gratitude for all the support I have received throughout this experience.

Firstly, I want to thank my PhD advisor, Jennifer Doudna, for giving me the opportunity to work in her lab and supporting me throughout my thesis. It is not an exaggeration to say that Jennifer has been my scientific idol since high school, when I first heard about her and collaborator, Emmanuelle Charpentier, and their research on a revolutionary genome engineering system and tool, CRISPR-Cas9. Jennifer, more than anyone I have ever met, has an instinct for what matters. She has taught me to laser focus on what the key point is: in a presentation, a research proposal, or a publication. Distilling your research into its critical elements is difficult, and can in fact be painful, because when you are in the scientific weeds you fall in love with the nuance and complexity. However, it has made my scientific writing, communication, and thinking dramatically better, and I am confident it will be fundamental to my ongoing success.

I want to thank my scientific colleagues and mentors within the Doudna lab. Jennifer Hamilton was my rotation mentor and learning about her incredible new tool, now called enveloped delivery vehicles, shaped my graduate career. I cannot wait to follow Azalea Therapeutics' accomplishments in the coming years. Kevin Wasko, who was initially my rotation student, has been my go-to person to ask all sorts of random questions, and has been an incredible person to work with and learn from. Matt Kan, my baymate, has given me lots of helpful context on how early-stage research fits into the therapeutic and clinical pipeline, and has also been a source of professional advice and wisdom. More recently, Wayne Ngo has become an invaluable mentor, providing me advice and encouragement on my scientific writing and project development. The Gene Fixers subgroup has been my lab within the lab, providing me with timely feedback, guidance, and advice. Lastly, the Doudna lab has been the best managed work environment I have ever been a part of, due to the excellent oversight of Kaihong and Jenny, who keep our instruments and experiments always running smoothly.

Before graduate school, I underestimated the importance of being in a biotech hub. The biotechnology nexus in the Bay Area has given me many opportunities I did not know existed prior to graduate school. From the excellent seminars at the Innovative Genomics Institute, to my internship at the Bakar BioEnginuity hub I have learned how scientific innovation gets translated into products and therapies that benefit society. I want to thank Livia and Wesley at Valitor for giving me the opportunity to join their team for the Summer and learn about preclinical development and the inner workings of an early-stage biotechnology company.

One of the biggest, unexpected gifts in graduate school was meeting my friends. As a life-long hard-core nerd, I have struggled at various points to connect with peers. At Berkeley, I felt an immediate connection to my friends, who studied different things, but had the same intensity. Most of them have graduated, or will be soon, and have

moved all over the country. I hope to remain in all their lives and hear about their exploits for years to come. Diego has fundamentally changed my graduate experience, and life. At my wedding, he was the best maid of honor I could imagine, reducing my tension with silly jokes, and by hawking spit into plants at the Bel-Air hotel. Aidan was always there for me when I needed to rant or talk and grabbing lunch and going on long walks always helped put everything into perspective. Orion, also known as my favorite root vegetable, the Onion, was always there when I just needed to dance, play board games, or just hang out. Darren expanded my social life dramatically, introducing me to music, people, and general good vibes. Dan was already ready for an adventure, whether it was out on a trail or a new culinary challenge. Neville, despite being frequently unavailable, was always there when it mattered. I have been extremely blessed with good friends, who have made my world and my life bigger, better, and who I am eternally grateful for.

I lucked out being born into my family, and without their support and encouragement I would never have considered entering a PhD in the first place. My mother always steps in when I need her, whether it is planning my wedding or lending me her car in a pinch. My dad has been there to celebrate the victories and thinking about going on safari after I graduate has gotten me through the last couple long months. My brother is an inspiration to me, who is one of the hardest workers I know, but has always shown me that success and happiness do not have to look the same for everyone. He has, more than anyone I know, always been himself, and I love him fiercely for it.

Lastly, my now husband, Jonathan, has been my fiercest supporter since we began our relationship over 10 years ago. He has moved twice for me to pursue my dreams, first to Madison for my undergraduate degree, and then to Berkeley for my PhD. He, more than anyone, has listened to my doubts, my frustrations, my triumphs and my rambling, exhausted semi-coherent free associations. He is who I tell the small details of my day to, and he always listens despite not being a scientist. Without his emotional, financial, and day-to-day support this would not have been possible. Jonathan, I love you with my whole heart, and I cannot wait for our next adventure.

CHAPTER ONE

Next-Generation CRISPR Ribonucleoproteins (RNPs) for Mammalian Gene Editing

Adapted in part from

Adler, B.A.,* Trinidad, M.* *et al.* **CasPEDIA Database: A Functional Classification System for Class 2 CRISPR-Cas Enzymes**. Nucleic Acids Research. (2024). 52(2):1002

1.1 Overview

1.1.1 Abstract

CRISPR genome editing tools continue to propel major advances in biological research, and offer new therapeutic avenues to treat genetic diseases. The idealized aim of mammalian genome engineering is to make any intended modification at the correct target(s) without any undesired consequences, such as off-target edits, immunogenicity, or unintended cellular perturbations. For *in vivo* therapeutic or research applications, there is the additional hurdle of safe and effective delivery of CRISPR effectors intracellularly, necessitating that gene editors are compact and stable enough to package into delivery vehicles or be directly delivered. We discuss progress towards engineering next-generation CRISPR ribonucleoproteins (RNPs) with broader and efficient genomic targeting capabilities, improved editing specificity, packability and nuclease activity, and outline key considerations and remaining critical challenges.

1.1.2 Introduction

Discovery of CRISPR genome editors[1], and consequent demonstration of their mammalian genome editing[2–4], has enabled a revolution in both fundamental biological research and therapeutic development. However, the evolved characteristics of the CRISPR-cas biological defense mechanisms are distinct from the desirable features of a precise mammalian genome engineering tool. Critical limitations of native CRISPR editors include their lack of specificity[4,5], limited targeting scope[6] and compatibility with *in vivo* delivery strategies[7,8]. To address these challenges, there has been explosive growth in the number and variety of characterized and engineered CRISPR effectors and tools established for mammalian genome engineering[9,10]. In 2024, following the approval of the first CRISPR-based therapy in 2023[11], there are more than 100 ongoing CRISPR clinical trials (clinicaltrials.gov), but only a handful of CRISPR editors have progressed to preclinical and clinical trials. Despite substantial progress made towards engineering CRISPR effectors that have improved characteristics, including increased editing specificity, PAM broadening or hyper-compactness, these novel variants are generally less robust than their native counterparts. The drawbacks of many engineered CRISPR editors are most apparent

when used in the most demanding contexts, including preclinical and clinical development of novel *in vivo* or *ex vivo* therapies, where genome editor doses are strictly limited.

Safe, specific, and efficient delivery of CRISPR editors to desired cell types is a requirement for successful therapies. In general, CRISPR editors can be delivered either as a nucleic acid, to be transcribed and/or translated in the target cell, or as an intact ribonucleoprotein complex (RNP)[12]. Importantly, mode of delivery has a dramatic impact on the safety and efficacy of CRISPR[13–15]. Therefore, there is extensive interplay between the engineering goals of delivery strategies and next-generation CRISPR editors. For example, reducing the period that CRISPR editors remain active in the cell can be accomplished either by delivering them as RNPs[14], or by engineering editors with substantially improved specificity[5]. Despite this, almost all CRISPR variants have been primarily studied in extended expression systems, such as lentiviral and plasmid-based expression[16]. The general concept of "you get what you screen for"[17] holds true in this context, and these variants often do not work well when CRISPR editor delivery is limited, such as in most therapeutic applications. In this review, we aim to discuss the engineering of CRISPR effectors to optimize their functionality at every stage of genome modification, and how this relates to on-going efforts to improve CRISPR therapeutic delivery.

For a CRISPR effector to successfully modify the human genome it must be delivered into the cell, traffic into the nucleus, and search through the six billion nucleotides in the human genome. Upon finding the target sequence, the genome modification is executed either by the active CRISPR nuclease[3] or an enzyme fused to the CRISPR RNP scaffold[9]. Throughout the editors entire residence in the nucleus, it is critical to minimize off-target editing, which for nucleases increases rates of chromosomal aberrations[18] and cytotoxicity[19–21]. Throughout this entire process, the CRISPR effector must remain guide-complexed and biochemically active in a cellular environment that is extremely different from the source organism[1]. In recent years, every step of this complex process has been extensively investigated and engineered, leading to a dramatic expansion of the CRISPR toolbox (Fig. 1).

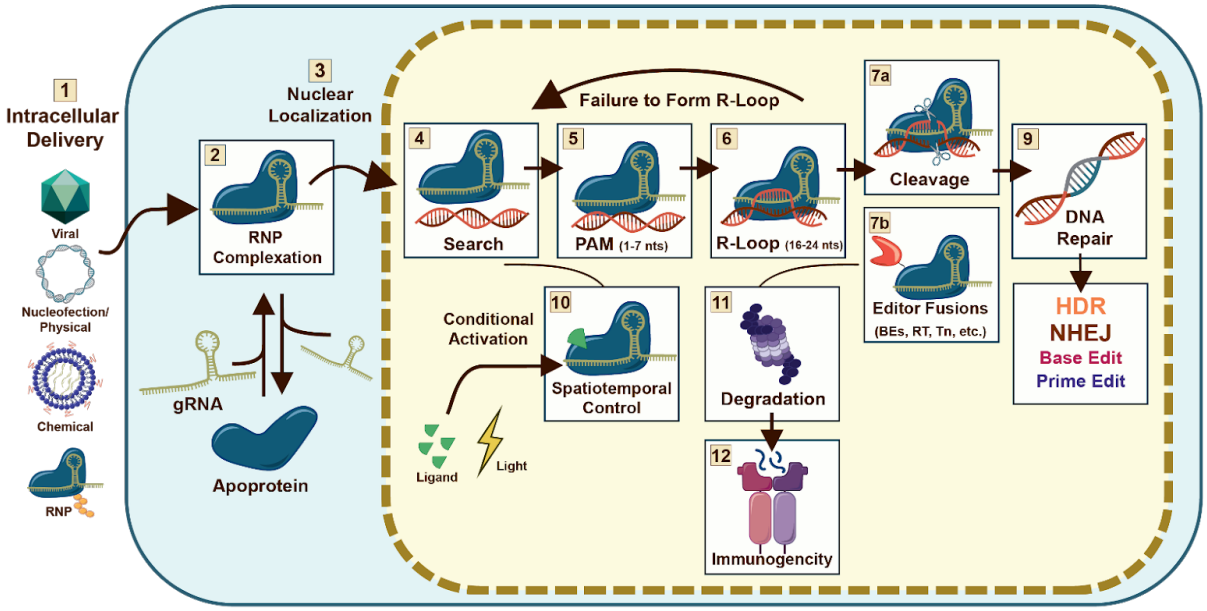

Figure 1.1: Engineering CRISPR-Cas effectors at Every Stage of Genome Modification

Step:	**Engineering Goals:**	**Approaches:**
(1) Intracellular Delivery	a. Compactness b. Penetrance c. Serum stability d. Surface charge for LNP encapsulation	a. (i) novel variants[7,22–26] (ii) deletion landscaping[27] b. (i) CPP/NLS[28–30] (ii) cell-targeting motifs[31] c. (i) thermostable variant characterization[32] d. Charge engineering[33,34]
(2) RNP complexation	Prevent guide/RNP degradation	(i) guide engineering[35] (ii) RNP pre-complexation[15] (iii) protein stability engineering[32,36]
(3) Nuclear Transport	a. Nuclear localization	a. (i) combinatorial NLS screening (ii) HDR template shuttling[37,38]
(4-5) Genomic Searching and PAM recognition	a. PAM Broadening and Diversification	a. (i) novel variants[39–41] (ii) PAM engineering[42]
(6) Binding and R-loop formation	a. Binding Specificity	a. (i) novel variants (ii) specificity engineering[5,43–46]
(7) Nuclease activity	a. Cleavage Specificity b. Cleavage Activity	a. (i) specificity engineering b. Increase nuclease activity[47–51]

(8) Editor Fusion constructs/RNA editing	(a) Edit without DSBs	(i) Base editors (BEs) (ii) Prime editors (iii)Transposases (iv)
(9) Genomic Repair	(a) increase HDR rate (b) Reduce on-target harmful genetic outcomes	(a) (i)Template shuttling[37] (ii) fusion of repair machinery[52] (iii) increased generation of staggered ends[53]
(10) Spatiotemporal control	a. Minimize or control RNP active time window	a. (i) Small molecule activation/inhibition[29] (ii) shortened half-life[30,31] (iii) Genetic control (tissue specific promoter, cell cycle)[54]
(11) Degradation	Prevent Cas9 degradation	inhibit degradation machinery[55]
(12) Reduced Immunogenicity	a. Prevent cell death in CRISPR engineered cells b. Minimize protein immunogenicity	a. (i) Prevent MHC presentation[32] (ii) T cell (T reg) tolerization (iii) spatiotemporal control[54] b. Get rid of immunogenic epitopes[56]

Terminology: Lipid nanoparticle (LNP), Cell Penetrating Peptide (CPP), Nuclear Localization Signal (NLS), Non-homologous end joining (NHEJ)

1.2 CRISPR-Cas System Diversity

In its native context, bacteria and archaea use RNA-guided endonucleases from CRISPR-Cas systems to bind and cleave foreign nucleic acids as part of their adaptive immune system[57]. These systems retain records of nucleic acid from previously encountered invaders in CRISPR arrays and then use these captured sequences, referred to as spacers, to direct CRISPR-Cas nucleases to destroy the nucleic acids of future pathogens[58]. This mechanism allows for CRISPR-Cas systems to be readily reprogrammed by simply swapping out the spacer sequence within a guide RNA but requires that the target sequence is flanked by the correct protospacer adjacent motif (PAM). The PAM requirement protects the source organism from erroneously cleaving its own genome, but also limits its targeting flexibility in engineering and therapeutic applications[1]. Identification and characterization of naturally occurring Cas effectors and their subsequent engineering for desirable properties have dramatically expanded the CRISPR toolbox. These variants, both natural and derived, will primarily be discussed in terms of Cas nucleases, but many of these engineering developments similarly apply to fusion editors[9], such as base, prime and epigenome editors. For fusion editor applications, users should consider whether a given CRISPR protein is compatible or has been previously optimized as a fusion editor[9,10].

CRISPR-Cas systems are classified into two main groups; Class 1 and Class 2 which are multi-component and single component nuclease systems, respectively. For most applications, having a single component Cas effector is advantageous,

making class 2 more widely used[10]. Class 2 is subdivided into three types- II, V, VI- which specify a distinct category of Cas effector[59,60]. Type II Cas9 and Type V Cas12 effectors are RNA-guided DNA nucleases most frequently used for DNA genome editing[9]. Type VI Cas13 variants preferentially target and cleave RNA. Recently, Cas13 variants have been utilized for RNA-targeting therapeutic strategies[61].

1.2.1 Cas9 Nucleases

In its native context, Cas9 nucleases are guided by CRISPR RNA (crRNA) that pair with trans-activating crRNA (tracrRNA) to form the functional guide RNA (gRNA)[62]. Many Cas9 applications make use of a single gRNA (sgRNA), formed from the engineered joining of the crRNA and tracrRNA into a single, convenient molecule[1]. The PAM for Cas9 orthologs is located directly 3' of the protospacer sequence on the DNA that is not complementary to the spacer sequence[1]. Mechanistically, following R-loop formation, the HNH nuclease domain cleaves the gRNA-bound target DNA strand, while the RuvC-like domain cleaves the PAM-containing non-target DNA strand 3 bp upstream of the PAM, within the protospacer[1,63], though some more recently discovered cas9 orthologs display different cleavage patterns. Cas9 can also generate staggered cutting that results in predictable 1-bp insertions[64,65]. Because Cas9 DNA cleavage is catalyzed by two independent nuclease domains, HNH and RuvC, selective deactivation of either or both domains generates nickase variants and dCas9 variants, both of which are useful for targeting of fused proteins to specific genomic loci[9].

In 2013, SpyCas9 was the first CRISPR gene editor shown to be effective at mammalian genome editing[3]. Since then, dozens of cas9 effectors have been shown to be capable of mammalian cell editing, as nucleases, nickases, or as fusion editors. These include orthologs from *Staphylococcus Aureus*[7,66,67], *Neisseria meningitidis*[68–70], *Campylobater jejuni*[71–73], and many other organisms (Table 1.1). Some of these natively characterized editors hold advantages to SpyCas9, such as smaller sizes[7,71] or broader PAMs[39,40]. Many of these variants have also been engineered to further improve desirable characteristics such as overall activity, specificity, or PAM diversification.

Despite the expansion of the CRISPR toolbox, SpyCas9 remains unequivocally the most used CRISPR editor in fundamental research and in clinical applications. This is partially because it was the first characterized CRISPR editor active in mammalian cells[3], but SpyCas9 also remains appealing because of its native broad PAM (NGG)[1], efficient nuclease activity, and high binding affinity[74] making it ideal as a fusion editor[10]. In addition, many tools and resources are available to SpyCas9 users, including guide design and off-target prediction algorithms[75,76], commercially available guide RNAs and reagents, and general protocols.

Despite these advantages and its continued widespread use, there is ample demand for alternative CRISPR genome editors. One of the biggest limitations of SpyCas9 is its size which precludes effective packaging into recombinant adeno associated virus (AAV)[7], an effective and highly utilized *in vivo* delivery strategy. Deleting portions of SpyCas9[27] to minimize its size has enabled characterization of biochemically critical domains but reduces its editing activity. SpyCas9 has a relatively broad NGG PAM, but still cannot target many desired target sites.

Investigation of other native CRISPR variants has dramatically increased the range of targetable regions by identifying editors with alternative PAM restrictions (Table 1.1; Table 1.2). Beyond expanding options for therapeutic editing, the hunt for other CRISPR effectors has also broadened the fundamental understanding of CRISPR systems, and has led to myriad tool development including diagnostics[77,78], live cell imaging[79,80], and molecular recording, among others.

Table 1.1: Source organisms and PAMs of naturally occurring Cas9 orthologs with Mammalian Gene Editing activity

Name	Species/Source	PAM (5' to 3')	Publication(s)
SpyCas9	*Streptococcus pyogenes*	NGG	[1]
SauCas9	*Staphylococcus aureus*	NNGRRT	[7]
SluCas9	*Staphylococcus lugdunensis*	NNGG	[22,24]
ScCas9	*Streptococcus canis*	NNG	[39,40]
Nme1Cas9	*Neisseria meningitidis*	NNNNGATT	[69]
Nme2Cas9	*Neisseria meningitidis*	NNNNCC	[68–70]
Nme3Cas9	*Neisseria meningitidis*	NNNNCAAA	[69]
CjeCas9	*Campylobacter jejuni*	NNNVRYAC	[72,73]
Stl1Cas9	*Streptococcus thermophilus 1*	NNAGAAW	[81,82]
Stl3Cas9	*Streptococcus thermophilus 3*	NGGNG	[81]
FnCas9	*Francisella novicida*	NNG or NGG	[41]
GeoCas9	*Geobacillus stearothermophilus*	NNNNCRAA	[32]
CdCas9	*Corynebacterium diphtheriae*	NNRHHHY	[83]
FrCas9	*Faecalibaculum rodentium*	NNTA	[84]
PpCas9	*Pasteurella pneumotropica*	NNNNRTT	[85]
GBS Cas9	*Streptococcus agalactiae*	NGG	[86]

1.2.1 Cas12 Nucleases

In 2015 AsCas12a[87], and related orthologs, were the first Cas12a nucleases characterized for mammalian genome editing. AsCas12a does not require a tracrRNA and can process its CRISPR array into multiple, useful crRNAs, allowing for easy guide multiplexing from a single transcript[88]. AsCas12a targets a thymine rich PAM (5'TTTV), which complements the guanine rich (5'NGG) SpyCas9 PAM. Worth noting, AsCas12a and related orthologs also exhibit indiscriminate single stranded DNA (ssDNA) cleavage upon binding DNA complementary to its spacer. This characteristic has been leveraged for its use in rapid and highly sensitive diagnostic testing[77,78,89].

In general, Cas12 nucleases possess a single RuvC-like nuclease domain that mediates cleavage of both strands of DNA[90]. Because Cas12 cleaves both the target and non-target strand with the same active site, engineering Cas12 effectors into nickase variants for base or prime editing applications is nontrivial[91]. Conveniently, many Cas12 nucleases are guided by a single crRNA, also facilitating applications that require multiplexing[92]. Unlike Cas9, Cas12 nucleases generate staggered cuts within the protospacer distal to the PAM sequence[87]. Staggered cuts, rather than the blunt cuts made by Cas9, may naturally facilitate HDR[93–95] which is desirable for

successful introduction of a transgene or precise gene repair. Some reports also suggest that many Cas12 effectors have naturally higher specificity than their Cas9 counterparts[96,97], though direct comparison of the specificity of different gene editors is complicated by their varying PAM requirements and DNA cleavage outcomes[96]. Cas12 variants have enormous diversity in terms of their substrate cleavage capabilities[98], size and architecture[10].

Table 1.2: Source organisms and PAMs of representative Cas12 orthologs with DNA Editing activity in human cells

Name	Species/Source	PAM (5' to 3')	Publication(s)
AsCas12a	*Acidaminococcus sp.*	TTTV	[96,97]
LbCas12a	Lachnospiraceae bacterium	TTTV	[96,97]
FnCas12a	*Francisella novicida*	TTTV	[99,100]
MbCas12a	*Moraxella bovoculi 237*	TTTV	[100]
ErCas12a	*Eubacterium rectale*	TTTN and CTTN	[101]
Un1Cas12f	Uncultured archaeon 1	TTTR	[23,25]
AsCas12f	*Acidibacillus sulfuroxidans*	NTTR	[48]
PlmCasX	Phyla Planctomycetes	TTCN	[26,102]
DpbCasX	Phyla Deltaproteobacteria	TTCN	[26,102]
CasPhi2 (Cas12j2)	Biggie phage 2	TGAA	[8]
BhCas12b	*Bacillus hisashii*	ATTN	[103]
AcCas12n	*Actinomadura craniellae*	AAN	[104]
IsDra2 (TnpB)	*Deinococcus radiodurans*	TTGAT	[105]
SpuFz1 (Fanzor)	*Spizellomyces punctatus*	TTAAN	[106]
Cas12j8	Biggie phage 8	TTN	[107]

1.2.3 Repair Pathways

There are many endogenous DNA repair mechanisms in mammalian cells to repair double stranded breaks (DSBs)[108]. Prior research with other targeted nucleases, such as zinc finger nucleases[109,110] and transcription activator-like effector nucleases (TALENs)[111,112], established an understanding of how targeted DSB lead to different repair outcomes. Many factors impact which repair pathway is predominately used by a cell, including cell-type, cell cycle and the type of DSB (blunt or staggered)[113]. DSB repair pathways fall into two general categories, those that ligate broken DNA end, termed end-joining, and those that use DNA templates for homology directed repair (HDR). End-joining repair mechanisms are efficient in most cells, but HDR efficiency

is often limited and can be inactive in post-mitotic cells[113,114], because it requires proteins that are principally expressed during the S and G2 stages of the cell cycle[115,116].

Conventional genome editing approaches rely on CRISPR nucleases to disrupt a target gene selectively and efficiently. Cas nuclease generated DSBs are repaired by non-homologous end joining (NHEJ) which either regenerates the original sequences, leaving it a substrate for re-cutting, or results in small insertions or deletions, termed indels, and preventing re-cutting[117]. The resulting indels from DSBs are not controllable, but they are also not random and can be predicted experimentally or through computational modeling[118,119]. In specific instances, end-joining primarily produces a single product, which is useful for certain types of reporter systems or therapeutic repair[118,120]. Most commonly NHEJ is utilized to disrupt target genes by disrupting their coding sequence, or by simultaneously utilizing two DSBs flanking the gene to remove it entirely[3,121].

For many editing applications, precise restoration or integration of an exogenous DNA sequence is required. HDR results in incorporation of desired exogenous templates at the cut site, allowing for replacement of a defective gene[113]. Repair templates contain the desired mutation flanked by homologous regions on either side of the DSB. For many clinically relevant cell types, particularly post mitotic cells[113,114], such as neurons or cardiomyocytes, or stem cells, HDR is typically inefficient. More generally, HDR efficiency is frequently a critical limitation of CRISPR-based therapeutic approaches, with outcomes depending on the type of repair template, the cell type, the cell cycle, the local chromatin context, and type of CRISPR nuclease[122]. Numerous methods to enhance HDR, including template engineering, and NHEJ inhibition, are extensively reviewed elsewhere[123], but several approaches involve directly fusing CRISPR effectors to DNA repair machinery to upregulate HDR[124–126].

Reliance on endogenous repair pathways remains a huge barrier to CRISPR-based gene therapies. Fusion editors, including base and prime editors, circumvent the reliance on DSB repair pathways, but still require endogenous repair machinery[9]. Most methods to measure editing specificity, such as CIRCLE-seq[127], Digenome-seq[128], GUIDE-seq[129], and SITE-seq[13], require DSBs to detect off target activity. Direct profiling methods to measure the editing specificity of fusion editors are only beginning to emerge[130], and most specificity comparisons leverage previously validated or predicted *in silico* off-targets.

1.3 Overcoming Limitations of CRISPR RNP for mammalian genome editing

1.3.1 Engineering CRISPR RNPs

The size and complexity of CRISPR effectors makes the application of many existing protein engineering techniques challenging. AlphaFold[131] and related computational models[132,133] have revolutionized *de novo* protein engineering, but are often hindered in CRISPR engineering applications due to a lack of high quality training data on nucleic acid binding protein interactions [134,135]. Therefore, it is unsurprising that the vast majority of CRISPR engineering efforts leverage structure-guided rationale design or directed

evolution, or a combination of these approaches. To improve editor specificity or to modify PAM targeting requirements, most engineering focuses on the residues and/or structural regions that interact with the DNA. Interestingly, identified mutations can sometimes yield similar improvement in multiple related orthologs[36,47,136].

Frequently, the optimization of one desirable characteristic such as PAM broadening or improved editing specificity results in loss of general activity or functionality[5,44]. Interestly, whether these engineering goals are fundamentally opposed due to underlying biochemical principles or a surmountable engineering problem remains a debate. For PAM broadening, recent evidence supports there being a inherent tradeoff between broad PAM recognition and genome editing effectiveness[137,138], because for minimal PAM variants, such as SpRY[6], the dramatic increase in PAM binding sites commensurately lengthens the search time compared to the native enzyme.

1.3.2 Nuclease activity

Most newly discovered CRISPR enzymes are inefficient nucleases or fusion scaffolds in mammalian cells, with notable exceptions including SpyCas9[2–4] and AsCas12a[87,96,97]. However, these enzymes often have other desirable properties such as compactness[8,25,48,69], thermostability[32,33,36,81,82], multiplexed gRNA processing[25,96], or naturally broad PAMs[39,40]. Utilizing these newly discovered variants requires first improving their activity, with engineering approaches outlined below (Table 1.3, Table 1.4).

Table 1.3 Engineering Cas9 Variants for improved nuclease activity

Derived from:	Name of variant:	Mutations:	Engineering Strategy:	Publication(s)
SpyCas9	vCas9 (Note: designed to improve HDR)	S55R, R976A, K1003A, T1314R	Rationale design of 14 residues, goal to make more staggered cuts	[53]
	iCas9	D147Y, P411T	Accidentally generated during plasmid construction	[51]
	OptiHF-SpCas9	Q695A, K848A, E923M, T924V, Q926A	Combinatorial mutagenesis	[139]

	Turbo Cas9	V842L, Q844R, F846Y, L847M, I852F	Computational design focused on HNH and RuvC	[140]

Table 1.4 Engineering Cas12 Variants for improved nuclease activity

Derived from:	Name of variant:	Mutations:	Engineering Strategy:	Publication(s)
LbCas12a	LbCas12a-KY	Q571K, C1003Y	Structure-guided	[141]
	impLbCas12a	D156R, G532R, K538V, Y542R, K595R	Structure-guided	[142]
	LbCas12a-Plus	D156R, R883K, R887A	Structure-guided	[143]
	LbCas12a-RVQ	G146R, R182V, E795Q	Directed evolution	[144]
AsCas12a	enAsCas12a	E174R/S542R/K548R	Structure-guided protein engineering	[145]
	AsCas12a-Ultra	M537R and F870L	Directed evolution	[47]
	AsCas12a-Plus	E174R, R951K, R955A	Structure-guided	[143]
	HyperFi-As	S186A/R301A/T315A/Q1014A/K414A	Rationale/structure-guided design	[146]
EbCas12a	enEbCas12a	D141R	Application of previously reported mutations[145]	[147]

LbdCas12a	hyperCas12a	D156R, D235R, E292R, D350R	First engineered for as dCas12a; structure-guided protein engineering	[50]
PlmCasX	PlmCasX(R1)	R-loop engineering	Guide engineering; truncation of stem loop structure	[102]
DpbCasX	DpbCasX(R3)	R-loop engineering	Guide engineering; truncation of stem loop structure	[102]
Un1cas12f	CasMINI(v3.1)	D143R, T147R, E151A	Gene activation screen in mammalian cells; Guide engineering	[23]
	ge4.1	N/A	Guide engineering; truncation of stem loop structure	[25]
AsCas12f	enAsCas12f	D196K, N199K, G276R, N328G, D364R	Deep mutational scanning and empirical design; guide truncation	[148]
CnCas12f1	CnCas12f1	N/A	Guide engineering; truncation of stem loop structure	[149]

SpaCas 12f1	SpaCas12 f1	N/A	Guide engineering; truncation of stem loop structure	[150]
BhCas1 2b	BhCas12b v4	K846R, S893R, E837G	Structure-guided	[103]
Cas12i2	ABR-001	D581R, I926R, V1030G	Structure guided and mutational scanning	[151]
	Cas-SF01	S7R, D233R, D267R, N369R, S433R	AI-guided prediction of structures and rational design	[152]
	hfCas12M ax	N243R,E33R, D892R	Structure guided; specifically arginine substitutions at the PAM-interacting (PI) REC and RuvC domains	[153]
Chimera	M44	NA	Screening of >500 combinatoria l variants	[154]
	ehCas12a	NA	Shuffling and mutagenesis of Cas12 variant library	[49]

Terminology: Deep mutational scanning (DMS)

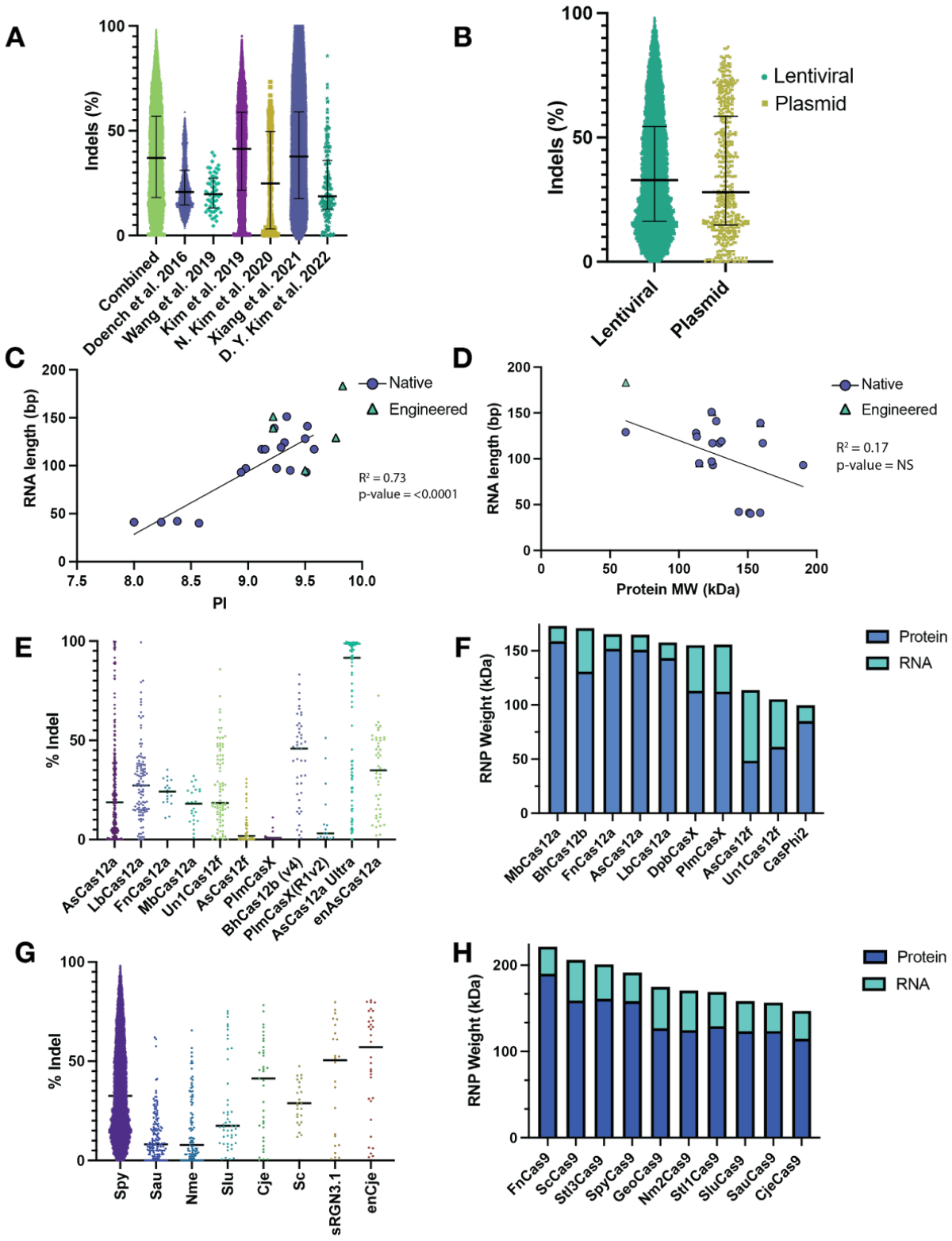
A
Indels (%)
100
50
0
Combined
Doench et al. 2016
Wang et al. 2019
Kim et al. 2019
N. Kim et al. 2020
Xiang et al. 2021
D. Y. Kim et al. 2022
B
Indels (%)
Lentiviral
Plasmid
C
RNA length (bp)
PI
Native
Engineered
R² = 0.73
p-value = <0.0001
D
RNA length (bp)
Protein MW (kDa)
Native
Engineered
R² = 0.17
p-value = NS
E
% Indel
AsCas12a
LbCas12a
FnCas12a
MbCas12a
Un1Cas12f
AsCas12f
PlmCasX
BhCas12b (v4)
PlmCasX(R1v2)
AsCas12a Ultra
enAsCas12a
F
RNP Weight (kDa)
Protein
RNA
MbCas12a
BhCas12b
FnCas12a
AsCas12a
LbCas12a
DpbCasX
PlmCasX
AsCas12f
Un1Cas12f
CasPhi2
G
% Indel
Spy
Sau
Nme
Slu
Cje
Sc
sRGN3.1
enCje
H
RNP Weight (kDa)
Protein
RNA
FnCas9
ScCas9
Stl3Cas9
SpyCas9
GeoCas9
Nm2Cas9
Stl1Cas9
SluCas9
SauCas9
CjeCas9

Figure 1.2: Comparing editing efficiencies of native and engineered CRISPR-Cas effectors in HEK293T

(A) SpyCas9 editing efficiency in large studies (> 50 endogenous loci targets) from 2016-2022 (B) Comparison editing efficiency resulting from extended expression of SpyCas9 lentiviral or plasmid delivery (C) PI vs guide length D) size vs guide length E) Complied Cas9 variant NHEJ comparison in 293 cells F) Cas9 variant RNP size comparison G) Cas12 variant NHEJ comparison in 293 cells H) Cas9 variant RNP size comparison. Studies included in this comparison were tested in HEK293T or derivatives with editors delivered by lentivirus or plasmid. Only included studies that targeted endogenous loci (not lentiviral integrated transgenes) and where the indel quantification was done with NGS. The studies included are listed in Supplemental Table 1.

1.3.3 Editing Specificity

Precise targeting by CRISPR effectors requires that they can robustly discriminate on-target sequences from similar off-target sequences throughout the genome. Protospacer sequences play an essential role in the specificity of CRISPR effectors, and guide optimization algorithms exist for the more commonly used enzymes such as SpyCas9[4,76,155] and AsCas12a[96,97]. While several native Cas9[69,70] and Cas12[96,97] orthologs reportedly have high fidelity than SpyCas9, a major engineering goal has been to develop editors with greater selectivity for on-target sequences over off-targets.

Increasing the specificity of gene editors requires raising the energetic barriers for off-target DNA cleavage[156]. Therefore, there may be an intrinsic tradeoff between overall nuclease activity and editing specificity[5,43,157]. This appears to be generally true, but certain top performing specificity variants, such as LZ3 cas9[5] and HiFi Cas9[16], claim to optimize both activity and specificity. Most specificity variants were generated and primarily studied in extended expression systems, such as lentiviral and plasmid-based expression[44]. Under extended expression, engineered high specificity SpyCas9 variants exhibit activity that is more comparable to WT SpyCas9, than when delivered transiently as a ribonucleoprotein or mRNA[16,44]. HiFi Cas9[16] was engineered with this limitation in mind and shown to improve specificity but maintain nuclease activity even when delivered to cells transiently as ribonucleoproteins.

To facilitate precise nuclease activity and to minimize off-targets many strategies to have spatiotemporal control over Cas9 have been engineered[54]. Extended expression of gene editors, for example resulting from viral delivery by AAV or lentivirus, increases the probability of unintended DSBs[13]. This has driven development of many spatiotemporal control methods to limit the active duration of gene editors in cells[54]. Many of these spatiotemporal control mechanisms are mediated by protein fusions or modifications to the protein or RNA sequence directly[54]. These strategies are extensively reviewed elsewhere, but spatiotemporal control strategies fall broadly into genetic regulation, chemical control, and physical control. Cas effectors have been engineered to be selectively activated or inhibited by small molecules including rapamycin[158], 4-hydroxytamoxifen[159,160] and degron domains[161]. These spatiotemporal control mechanisms have been shown to promote specificity in

vitro, but suffer from similar limitations as engineered specificity variants, in that they fail to work as robustly as their native counterparts.

CRISPR effectors are two component systems and gRNA engineering is critical to the overall editing efficacy and specificity. For extended expression systems, including plasmid and lentiviral delivery, truncation of the protospacer sequence to have less than 20 bp sequence homology[162] increases overall SpyCas9 editing specificity. This improvement appears counterintuitive because it requires a shortened complementary region but is consistent with protein engineering strategies that aim to destabilize the interaction of the CRISPR RNP with the off-target sequence[156]. Modifications of the stem loop structure of the guide scaffold can similarly increase editing specificity by weakening direct interactions between the Cas effector and DNA[163].

For mRNA and direct RNP delivery strategies, including LNP[164], electroporation[165] and peptide mediated delivery[166], chemical guide engineering can play a critical role in the overall editing efficacy and specificity[15]. The particular chemical modifications of the guides is extensively reviewed[167,168] elsewhere but has been demonstrated to dramatically improve the specificity of Cas9 and Cas12 orthologs[167].

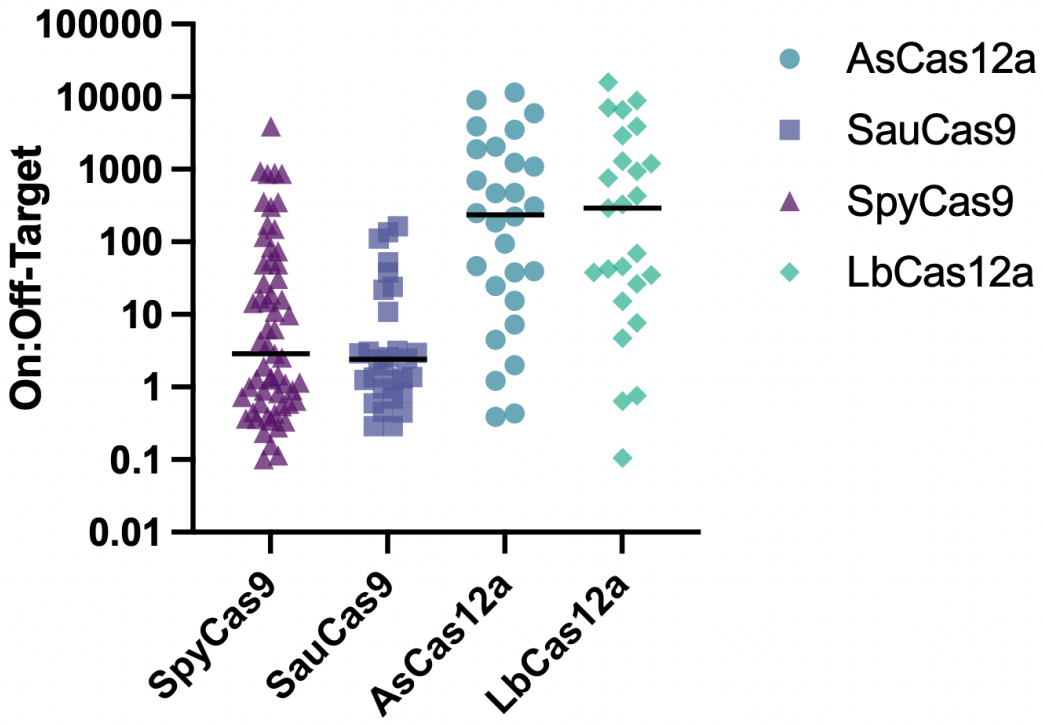

Figure 1.3 Comparison of reported editing specificity for frequently used CRISPR-Cas genome editors.

Reported specificity values for SpyCas9, SauCas9, AsCas12a and LbCas12a. Specificity readout inclusion criteria was that CRISPR editors were delivered by

lentivirus or plasmid. Data was publicly available. Specificity analysis methods included were Guide-seq[129] and Digenome-seq[128]. Publications: SpyCas9[5,24,40,128,136,169] SauCas9[7,170,171] AsCas12a[25,96,97] LbCas12a [96,97]

Table 1.5: Engineered Cas9 Variants with improved targeting specificity

Derived from:	Name of variant:	Mutations made:	Engineering Strategy:	Publication(s)
SauCas9	SauCas9-HF	R245A, N413A, N419A, R654A	Empirical design; mutations around amino acids within 3.0 Å of target DNA strand	[170]
	efSaCas9	N260D	Directed Evolution in human cells	[171]
	KKH-SaCas9-SAV1* (*derived from KKH-SaCas9)	Y239H, N419D, R499A, Q500A, Y651H, *E782K, *N968K, *R1015H * new mutation	Structure-guided combinatorial mutagenesis	[172]
SpyCas9	eSpCas9(1.1)	K848A, K1003A, R1060A	Structure Guided engineering	[136]
	SpCas9-HF1	N497A, R661A, Q695A, Q926A	Rational Design through analysis of protein-DNA interaction points	[173]
	HeFSpCas9* (*2nd Generation, combined eSpCas9 and SpyCas9-HF1)	N497A, R661A, Q695A, K848A, Q926A, K1003A, R1060A	Combining mutations from eSpCas9 and SpCas9-HF1	[174]
	evoCas9	M495V, Y515N, K526E,R661Q	Directed evolution by	[169]

			random mutagenesis of the REC domain	
	HypaCas9	N692A, M694A, Q695A, H698A	Rational design	[45]
	xCas9 (3.7)	A262T, R324L, S409I, E480K, E543D, M694I, E1219V	Phage assisted continuous evolution	[175]
	Sniper-Cas9	F539S, M763I, K890N	Directed evolution with negative selection screen; Error prone PCR and DNA shuffling	[176]
	Sniper2L-Cas9* (*2nd generation, derived from Sniper-Cas9)	F539S, M763I, K890N, E1007L* *new mutation	Directed evolution	[46]
	iSniperCas (*2nd generation, derived from Sniper-Cas9)	D147Y*, P411T*, F539S, M763I, K890N *new mutation	Rational design and random mutagenesis	[177]
	HiFi Cas9	R691A	Directed evolution in bacteria; Validation in human cell lines with transient delivery (RNP)	[16]
	SuperFi-Cas9	Y1010D,Y1013D, Y1016D, V1018D R1019D, Q1027D K1031D	Structure guided; targeted toward regions involved in mismatch tolerance	[178,179]

	SpartaCas	D23A, Y128V, S1216V D1251G	Directed Evolution with scanning mutagenesis and phage based selection	[180]
	LZ3Cas9	N690C, G915M, T769I, N980K	Targeted mutagenesis of RuvC and HNH domains, L1 and L2 linkers (173 residues)	[5]
	HSC1.2 Cas9	V842L, Q844R, F846Y, L847M, I852F	Rational design from crystal structure	[181]
	Cas9 V3	N497A, K510A, R661A	Rationale design to enhance hydrophobic interactions of REC3/HNH and guide	[182]
	FeCas9* (*2nd generation, Derived from eCas9)	K848A, K1003A, R1060A, D1135E* *new mutation	Rationale design to destabilize off target binding	[183]
	rCas9HF (*2nd generation, Derived from evoCas9)	K526E	EvoCas9 mutations screened and optimized for RNP delivery	[44]
ScCas9	Sc++-HF	R701A, T1227K, Loop modification	Rationale design, substituting positively charged residues into PAM-interaction	[40]

			domain, Loop engineering (subsitution from *S. anginosus*)	
Slu(g)Cas9	SlugCas9-HF	R247A, N415A, T421A, R656A	Pairwise alignment applying mutations from SauCas9-HF engineering[170]	[22]

1.3.4 Broadening or retargeting the PAM

Expanding or retargeting CRISPR effectors has been a major focus of CRISPR engineering. A primary requirement for the binding of a CRISPR effector is the presence of its PAM sequence. The two most broadly used CRISPR effectors, SpyCas9 and AsCas12a, both have relatively broad PAM targeting constraints (5'NGG and 5'TTTV, respectively). However, these PAMs constrain targeting and can affect editing flexibility in fundamental and clinically relevant applications. The discovery and characterization of naturally occurring orthologs has vastly expanded the possible realm of targetable sites (Table 1.1; Table 1.2). Some natural variants, such as ScCas9[39], have extremely minimal PAMs (5'NNG), but have other drawbacks, such as large size[41] or low nuclease activity[40,41], that limit their utility. Therefore, PAM availability remains a common limitation even with the discovery of these natural Cas proteins, leading to the engineering of less restricted or diversified Cas9 and Cas12 variants.

The earliest Cas9 variants with altered PAM specificity were developed through a combination of rational design and directed evolution[66,67]. PAM engineering is particularly amenable to a structure guided approach in part because there is a limited number of residues that are directly involved with PAM recognition[66].

Similar to the engineered Cas specificity variants, the Cas variants engineered for broadened or diversified PAMs typically perform worse than their, particularly in the context of transient delivery[137,138]. Recent work has argued that this is due to a fundamental tradeoff between broad PAM recognition and genome editing effectiveness[137,138]. As PAM targeting broadens, the number of potential PAM binding sites dramatically increases, leading to extended search time requirements[137,138]. This appears to support the strategy of PAM diversification rather than broadening. However, in practice many native orthologs, such as GeoCas9[32], and engineered variants that target longer PAMs perform poorly[66]. Unfortunately, it is difficult to disentangle whether this is an inherent biochemical tradeoff or due to suboptimal engineering.

Table 1.6: Engineered Cas9 PAM Variants

Derived from:	Variant name:	PAM (5' to 3') * = lesser activity	Mutations:	Engineering strategies:	Publication(s)
SpyCas9	VQR	NGAN	D1135V, R1335Q, T1337R	Directed evolution and rational design disrupting 3rd nucleotide of PAM domain	[66]
	EQR	NGNG	D1135E,R1335Q, T1337R	Directed evolution and rational design	[66]
	VRER	NGCG	D1135V,G1218R, R1335E,T1337R	Directed evolution and rational design	[66]
	QQR1	NAAG	G1218R,N1286Q, I1331F,D1332K, R1333Q,R1335Q, T1337R	Structure guided	[184]
	SpG	NGN	D1135L,S1136W, G1218K,E1219Q, R1335Q, T1337R	Structure guided	[6]
	SpRY	NRN	D1135L, S1136W, G1218K, E1219Q, R1335Q, T1337R, L1111R, A1322R, A61R, N1317R, R1333P	Structure guided	[6]
	HF1-SpRY* (2nd generation, HF1	NRN	A61R, N497A, R661A, Q695A, Q926A,	Combination of previously engineered variants	[185]

	and SpRY)		L1111R, D1135L, S1136W, G1218K, E1219Q, N1317R, A1322R, R1333P, R1335Q, T1337R		
	xCas9(3.7)	NG, GAA, GAT	A262T, R324L, S409I, E480K,E543D, M694I, E1219V	Phage assisted directed evolution	[175]
	NRRH	NRRH	D10T, I322V, S409I, E427G, R654L, R753G, R1114G, D1135N, V1139A, D1180G, E1219V, Q1221H, A1320V, R1333K	Phage assisted directed evolution	[186]
	NRTH	NRTH	D10T, I322V, S409I, E427G, R654L, R753G, R1114G,D1135, D1180G, G1218S, E1219V, Q1221H, P1249S, E1253K, P1321S, D1332G, R1335L	Phage assisted directed evolution	[186]
	NRCH	NRCH	D10T, I322V,	Phage assisted	[186]

			S409I, E427G, R654L, R753G, R1114G, D1135N, E1219V, D1332N, R1335Q, T1337N, S1338T, H1349R	directed evolution	
	NG	NG	R1335V/L1111R/D1135V/G1218R/E1219F/A1322R/T1337R	Structure guided rational design to stabilize PAM interaction	[187]
	SpdNG-LWQT	NRN *NYN *less activity	D10A, H840A, R1335V, L1111R, G1218R, E1219F, A1322R, R1333Q, V1335T, T1337R	Structure guided rational design	[188]
	VRKG	NAG	D1135V, S1136R, D1332K, R1333G	Directed evolution	[189]
	SpCas9-NRRH	NRRH	D10T, I322V, S409I, E427G, R654L, R753G, R1114G, D1135N, V1139A, D1180G, E1219V, Q1221H, A1320V, R1333K	Directed evolution, Continuous evolution	[186]
SpyCas9/SmacCas9	iSpyMac	NAA	Fusion w/ SmacCas9;	Structural guided fusion of two Cas9 proteins,	[191]

			R221K/N394K[190]	SpyCas9 and SmacCas9	
SpyCas9/ScCas9	SpRyc	NNN	N-terminus (1–1119) from Sc ++ and PID (1111–1368) from SpRY	Structural guided fusion of high SpyCas9 (SpRY) and ScCas9	[192]
SauCas9	KKH	NNNRRT	E782K/N968K/R1015H	Directed evolution	[67]
	SaCas9-NR* (*2nd generation, derived from KKH)	NN*N*RRT	E782K/N968K/R1015H, Y239H* *new mutation	Computational design	[193]
FnCas9	RHA FnCas9	YG	E1369R/E1449H/R1556A	Structure guided protein engineering	[194]
	enFnCas9	NGR	Refers to multiple variants	Structure guided protein engineering	[195]
CjeCas9	evo*Cj*Cas9	N4AH, N5HA	E789K	Continuous Directed Evolution	[196]

Table 1.7: Engineered Cas12 PAM Variants

Derived from:	Variant name:	PAM (5' to 3') * = lesser activity	Mutations:	Engineering strategies:	Publication(s)
AsCas12a	enAsCas12a	TYCN/TATN	E174R, S542R, K548R	In vitro PAM determination assay (PAMDA); Validation in HEK293T	[145]

	RVR	TATV	S542R, K548V, N552R	Structure-guided mutatgenesis	[197]
	RR	TYCV	S542R, K607R	Structure-guided mutagenesis	[197]
	KK		R951K, R955K	Structure-guided mutagenesis	[143]
	KA		R951K, R955K	Structure-guided mutagenesis	[143]
LbCas12a	RVRR	TNTN	G532R, K538V, Y542R, K595R	Plasmid based PAM screening (GFxFP); Validation in HEK293T	[142]
	As-K548R	YYN	K548R	Structure-guided mutagenesis (4 key residues previously established[142])	[198]
FnCas12a	eaFnCas12a-RR	TATV/TYCV	Q125R,N607R, K671R	Directed evolution	[99]

1.3.5 Immunogenicity

CRISPR effectors are composed of foreign proteins and RNA sequences which illicit immune responses in humans, potentially reducing their therapeutic effectiveness [21,56]. Many CRISPR effectors, including SpyCas9, are derived from common bacteria and are therefore recognized by the adaptive immune system[199]. However, immune responses have been detected even in naive individuals, with activation of T and B cells reported upon delivery of SpyCas and SauCas9 in naive mice[200,201]. For *ex vivo* clinical therapies it is relatively straightforward to confirm that the gene editor used therapeutically is undetectable prior to infusion of edited cells [202], but this approach is generally limited to hematopoietic target indications. Immunogenicity concerns are one reason why many early in vivo CRISPR clinical trials have focused on relatively immune privileged sites, such as the human eye (NCT03872479). Extended expression of gene editors, resulting from delivery by AAV or lentivirus, has been shown to be more immunogenic than transient RNP delivery[19–21]. Extensive

engineering efforts have focused on directly modifying the protein or guide to lessen recognition by the adaptive or innate immune system[203].

In human cells, foreign RNAs are typically recognized in the cytosol by pathogen-associated molecular receptors, which trigger a signaling cascade that upregulates type 1 interferons and related genes[204]. These pathways are triggered by the 5' triphosphate group present on CRISPR gRNA[20] generated by in vitro transcription, which can be mitigated by synthetic modification of the guide termini.

For CRISPR protein engineering, what sequences or structural motifs cause immune responses is often unclear, but immunosuppression during the gene editor delivery window has been shown to facilitate in vivo therapeutic editing[205]. An interesting alternative strategy involves engineering variants of SpyCas9 that are less immunogenic through targeted mutations that eliminate immunodominant epitopes[56].

1.3.6 Engineering for delivery

CRISPR-based genome editing therapies have enormous potential to cure genetic diseases. Despite this promise, safe and effective delivery of genome editors remains a challenge for both therapeutic development and fundamental research [12,206]. In general, CRISPR editors can be delivered either as a nucleic acid, to be transcribed and/or translated in the target cell, or as an intact ribonucleoprotein complex (RNP) [12]. Transient delivery of editors offer distinct advantages including shorter intracellular lifetimes that minimize off-target edits [14] and reduce immunogenicity [19–21]. While delivery of CRISPR editors to the interior of cells remains a critical therapeutic challenge [207], extensive engineering efforts have generated multiple promising *ex vivo* and *in vivo* delivery strategies [12,206]. RNP electroporation is a common strategy, with widespread use in CRISPR genome editing therapies [208,209]. RNP electroporation is less cytotoxic than nucleic acid electroporation [30], is efficient in primary cells and has higher specificity than delivery systems that result in extended genome editor expression [14]. However, RNP electroporation requires an *ex vivo* approach, limiting its therapeutic utility. Furthermore, electroporation can impact cell viability [166] and lead to high manufacturing costs for cell-based therapies [166].

For in vivo delivery there are two broad categories of delivery vehicles: viral and non-viral. Viral vectors, lacking replicative capacity, are broadly utilized and leverage the native transduction and delivery efficiency of viruses. The most broadly utilized are adeno associated viral (AAV) vectors, with different variants exhibiting a wide range of tropisms for clinically relevant tissues including the eye and central nervous system (CNS). For CRISPR applications, the minimal packaging capacity of AAV, which typically is around 5 kb, is limited. Following transduction, AAVs express their cargo as a long-lived episome. Lentiviral vectors, which are a subtype of retrovirus, express larger transgenes (~10 kb) following genomic integration. Importantly both viral vectors are capable of transducing post-mitotic cell types. The extended expression of CRISPR editors following viral delivery poses a serious safety risk, increasing the probability of unintended edits, cellular perturbations, and immunogenicity risk. In addition, lentiviral integration can lead to insertional oncogenesis, with a retroviral gene therapy resulting in four out of nine patients developing leukemia[210,211].

SpyCas9 exhibits high activity in mammalian cells, and still by far the most used CRISPR gene editor at 4.1 kilobases (kb), is too large to enable co-packaging of SpyCas9 and gRNA into AAV vectors. In 2015, SauCas9, a natural Cas9 ortholog, was identified as a mammalian genome editor[7] that, at 3.2 kb, is small enough to fit robustly into AAV. SauCas9's early discovery and compact size led to its widespread use in AAV gene therapy clinical trial development and is currently in trials to treat leber congenital amaurosis (NCT03872479) and HIV-1 (NCT05144386). Despite these successes, SauCas9 exhibits lower nuclease activity than SpyCas9 and stricter PAM requirements (5′NNGRRT), driving the characterization and development of other smaller Cas9 variants. CjeCas9 and SluCas9 are two notable examples, both of which have been extensively engineered for mammalian genome engineering applications. Wild-type (WT) CjeCas9 is a highly effective nuclease, but has stringent PAM constraints(5′-NNNNACAC-3′ or 5′-NNNNRYAC-3′). Worth noting, CjeCas9 apoprotein indiscriminately cleaves single stranded DNA (ssDNA) leading to cytotoxicity and cell death[71], which potentially minimize its broad utility as a gene editor.

In recent years, several increasingly hypercompact Cas12 systems have been characterized including Cas12e[26,102], previously CasX (~1000 AA), Cas12j[8], previously CasPhi (~750 AA), and Cas12f[23,48] (~450 AA). These hypercompact variants are small enough to be packaged into AAV, even as fusion editors, along with multiple guides.

Table 1.8: RNP weight of representative Cas9 Variants

Name	Protein Weight (kDa)	Scaffold Length	RNP Weight (kDa)	Publication(s)
SpyCas9	158.4	97	191.5	[1]
SauCas9	123.8	97	156.7	[7]
SluCas9	123.7	151	158.5	[22,24]
ScCas9	159.2	139	206.4	[39,40]
Nm2Cas9	124.7	136	170.7	[68–70]
CjeCas9	114.8	95	147.1	[72,73]
Stl1Cas9	129.5	117	169.1	[81,82]
Stl3Cas9	161.1	117	200.9	[81]
FnCas9	190.3	93	221.8	[41]
GeoCas9	127.1	141	174.9	[32]

Table 1.9: RNP weight of representative Cas12 Variants

Name	Protein Weight (kDa)	Scaffold Length	RNP Weight (kDa)	Publication(s)
AsCas12a	151.1	41	164.9	[96,97]
LbCas12a	143.5	42	157.8	[96,97]
FnCas12a	151.9	40	165.5	[99,100]
MbCas12a	159.1	41	172.9	[100]
Un1Cas12f	61.4	129	105.2	[23]
AsCas12f	48.7	193	113.8	[48]
PlmCas12e (PlmCasX)	112.5	128	115.9	[26,102]

DpbCas12e (DpbCasX)	113.1	124	155.2	[26,102]
CasPhi2	85.2	43	99.8	[8]
BhCas12b	130.9	119	171.0	[103]

1.4 Conclusions

From their initial discovery, CRISPR-Cas systems have rapidly developed into powerful tools for fundamental research and clinical development. In 2023, Casgevy, a treatment for sickle cell disease developed by Vertex and CRISPR therapeutics, was the first CRISPR based gene therapy approved by the FDA. With more than 100 other CRISPR clinical trials in progress it is looking to be the first of many. In 2024, a mere 12 years since SpyCas9 was first demonstrated as a RNA-guided endonuclease[1], there are now hundreds of characterized orthologs and engineered Cas proteins demonstrated to work in mammalian cells, and thousands more characterized *in silico*[59,60]. These variants seek to address the critical limitations of native CRISPR editors including their lack of specificity[4,5], limited targeting scope[6] and compatibility with *in vivo* delivery strategies[7,8]. However, the majority of variants are developed within a narrow scope, specifically with extended expression, by plasmid or lentiviral delivery, in HEK293T or derivative cell lines. It is therefore, unsurprising that many of these variants fail to work robustly in more demanding contexts, and with some notable exceptions, such as AsCas12a-ultra[47], failed to be utilized outside of the early stage research. In addition, though HEK293T are a useful model system, they fail to capture the well-documented variability between cell lines. The epigenetic context varies substantially by cell type, and clinically relevant cell lines, such as hematopoietic stem cells, are much more sensitive to cytotoxicity resulting from indiscriminate DNA cleavage[212–215]. Numerous papers have shown that editing[16,165] and specificity[15,44] is extremely dependent on delivery context. Therefore, it is critical that future engineering develops or validates its variants in the context of transient delivery, which better represents the dosage limited context of therapeutic delivery.

Supplemental table 1: Comparison of CRISPR-Cas effectors on-target activity in HEK293T at endogenous loci.

Studies included in this comparison were tested in HEK293T or derivatives with editors delivered by lentivirus or plasmid. Only included studies that targeted endogenous loci (not lentiviral integrated transgenes) and where the indel quantification was done with NGS.

#	Publication	Editors	Included	If not, why?
1	[24]	SpyCas9, SluCas9, sRGN3.1	N	RNP nucleoporation, not lentiviral or plasmid
2	[216]	SpyCas9	Y	

3	[103]	BhCas12b, BhCas12b(v4)	Y	
4	[43]	SpyCas9	Y	
5	[39]	SpyCas9, ScCas9	Y	
6	[72]	SpyCas9, CjeCas9	Y	
7	[217]	SpyCas9	Y	
8	[40]	SpyCas9, ScCas9	Y	
9	[25]	SpyCas9, Un1Cas12f	Y	
10	[157]	SpyCas9	Y	
11	[121]	SpyCas9	Y	
12	[175]	SpyCas9	Y	
13	[169]	SpyCas9	Y	
14	[136]	SpyCas9	Y	
15	[3]	SpyCas9	Y	
16	[47]	AsCas12a, LbCas12a, AsCas12a Ultra	Y	
17	[218]	AsCas12a, LbCas12a	Y	
18	[219]	AsCas12a	Y	
19	[100]	MbCas12a, FnCas12a, AsCas12a, LbCas12a	Y	
20	[220]	FnCas12a, AsCas12a	Y	
21	[221]	SpyCas9, SauCas9, St3Cas9, AsCas12a	Y	
22	[222]	AsCas12a	Y	
23	[223]	16 Cas12a Orthologs	N	Data inaccessible
24	[87]	AsCas12a, LbCas12a, FnCas12a	Y	
25	[224]	SpyCas9, AsCas12a	N	Fusion guides

26	[225]	AsCas12a	N	Cho
27	[96]	AsCas12a, LbCas12a	N	U2OS
28	[226]	AsCas12a, LbCas12a	N	Synthetic locus, not endogenous loci
29	[227]	AsCas12a, LbCas12a	N	Synthetic guides
30	[228]	LbCas12a, FnCas12a	Y	
31	[22]	SauCas9, SluCas9, ShaCas9, SlutrCas9	Y	
32	[48]	AsCas12f	Y	
33	[7]	SauCas9, SpyCas9	Y	
34	[170]	SauCas9	Y	
35	[73]	SauCas9, CjeCas9	Y	
36	[69]	NmeCas9	Y	
37	[229]	NmeCas9	Y	
38	[70]	NmeCas9	Y	
39	[141]	LbCas12a, MbCas12a, Lb2Cas12a	Y	
40	[230]	SauCas9, SauriCas9	In progress (SauCas9 only)	
41	[231]	SpyCas9	N	HCT116
42	[232]	Fdcas9	N	Fusion Construct w/ FokI endonuclease
43	[233]	SpyCas9	Y	
44	[234]	SpyCas9	N	Not applicable (mismatched guides)

45	[235]	SpyCas9	N	
46	[236]	SpyCas9	N	Loss of Function
47	[237]	SpyCas9	N	Recorded Relative Mutation Rate
48	[238]	SpyCas9	N	KBM7 and HL60
49	[143]	AsCas12a	In Progress	
50	[145]	AsCas12a, EnAsCas12a	Y	
51	[66]	SpyCas9, Stl1Cas9, SauCas9	N	U2OS
52	[142]	LbCas12a, AsCas12a, MbCas12a, FnCas12a	In progress	
53	[99]	FnCas12a, eaFnCas12a		
54	[191]	SpyMac, iSpyMac	Y	
55	[23]	CasMINI3.1	In Progress	
56	[239]	SpyCas9	N	T7EI
57	[240]	SpyCas9	Y	
58	[221]	SpyCas9, Stl1, Nme, Sau		
59	[101]	SpyCas9, MAD7	N	T7EI

References

1. Jinek, M. *et al.* A programmable dual-RNA-guided DNA endonuclease in adaptive bacterial immunity. *Science* **337**, 816–821 (2012).
2. Jinek, M. *et al.* RNA-programmed genome editing in human cells. *Elife* **2**, e00471 (2013).
3. Mali, P. *et al.* RNA-guided human genome engineering via Cas9. *Science* **339**, 823–826 (2013).
4. Hsu, P. D. *et al.* DNA targeting specificity of RNA-guided Cas9 nucleases. *Nat. Biotechnol.* **31**, 827–832 (2013).
5. Schmid-Burgk, J. L. *et al.* Highly Parallel Profiling of Cas9 Variant Specificity. *Mol. Cell* **78**, 794–800.e8 (2020).

6. Walton, R. T., Christie, K. A., Whittaker, M. N. & Kleinstiver, B. P. Unconstrained genome targeting with near-PAMless engineered CRISPR-Cas9 variants. *Science* **368**, 290–296 (2020).
7. Ran, F. A. *et al.* In vivo genome editing using Staphylococcus aureus Cas9. *Nature* **520**, 186–191 (2015).
8. Pausch, P. *et al.* CRISPR-CasΦ from huge phages is a hypercompact genome editor. *Science* **369**, 333–337 (2020).
9. Anzalone, A. V., Koblan, L. W. & Liu, D. R. Genome editing with CRISPR-Cas nucleases, base editors, transposases and prime editors. *Nat. Biotechnol.* **38**, 824–844 (2020).
10. Adler, B. A. *et al.* CasPEDIA Database: a functional classification system for class 2 CRISPR-Cas enzymes. *Nucleic Acids Res.* **52**, D590–D596 (2024).
11. Wong, C. UK first to approve CRISPR treatment for diseases: what you need to know. *Nature* **623**, 676–677 (2023).
12. Raguram, A., Banskota, S. & Liu, D. R. Therapeutic in vivo delivery of gene editing agents. *Cell* **185**, 2806–2827 (2022).
13. Cameron, P. *et al.* Mapping the genomic landscape of CRISPR-Cas9 cleavage. *Nat. Methods* **14**, 600–606 (2017).
14. Jang, H.-K. *et al.* High-purity production and precise editing of DNA base editing ribonucleoproteins. *Sci Adv* **7**, (2021).
15. Hendel, A. *et al.* Chemically modified guide RNAs enhance CRISPR-Cas genome editing in human primary cells. *Nat. Biotechnol.* **33**, 985–989 (2015).
16. Vakulskas, C. A. *et al.* A high-fidelity Cas9 mutant delivered as a ribonucleoprotein complex enables efficient gene editing in human hematopoietic stem and progenitor cells. *Nat. Med.* **24**, 1216–1224 (2018).
17. Schmidt-Dannert, C. & Arnold, F. H. Directed evolution of industrial enzymes. *Trends Biotechnol.* **17**, 135–136 (1999).
18. Tsuchida, C. A. *et al.* Mitigation of chromosome loss in clinical CRISPR-Cas9-engineered T cells. *Cell* **186**, 4567–4582.e20 (2023).
19. Wienert, B., Shin, J., Zelin, E., Pestal, K. & Corn, J. E. In vitro-transcribed guide RNAs trigger an innate immune response via the RIG-I pathway. *PLoS Biol.* **16**, e2005840 (2018).
20. Kim, S. *et al.* CRISPR RNAs trigger innate immune responses in human cells. *Genome Res.* **28**, 367–373 (2018).
21. Charlesworth, C. T. *et al.* Identification of preexisting adaptive immunity to Cas9 proteins in humans. *Nat. Med.* **25**, 249–254 (2019).
22. Hu, Z. *et al.* Discovery and engineering of small SlugCas9 with broad targeting range and high specificity and activity. *Nucleic Acids Res.* **49**, 4008–4019 (2021).
23. Xu, X. *et al.* Engineered miniature CRISPR-Cas system for mammalian genome regulation and editing. *Mol. Cell* **81**, 4333–4345.e4 (2021).
24. Schmidt, M. J. *et al.* Improved CRISPR genome editing using small highly active and specific engineered RNA-guided nucleases. *Nat. Commun.* **12**, 4219 (2021).
25. Kim, D. Y. *et al.* Efficient CRISPR editing with a hypercompact Cas12f1 and engineered guide RNAs delivered by adeno-associated virus. *Nat. Biotechnol.* **40**, 94–102 (2022).
26. Liu, J.-J. *et al.* CasX enzymes comprise a distinct family of RNA-guided genome editors. *Nature* **566**, 218–223 (2019).
27. Shams, A. *et al.* Comprehensive deletion landscape of CRISPR-Cas9 identifies minimal RNA-guided DNA-binding modules. *Nat. Commun.* **12**, 5664 (2021).
28. Ramakrishna, S. *et al.* Gene disruption by cell-penetrating peptide-mediated delivery of Cas9 protein and guide RNA. *Genome Res.* **24**, 1020–1027 (2014).

29. Staahl, B. T. *et al.* Efficient genome editing in the mouse brain by local delivery of engineered Cas9 ribonucleoprotein complexes. *Nat. Biotechnol.* **35**, 431–434 (2017).
30. Kim, S., Kim, D., Cho, S. W., Kim, J. & Kim, J.-S. Highly efficient RNA-guided genome editing in human cells via delivery of purified Cas9 ribonucleoproteins. *Genome Res.* **24**, 1012–1019 (2014).
31. Rouet, R. *et al.* Receptor-Mediated Delivery of CRISPR-Cas9 Endonuclease for Cell-Type-Specific Gene Editing. *J. Am. Chem. Soc.* **140**, 6596–6603 (2018).
32. Harrington, L. B. *et al.* A thermostable Cas9 with increased lifetime in human plasma. *Nat. Commun.* **8**, 1424 (2017).
33. Chen, K. *et al.* Lung and liver editing by lipid nanoparticle delivery of a stable CRISPR-Cas9 RNP. *bioRxivorg* (2023) doi:10.1101/2023.11.15.566339.
34. Wang, M. *et al.* Efficient delivery of genome-editing proteins using bioreducible lipid nanoparticles. *Proc. Natl. Acad. Sci. U. S. A.* **113**, 2868–2873 (2016).
35. Dong, C., Gou, Y. & Lian, J. SgRNA engineering for improved genome editing and expanded functional assays. *Curr. Opin. Biotechnol.* **75**, 102697 (2022).
36. Eggers, A. R. *et al.* Rapid DNA unwinding accelerates genome editing by engineered CRISPR-Cas9. *Cell* **187**, 3249–3261.e14 (2024).
37. Nguyen, D. N. *et al.* Polymer-stabilized Cas9 nanoparticles and modified repair templates increase genome editing efficiency. *Nat. Biotechnol.* **38**, 44–49 (2020).
38. Lin-Shiao, E. *et al.* CRISPR-Cas9-mediated nuclear transport and genomic integration of nanostructured genes in human primary cells. *Nucleic Acids Res.* **50**, 1256–1268 (2022).
39. Chatterjee, P., Jakimo, N. & Jacobson, J. M. Minimal PAM specificity of a highly similar SpCas9 ortholog. *Sci. Adv.* **4**, eaau0766 (2018).
40. Chatterjee, P. *et al.* An engineered ScCas9 with broad PAM range and high specificity and activity. *Nat. Biotechnol.* **38**, 1154–1158 (2020).
41. Acharya, S. *et al.* Francisella novicida Cas9 interrogates genomic DNA with very high specificity and can be used for mammalian genome editing. *Proc. Natl. Acad. Sci. U. S. A.* **116**, 20959–20968 (2019).
42. Christie, K. A. & Kleinstiver, B. P. Making the cut with PAMless CRISPR-Cas enzymes. *Trends Genet.* **37**, 1053–1055 (2021).
43. Kim, N. *et al.* Prediction of the sequence-specific cleavage activity of Cas9 variants. *Nat. Biotechnol.* **38**, 1328–1336 (2020).
44. Pedrazzoli, E. *et al.* An optimized SpCas9 high-fidelity variant for direct protein delivery. *Mol. Ther.* **31**, 2257–2265 (2023).
45. Chen, J. S. *et al.* Enhanced proofreading governs CRISPR-Cas9 targeting accuracy. *Nature* **550**, 407–410 (2017).
46. Kim, Y.-H. *et al.* Sniper2L is a high-fidelity Cas9 variant with high activity. *Nat. Chem. Biol.* **19**, 972–980 (2023).
47. Zhang, L. *et al.* AsCas12a ultra nuclease facilitates the rapid generation of therapeutic cell medicines. *Nat. Commun.* **12**, 3908 (2021).
48. Wu, Z. *et al.* Programmed genome editing by a miniature CRISPR-Cas12f nuclease. *Nat. Chem. Biol.* **17**, 1132–1138 (2021).
49. Liu, Z., Liu, H., Huang, C., Zhou, Q. & Luo, Y. Hybrid Cas12a variants with relaxed PAM requirements expand genome editing compatibility. *ACS Synth. Biol.* **13**, 1809–1819 (2024).
50. Guo, L. Y. *et al.* Multiplexed genome regulation in vivo with hyper-efficient Cas12a. *Nat. Cell Biol.* **24**, 590–600 (2022).
51. Bao, Z. *et al.* Homology-integrated CRISPR-Cas (HI-CRISPR) system for one-step multigene disruption in Saccharomyces cerevisiae. *ACS Synth. Biol.* **4**, 585–594 (2015).

52. Tabassum, T., Pietrogrande, G., Healy, M. & Wolvetang, E. J. CRISPR-Cas9 direct fusions for improved genome editing via enhanced homologous recombination. *Int. J. Mol. Sci.* **24**, 14701 (2023).
53. Chauhan, V. P., Sharp, P. A. & Langer, R. Altered DNA repair pathway engagement by engineered CRISPR-Cas9 nucleases. *Proc. Natl. Acad. Sci. U. S. A.* **120**, e2300605120 (2023).
54. Zhuo, C. *et al.* Spatiotemporal control of CRISPR/Cas9 gene editing. *Signal Transduct Target Ther* **6**, 238 (2021).
55. Chen, J. *et al.* Engineered Cas9 variants bypass Keap1-mediated degradation in human cells and enhance epigenome editing efficiency. *Nucleic Acids Res.* gkae761 (2024).
56. Ferdosi, S. R. *et al.* Multifunctional CRISPR-Cas9 with engineered immunosilenced human T cell epitopes. *Nat. Commun.* **10**, 1842 (2019).
57. Hille, F. *et al.* The biology of CRISPR-Cas: Backward and forward. *Cell* **172**, 1239–1259 (2018).
58. McGinn, J. & Marraffini, L. A. Molecular mechanisms of CRISPR-Cas spacer acquisition. *Nat. Rev. Microbiol.* **17**, 7–12 (2019).
59. Koonin, E. V., Gootenberg, J. S. & Abudayyeh, O. O. Discovery of diverse CRISPR-Cas systems and expansion of the genome engineering toolbox. *Biochemistry* **62**, 3465–3487 (2023).
60. Koonin, E. V. & Makarova, K. S. Origins and evolution of CRISPR-Cas systems. *Philos. Trans. R. Soc. Lond. B Biol. Sci.* **374**, 20180087 (2019).
61. Xu, C. *et al.* Programmable RNA editing with compact CRISPR-Cas13 systems from uncultivated microbes. *Nat. Methods* **18**, 499–506 (2021).
62. Deltcheva, E. *et al.* CRISPR RNA maturation by trans-encoded small RNA and host factor RNase III. *Nature* **471**, 602–607 (2011).
63. Jiang, F. & Doudna, J. A. CRISPR-Cas9 structures and mechanisms. *Annu. Rev. Biophys.* **46**, 505–529 (2017).
64. Liu, M. *et al.* Global detection of DNA repair outcomes induced by CRISPR-Cas9. *Nucleic Acids Res.* **49**, 8732–8742 (2021).
65. Yin, J. & Hu, J. The origin of unwanted editing byproducts in gene editing. *Acta Biochim. Biophys. Sin. (Shanghai)* **54**, 767–781 (2022).
66. Kleinstiver, B. P. *et al.* Engineered CRISPR-Cas9 nucleases with altered PAM specificities. *Nature* **523**, 481–485 (2015).
67. Kleinstiver, B. P. *et al.* Broadening the targeting range of Staphylococcus aureus CRISPR-Cas9 by modifying PAM recognition. *Nat. Biotechnol.* **33**, 1293–1298 (2015).
68. Lee, C. M., Cradick, T. J. & Bao, G. The Neisseria meningitidis CRISPR-Cas9 System Enables Specific Genome Editing in Mammalian Cells. *Mol. Ther.* **24**, 645–654 (2016).
69. Edraki, A. *et al.* A Compact, High-Accuracy Cas9 with a Dinucleotide PAM for In Vivo Genome Editing. *Mol. Cell* **73**, 714–726.e4 (2019).
70. Amrani, N. *et al.* NmeCas9 is an intrinsically high-fidelity genome-editing platform. *Genome Biol.* **19**, 214 (2018).
71. Saha, C. *et al.* Guide-free Cas9 from pathogenic Campylobacter jejuni bacteria causes severe damage to DNA. *Sci. Adv.* **6**, eaaz4849 (2020).
72. Nakagawa, R. *et al.* Engineered Campylobacter jejuni Cas9 variant with enhanced activity and broader targeting range. *Commun Biol* **5**, 211 (2022).
73. Kim, E. *et al.* In vivo genome editing with a small Cas9 orthologue derived from Campylobacter jejuni. *Nat. Commun.* **8**, 14500 (2017).
74. Gong, S., Yu, H. H., Johnson, K. A. & Taylor, D. W. DNA Unwinding Is the Primary Determinant of CRISPR-Cas9 Activity. *Cell Rep.* **22**, 359–371 (2018).

75. Clement, K. *et al.* CRISPResso2 provides accurate and rapid genome editing sequence analysis. *Nat. Biotechnol.* **37**, 224–226 (2019).
76. Labun, K. *et al.* CHOPCHOP v3: expanding the CRISPR web toolbox beyond genome editing. *Nucleic Acids Res.* **47**, W171–W174 (2019).
77. Chen, J. S. *et al.* CRISPR-Cas12a target binding unleashes indiscriminate single-stranded DNase activity. *Science* **360**, 436–439 (2018).
78. Gootenberg, J. S. *et al.* Multiplexed and portable nucleic acid detection platform with Cas13, Cas12a, and Csm6. *Science* **360**, 439–444 (2018).
79. Yang, L.-Z. *et al.* Dynamic imaging of RNA in living cells by CRISPR-Cas13 systems. *Mol. Cell* **76**, 981–997.e7 (2019).
80. Tang, H. *et al.* Live-cell RNA imaging using the CRISPR-dCas13 system with modified sgRNAs appended with fluorescent RNA aptamers. *Chem. Sci.* **13**, 14032–14040 (2022).
81. Müller, M. *et al.* Streptococcus thermophilus CRISPR-Cas9 Systems Enable Specific Editing of the Human Genome. *Mol. Ther.* **24**, 636–644 (2016).
82. Agudelo, D. *et al.* Versatile and robust genome editing with Streptococcus thermophilus CRISPR1-Cas9. *Genome Res.* **30**, 107–117 (2020).
83. Hirano, S. *et al.* Structural basis for the promiscuous PAM recognition by Corynebacterium diphtheriae Cas9. *Nat. Commun.* **10**, 1968 (2019).
84. Cui, Z. *et al.* FrCas9 is a CRISPR/Cas9 system with high editing efficiency and fidelity. *Nat. Commun.* **13**, 1425 (2022).
85. Fedorova, I. *et al.* PpCas9 from Pasteurella pneumotropica - a compact Type II-C Cas9 ortholog active in human cells. *Nucleic Acids Res.* **48**, 12297–12309 (2020).
86. Gopalakrishna, K. P. *et al.* Group B Streptococcus Cas9 variants provide insight into programmable gene repression and CRISPR-Cas transcriptional effects. *Commun. Biol.* **6**, 620 (2023).
87. Zetsche, B. *et al.* Cpf1 is a single RNA-guided endonuclease of a class 2 CRISPR-Cas system. *Cell* **163**, 759–771 (2015).
88. Zetsche, B. *et al.* Multiplex gene editing by CRISPR-Cpf1 using a single crRNA array. *Nat. Biotechnol.* **35**, 31–34 (2017).
89. Li, S.-Y. *et al.* CRISPR-Cas12a-assisted nucleic acid detection. *Cell Discov* **4**, 20 (2018).
90. Tao, J., Bauer, D. E. & Chiarle, R. Assessing and advancing the safety of CRISPR-Cas tools: from DNA to RNA editing. *Nat. Commun.* **14**, 212 (2023).
91. Yamano, T. *et al.* Crystal structure of Cpf1 in complex with guide RNA and target DNA. *Cell* **165**, 949–962 (2016).
92. Gier, R. A. *et al.* High-performance CRISPR-Cas12a genome editing for combinatorial genetic screening. *Nat. Commun.* **11**, 3455 (2020).
93. Singh, D. *et al.* Real-time observation of DNA target interrogation and product release by the RNA-guided endonuclease CRISPR Cpf1 (Cas12a). *Proc. Natl. Acad. Sci. U. S. A.* **115**, 5444–5449 (2018).
94. Hewes, A. M., Sansbury, B. M. & Kmiec, E. B. The diversity of genetic outcomes from CRISPR/Cas gene editing is regulated by the length of the symmetrical donor DNA template. *Genes (Basel)* **11**, 1160 (2020).
95. Moreno-Mateos, M. A. *et al.* CRISPR-Cpf1 mediates efficient homology-directed repair and temperature-controlled genome editing. *Nat. Commun.* **8**, 2024 (2017).
96. Kleinstiver, B. P. *et al.* Genome-wide specificities of CRISPR-Cas Cpf1 nucleases in human cells. *Nat. Biotechnol.* **34**, 869–874 (2016).
97. Kim, D. *et al.* Genome-wide analysis reveals specificities of Cpf1 endonucleases in human cells. *Nat. Biotechnol.* **34**, 863–868 (2016).

98. Harrington, L. B. *et al.* Programmed DNA destruction by miniature CRISPR-Cas14 enzymes. *Science* **362**, 839–842 (2018).
99. Liu, X. *et al.* Engineered FnCas12a with enhanced activity through directional evolution in human cells. *J. Biol. Chem.* **296**, 100394 (2021).
100. Tóth, E. *et al.* Mb- and FnCpf1 nucleases are active in mammalian cells: activities and PAM preferences of four wild-type Cpf1 nucleases and of their altered PAM specificity variants. *Nucleic Acids Res.* **46**, 10272–10285 (2018).
101. Liu, Z. *et al.* ErCas12a CRISPR-MAD7 for Model Generation in Human Cells, Mice, and Rats. *CRISPR J* **3**, 97–108 (2020).
102. Tsuchida, C. A. *et al.* Chimeric CRISPR-CasX enzymes and guide RNAs for improved genome editing activity. *Mol. Cell* **82**, 1199–1209.e6 (2022).
103. Strecker, J. *et al.* Engineering of CRISPR-Cas12b for human genome editing. *Nat. Commun.* **10**, 212 (2019).
104. Chen, W. *et al.* Cas12n nucleases, early evolutionary intermediates of type V CRISPR, comprise a distinct family of miniature genome editors. *Mol. Cell* **83**, 2768–2780.e6 (2023).
105. Karvelis, T. *et al.* Transposon-associated TnpB is a programmable RNA-guided DNA endonuclease. *Nature* **599**, 692–696 (2021).
106. Saito, M. *et al.* Fanzor is a eukaryotic programmable RNA-guided endonuclease. *Nature* **620**, 660–668 (2023).
107. Wang, Y. *et al.* A highly specific CRISPR-Cas12j nuclease enables allele-specific genome editing. *Sci. Adv.* **9**, eabo6405 (2023).
108. Ciccia, A. & Elledge, S. J. The DNA damage response: making it safe to play with knives. *Mol. Cell* **40**, 179–204 (2010).
109. Carroll, D. Genome engineering with zinc-finger nucleases. *Genetics* **188**, 773–782 (2011).
110. Urnov, F. D., Rebar, E. J., Holmes, M. C., Zhang, H. S. & Gregory, P. D. Genome editing with engineered zinc finger nucleases. *Nat. Rev. Genet.* **11**, 636–646 (2010).
111. Boch, J. *et al.* Breaking the code of DNA binding specificity of TAL-type III effectors. *Science* **326**, 1509–1512 (2009).
112. Christian, M. *et al.* Targeting DNA double-strand breaks with TAL effector nucleases. *Genetics* **186**, 757–761 (2010).
113. Chapman, J. R., Taylor, M. R. G. & Boulton, S. J. Playing the end game: DNA double-strand break repair pathway choice. *Mol. Cell* **47**, 497–510 (2012).
114. Rees, H. A. & Liu, D. R. Base editing: precision chemistry on the genome and transcriptome of living cells. *Nat. Rev. Genet.* **19**, 770–788 (2018).
115. Heyer, W.-D., Ehmsen, K. T. & Liu, J. Regulation of homologous recombination in eukaryotes. *Annu. Rev. Genet.* **44**, 113–139 (2010).
116. Moynahan, M. E. & Jasin, M. Mitotic homologous recombination maintains genomic stability and suppresses tumorigenesis. *Nat. Rev. Mol. Cell Biol.* **11**, 196–207 (2010).
117. Brinkman, E. K. *et al.* Kinetics and fidelity of the repair of Cas9-induced double-strand DNA breaks. *Mol. Cell* **70**, 801–813.e6 (2018).
118. Shen, M. W. *et al.* Predictable and precise template-free CRISPR editing of pathogenic variants. *Nature* **563**, 646–651 (2018).
119. van Overbeek, M. *et al.* DNA repair profiling reveals nonrandom outcomes at Cas9-mediated breaks. *Mol. Cell* **63**, 633–646 (2016).
120. Iyer, S. *et al.* Precise therapeutic gene correction by a simple nuclease-induced double-stranded break. *Nature* **568**, 561–565 (2019).
121. Cong, L. *et al.* Multiplex genome engineering using CRISPR/Cas systems. *Science* **339**, 819–823 (2013).

122. Yeh, C. D., Richardson, C. D. & Corn, J. E. Advances in genome editing through control of DNA repair pathways. *Nat. Cell Biol.* **21**, 1468–1478 (2019).
123. Leal, A. F., Herreno-Pachón, A. M., Benincore-Flórez, E., Karunathilaka, A. & Tomatsu, S. Current strategies for increasing knock-in efficiency in CRISPR/Cas9-based approaches. *Int. J. Mol. Sci.* **25**, 2456 (2024).
124. Jayavaradhan, R. *et al.* CRISPR-Cas9 fusion to dominant-negative 53BP1 enhances HDR and inhibits NHEJ specifically at Cas9 target sites. *Nat. Commun.* **10**, 2866 (2019).
125. Charpentier, M. *et al.* CtIP fusion to Cas9 enhances transgene integration by homology-dependent repair. *Nat. Commun.* **9**, 1133 (2018).
126. Reint, G. *et al.* Rapid genome editing by CRISPR-Cas9-POLD3 fusion. *Elife* **10**, e75415 (2021).
127. Tsai, S. Q. *et al.* CIRCLE-seq: a highly sensitive in vitro screen for genome-wide CRISPR-Cas9 nuclease off-targets. *Nat. Methods* **14**, 607–614 (2017).
128. Kim, D. *et al.* Digenome-seq: genome-wide profiling of CRISPR-Cas9 off-target effects in human cells. *Nat. Methods* **12**, 237–43, 1 p following 243 (2015).
129. Tsai, S. Q. *et al.* GUIDE-seq enables genome-wide profiling of off-target cleavage by CRISPR-Cas nucleases. *Nat. Biotechnol.* **33**, 187–197 (2015).
130. Lei, Z., Meng, H., Rao, X., Zhao, H. & Yi, C. Detect-seq, a chemical labeling and biotin pull-down approach for the unbiased and genome-wide off-target evaluation of programmable cytosine base editors. *Nat. Protoc.* **18**, 2221–2255 (2023).
131. Jumper, J. *et al.* Highly accurate protein structure prediction with AlphaFold. *Nature* **596**, 583–589 (2021).
132. Baek, M. *et al.* Accurate prediction of protein structures and interactions using a three-track neural network. *Science* **373**, 871–876 (2021).
133. van Kempen, M. *et al.* Fast and accurate protein structure search with Foldseek. *Nat. Biotechnol.* **42**, 243–246 (2024).
134. Schneider, B. *et al.* When will RNA get its AlphaFold moment? *Nucleic Acids Res.* **51**, 9522–9532 (2023).
135. Baek, M. *et al.* Accurate prediction of protein-nucleic acid complexes using RoseTTAFoldNA. *Nat. Methods* **21**, 117–121 (2024).
136. Slaymaker, I. M. *et al.* Rationally engineered Cas9 nucleases with improved specificity. *Science* **351**, 84–88 (2016).
137. Hibshman, G. N. *et al.* Unraveling the mechanisms of PAMless DNA interrogation by SpRY-Cas9. *Nat. Commun.* **15**, 3663 (2024).
138. Shi, H. *et al.* Rapid two-step target capture ensures efficient CRISPR-Cas9-guided genome editing. *bioRxiv* 2024.10.01.616117 (2024) doi:10.1101/2024.10.01.616117.
139. Choi, G. C. G. *et al.* Combinatorial mutagenesis en masse optimizes the genome editing activities of SpCas9. *Nat. Methods* **16**, 722–730 (2019).
140. Vos, P. D. *et al.* Computationally designed hyperactive Cas9 enzymes. *Nat. Commun.* **13**, 3023 (2022).
141. Tran, M. H. *et al.* A more efficient CRISPR-Cas12a variant derived from Lachnospiraceae bacterium MA2020. *Mol. Ther. Nucleic Acids* **24**, 40–53 (2021).
142. Tóth, E. *et al.* Improved LbCas12a variants with altered PAM specificities further broaden the genome targeting range of Cas12a nucleases. *Nucleic Acids Res.* **48**, 3722–3733 (2020).
143. Huang, H. *et al.* Engineered Cas12a-Plus nuclease enables gene editing with enhanced activity and specificity. *BMC Biol.* **20**, 91 (2022).
144. Zhang, L. *et al.* Boosting genome editing efficiency in human cells and plants with novel LbCas12a variants. *Genome Biol.* **24**, 102 (2023).

145. Kleinstiver, B. P. *et al.* Engineered CRISPR-Cas12a variants with increased activities and improved targeting ranges for gene, epigenetic and base editing. *Nat. Biotechnol.* **37**, 276–282 (2019).
146. Chen, P. *et al.* Engineering of Cas12a nuclease variants with enhanced genome-editing specificity. *PLoS Biol.* **22**, e3002514 (2024).
147. Wang, H. *et al.* Engineering of a compact, high-fidelity EbCas12a variant that can be packaged with its crRNA into an all-in-one AAV vector delivery system. *PLoS Biol.* **22**, e3002619 (2024).
148. Hino, T. *et al.* An AsCas12f-based compact genome-editing tool derived by deep mutational scanning and structural analysis. *Cell* **186**, 4920–4935.e23 (2023).
149. Su, M. *et al.* Molecular basis and engineering of miniature Cas12f with C-rich PAM specificity. *Nat. Chem. Biol.* **20**, 180–189 (2024).
150. Wang, Y. *et al.* Guide RNA engineering enables efficient CRISPR editing with a miniature Syntrophomonas palmitatica Cas12f1 nuclease. *Cell Rep.* **40**, 111418 (2022).
151. McGaw, C. *et al.* Engineered Cas12i2 is a versatile high-efficiency platform for therapeutic genome editing. *Nat. Commun.* **13**, 2833 (2022).
152. Duan, Z. *et al.* An engineered Cas12i nuclease that is an efficient genome editing tool in animals and plants. *Innovation (Camb.)* **5**, 100564 (2024).
153. Zhang, H. *et al.* An engineered xCas12i with high activity, high specificity, and broad PAM range. *Protein Cell* **14**, 538–543 (2023).
154. Liu, R. M. *et al.* Synthetic chimeric nucleases function for efficient genome editing. *Nat. Commun.* **10**, 5524 (2019).
155. Listgarten, J. *et al.* Prediction of off-target activities for the end-to-end design of CRISPR guide RNAs. *Nat Biomed Eng* **2**, 38–47 (2018).
156. Pacesa, M. *et al.* Structural basis for Cas9 off-target activity. *Cell* **185**, 4067–4081.e21 (2022).
157. Kim, H. K. *et al.* High-throughput analysis of the activities of xCas9, SpCas9-NG and SpCas9 at matched and mismatched target sequences in human cells. *Nat Biomed Eng* **4**, 111–124 (2020).
158. Zetsche, B., Volz, S. E. & Zhang, F. A split-Cas9 architecture for inducible genome editing and transcription modulation. *Nat. Biotechnol.* **33**, 139–142 (2015).
159. Davis, K. M., Pattanayak, V., Thompson, D. B., Zuris, J. A. & Liu, D. R. Small molecule-triggered Cas9 protein with improved genome-editing specificity. *Nat. Chem. Biol.* **11**, 316–318 (2015).
160. Liu, K. I. *et al.* A chemical-inducible CRISPR-Cas9 system for rapid control of genome editing. *Nat. Chem. Biol.* **12**, 980–987 (2016).
161. Nabet, B. *et al.* The dTAG system for immediate and target-specific protein degradation. *Nat. Chem. Biol.* **14**, 431–441 (2018).
162. Fu, Y., Sander, J. D., Reyon, D., Cascio, V. M. & Joung, J. K. Improving CRISPR-Cas nuclease specificity using truncated guide RNAs. *Nat. Biotechnol.* **32**, 279–284 (2014).
163. Kocak, D. D. *et al.* Increasing the specificity of CRISPR systems with engineered RNA secondary structures. *Nat. Biotechnol.* **37**, 657–666 (2019).
164. Cheng, Q. *et al.* Selective organ targeting (SORT) nanoparticles for tissue-specific mRNA delivery and CRISPR-Cas gene editing. *Nat. Nanotechnol.* **15**, 313–320 (2020).
165. Jacobi, A. M. *et al.* Simplified CRISPR tools for efficient genome editing and streamlined protocols for their delivery into mammalian cells and mouse zygotes. *Methods* **121-122**, 16–28 (2017).
166. Foss, D. V. *et al.* Peptide-mediated delivery of CRISPR enzymes for the efficient editing of primary human lymphocytes. *Nat Biomed Eng* **7**, 647–660 (2023).
167. Rozners, E. Chemical modifications of CRISPR RNAs to improve gene-editing activity and specificity. *J. Am. Chem. Soc.* **144**, 12584–12594 (2022).

168. Chen, Q., Zhang, Y. & Yin, H. Recent advances in chemical modifications of guide RNA, mRNA and donor template for CRISPR-mediated genome editing. *Adv. Drug Deliv. Rev.* **168**, 246–258 (2021).
169. Casini, A. *et al.* A highly specific SpCas9 variant is identified by in vivo screening in yeast. *Nat. Biotechnol.* **36**, 265–271 (2018).
170. Tan, Y. *et al.* Rationally engineered Staphylococcus aureus Cas9 nucleases with high genome-wide specificity. *Proc. Natl. Acad. Sci. U. S. A.* **116**, 20969–20976 (2019).
171. Xie, H. *et al.* High-fidelity SaCas9 identified by directional screening in human cells. *PLoS Biol.* **18**, e3000747 (2020).
172. Yuen, C. T. L. *et al.* High-fidelity KKH variant of Staphylococcus aureus Cas9 nucleases with improved base mismatch discrimination. *Nucleic Acids Res.* **50**, 1650–1660 (2022).
173. Kleinstiver, B. P. *et al.* High-fidelity CRISPR-Cas9 nucleases with no detectable genome-wide off-target effects. *Nature* **529**, 490–495 (2016).
174. Kulcsár, P. I. *et al.* Crossing enhanced and high fidelity SpCas9 nucleases to optimize specificity and cleavage. *Genome Biol.* **18**, 190 (2017).
175. Hu, J. H. *et al.* Evolved Cas9 variants with broad PAM compatibility and high DNA specificity. *Nature* **556**, 57–63 (2018).
176. Lee, J. K. *et al.* Directed evolution of CRISPR-Cas9 to increase its specificity. *Nat. Commun.* **9**, 3048 (2018).
177. Spasskaya, D. S. *et al.* Improving the on-target activity of high-fidelity Cas9 editors by combining rational design and random mutagenesis. *Appl. Microbiol. Biotechnol.* **107**, 2385–2401 (2023).
178. Bravo, J. P. K. *et al.* Structural basis for mismatch surveillance by CRISPR-Cas9. *Nature* **603**, 343–347 (2022).
179. Kulcsár, P. I., Tálas, A., Ligeti, Z., Krausz, S. L. & Welker, E. SuperFi-Cas9 exhibits remarkable fidelity but severely reduced activity yet works effectively with ABE8e. *Nat. Commun.* **13**, 6858 (2022).
180. Cerchione, D. *et al.* SMOOT libraries and phage-induced directed evolution of Cas9 to engineer reduced off-target activity. *PLoS One* **15**, e0231716 (2020).
181. Zuo, Z. *et al.* Rational engineering of CRISPR-Cas9 nuclease to attenuate position-dependent off-target effects. *CRISPR J.* **5**, 329–340 (2022).
182. Wang, G. H. *et al.* The development of SpCas9 variants with high specificity and efficiency based on the HH theory. *Mol. Biol.* **58**, 133–146 (2024).
183. Yin, J. *et al.* Optimizing genome editing strategy by primer-extension-mediated sequencing. *Cell Discov.* **5**, 18 (2019).
184. Anders, C., Bargsten, K. & Jinek, M. Structural Plasticity of PAM Recognition by Engineered Variants of the RNA-Guided Endonuclease Cas9. *Mol. Cell* **61**, 895–902 (2016).
185. Zhang, W. *et al.* In-depth assessment of the PAM compatibility and editing activities of Cas9 variants. *Nucleic Acids Res.* **49**, 8785–8795 (2021).
186. Miller, S. M. *et al.* Continuous evolution of SpCas9 variants compatible with non-G PAMs. *Nat. Biotechnol.* **38**, 471–481 (2020).
187. Nishimasu, H. *et al.* Engineered CRISPR-Cas9 nuclease with expanded targeting space. *Science* **361**, 1259–1262 (2018).
188. Wang, J. *et al.* Engineering a PAM-flexible SpdCas9 variant as a universal gene repressor. *Nat. Commun.* **12**, 6916 (2021).
189. Goldberg, G. W. *et al.* Engineered dual selection for directed evolution of SpCas9 PAM specificity. *Nat. Commun.* **12**, 349 (2021).
190. Spencer, J. M. & Zhang, X. Deep mutational scanning of S. pyogenes Cas9 reveals important functional domains. *Sci. Rep.* **7**, 16836 (2017).

191. Chatterjee, P. *et al.* A Cas9 with PAM recognition for adenine dinucleotides. *Nat. Commun.* **11**, 2474 (2020).
192. Zhao, L. *et al.* PAM-flexible genome editing with an engineered chimeric Cas9. *Nat. Commun.* **14**, 6175 (2023).
193. Luan, B., Xu, G., Feng, M., Cong, L. & Zhou, R. Combined computational-experimental approach to explore the molecular mechanism of SaCas9 with a broadened DNA targeting range. *J. Am. Chem. Soc.* **141**, 6545–6552 (2019).
194. Hirano, H. *et al.* Structure and Engineering of Francisella novicida Cas9. *Cell* **164**, 950–961 (2016).
195. Acharya, S. *et al.* PAM-flexible Engineered FnCas9 variants for robust and ultra-precise genome editing and diagnostics. *Nat. Commun.* **15**, 5471 (2024).
196. Schmidheini, L. *et al.* Continuous directed evolution of a compact CjCas9 variant with broad PAM compatibility. *Nat. Chem. Biol.* **20**, 333–343 (2024).
197. Gao, L. *et al.* Engineered Cpf1 variants with altered PAM specificities. *Nat. Biotechnol.* **35**, 789–792 (2017).
198. Zhou, J. *et al.* Cas12a variants designed for lower genome-wide off-target effect through stringent PAM recognition. *Mol. Ther.* **30**, 244–255 (2022).
199. Crudele, J. M. & Chamberlain, J. S. Cas9 immunity creates challenges for CRISPR gene editing therapies. *Nat. Commun.* **9**, 3497 (2018).
200. Nelson, C. E. *et al.* Long-term evaluation of AAV-CRISPR genome editing for Duchenne muscular dystrophy. *Nat. Med.* **25**, 427–432 (2019).
201. Chew, W. L. *et al.* A multifunctional AAV-CRISPR-Cas9 and its host response. *Nat. Methods* **13**, 868–874 (2016).
202. Stadtmauer, E. A. *et al.* CRISPR-engineered T cells in patients with refractory cancer. *Science* **367**, eaba7365 (2020).
203. Ewaisha, R. & Anderson, K. S. Immunogenicity of CRISPR therapeutics-Critical considerations for clinical translation. *Front. Bioeng. Biotechnol.* **11**, 1138596 (2023).
204. Kell, A. M. & Gale, M., Jr. RIG-I in RNA virus recognition. *Virology* **479-480**, 110–121 (2015).
205. Gillmore, J. D. *et al.* CRISPR-Cas9 In Vivo Gene Editing for Transthyretin Amyloidosis. *N. Engl. J. Med.* **385**, 493–502 (2021).
206. Sinclair, F., Begum, A. A., Dai, C. C., Toth, I. & Moyle, P. M. Recent advances in the delivery and applications of nonviral CRISPR/Cas9 gene editing. *Drug Deliv. Transl. Res.* **13**, 1500–1519 (2023).
207. Porello, I. & Cellesi, F. Intracellular delivery of therapeutic proteins. New advancements and future directions. *Front. Bioeng. Biotechnol.* **11**, 1211798 (2023).
208. Frangoul, H. *et al.* CRISPR-Cas9 gene editing for sickle cell disease and β-thalassemia. *N. Engl. J. Med.* **384**, 252–260 (2021).
209. Hanna, R. *et al.* S264: Edit-301 shows promising preliminary safety and efficacy results in the phase i/ii clinical trial (Ruby) of patients with severe sickle cell disease using highly specific and efficient ascas12a enzyme. *HemaSphere* **7**, e05170e0 (2023).
210. Hacein-Bey-Abina, S. *et al.* Insertional oncogenesis in 4 patients after retrovirus-mediated gene therapy of SCID-X1. *J. Clin. Invest.* **118**, 3132–3142 (2008).
211. Hacein-Bey-Abina, S. *et al.* LMO2-associated clonal T cell proliferation in two patients after gene therapy for SCID-X1. *Science* **302**, 415–419 (2003).
212. Hendriks, D., Clevers, H. & Artegiani, B. CRISPR-Cas tools and their application in genetic engineering of human stem cells and organoids. *Cell Stem Cell* **27**, 705–731 (2020).
213. Haapaniemi, E., Botla, S., Persson, J., Schmierer, B. & Taipale, J. CRISPR-Cas9 genome editing induces a p53-mediated DNA damage response. *Nat. Med.* **24**, 927–930 (2018).

214. Ihry, R. J. *et al.* p53 inhibits CRISPR-Cas9 engineering in human pluripotent stem cells. *Nat. Med.* **24**, 939–946 (2018).
215. Kosicki, M., Tomberg, K. & Bradley, A. Repair of double-strand breaks induced by CRISPR-Cas9 leads to large deletions and complex rearrangements. *Nat. Biotechnol.* **36**, 765–771 (2018).
216. Wang, D. *et al.* Optimized CRISPR guide RNA design for two high-fidelity Cas9 variants by deep learning. *Nat. Commun.* **10**, 4284 (2019).
217. Doench, J. G. *et al.* Optimized sgRNA design to maximize activity and minimize off-target effects of CRISPR-Cas9. *Nat. Biotechnol.* **34**, 184–191 (2016).
218. Kim, H. K. *et al.* In vivo high-throughput profiling of CRISPR-Cpf1 activity. *Nat. Methods* **14**, 153–159 (2017).
219. Kim, H. K. *et al.* Deep learning improves prediction of CRISPR-Cpf1 guide RNA activity. *Nat. Biotechnol.* **36**, 239–241 (2018).
220. Tu, M. *et al.* A 'new lease of life': FnCpf1 possesses DNA cleavage activity for genome editing in human cells. *Nucleic Acids Res.* **45**, 11295–11304 (2017).
221. Chari, R., Yeo, N. C., Chavez, A. & Church, G. M. sgRNA Scorer 2.0: A Species-Independent Model To Predict CRISPR/Cas9 Activity. *ACS Synth. Biol.* **6**, 902–904 (2017).
222. Kim, Y. *et al.* Generation of knockout mice by Cpf1-mediated gene targeting. *Nat. Biotechnol.* **34**, 808–810 (2016).
223. Zetsche, B., Abudayyeh, O. O., Gootenberg, J. S., Scott, D. A. & Zhang, F. A survey of genome editing activity for 16 Cas12a orthologs. *Keio J. Med.* **69**, 59–65 (2020).
224. Kweon, J. *et al.* Fusion guide RNAs for orthogonal gene manipulation with Cas9 and Cpf1. *Nat. Commun.* **8**, 1723 (2017).
225. Schmieder, V. *et al.* Enhanced Genome Editing Tools For Multi-Gene Deletion Knock-Out Approaches Using Paired CRISPR sgRNAs in CHO Cells. *Biotechnol. J.* **13**, e1700211 (2018).
226. Zhong, G., Wang, H., Li, Y., Tran, M. H. & Farzan, M. Cpf1 proteins excise CRISPR RNAs from mRNA transcripts in mammalian cells. *Nat. Chem. Biol.* **13**, 839–841 (2017).
227. Li, B. *et al.* Engineering CRISPR-Cpf1 crRNAs and mRNAs to maximize genome editing efficiency. *Nat Biomed Eng* **1**, (2017).
228. Liu, P. *et al.* Enhanced Cas12a editing in mammalian cells and zebrafish. *Nucleic Acids Res.* **47**, 4169–4180 (2019).
229. Ibraheim, R. *et al.* Self-inactivating, all-in-one AAV vectors for precision Cas9 genome editing via homology-directed repair in vivo. *Nat. Commun.* **12**, 6267 (2021).
230. Hu, Z. *et al.* A compact Cas9 ortholog from Staphylococcus Auricularis (SauriCas9) expands the DNA targeting scope. *PLoS Biol.* **18**, e3000686 (2020).
231. Hand, T. H. *et al.* Catalytically Enhanced Cas9 through Directed Protein Evolution. *CRISPR J* **4**, 223–232 (2021).
232. Aouida, M. *et al.* Efficient fdCas9 Synthetic Endonuclease with Improved Specificity for Precise Genome Engineering. *PLoS One* **10**, e0133373 (2015).
233. Xiang, X. *et al.* Enhancing CRISPR-Cas9 gRNA efficiency prediction by data integration and deep learning. *Nat. Commun.* **12**, 3238 (2021).
234. Kim, D., Kim, D.-E., Lee, G., Cho, S.-I. & Kim, J.-S. Genome-wide target specificity of CRISPR RNA-guided adenine base editors. *Nat. Biotechnol.* **37**, 430–435 (2019).
235. Xu, H. *et al.* Sequence determinants of improved CRISPR sgRNA design. *Genome Res.* **25**, 1147–1157 (2015).
236. Hart, T. *et al.* High-Resolution CRISPR Screens Reveal Fitness Genes and Genotype-Specific Cancer Liabilities. *Cell* **163**, 1515–1526 (2015).

237. Chari, R., Mali, P., Moosburner, M. & Church, G. M. Unraveling CRISPR-Cas9 genome engineering parameters via a library-on-library approach. *Nat. Methods* **12**, 823–826 (2015).
238. Wang, T., Wei, J. J., Sabatini, D. M. & Lander, E. S. Genetic screens in human cells using the CRISPR-Cas9 system. *Science* **343**, 80–84 (2014).
239. Fu, Y. *et al.* High-frequency off-target mutagenesis induced by CRISPR-Cas nucleases in human cells. *Nat. Biotechnol.* **31**, 822–826 (2013).
240. Kim, H. K. *et al.* SpCas9 activity prediction by DeepSpCas9, a deep learning-based model with high generalization performance. *Sci Adv* **5**, eaax9249 (2019).

CHAPTER TWO

Packaged delivery of CRISPR-Cas9 ribonucleoproteins accelerates genome editing

Reproduced in part with permission from all co-authors:

Karp, H. *et al.* **Packaged delivery of CRISPR-Cas9 ribonucleoproteins accelerates genome editing**. In review at Nucleic Acids Research.

2.1 Abstract

Effective genome editing requires a sufficient dose of CRISPR-Cas9 ribonucleoproteins (RNPs) to enter the target cell while minimizing immune responses, off-target editing and cytotoxicity. Clinical use of Cas9 RNPs currently entails electroporation into cells *ex vivo*, but no systematic comparison of this method to packaged RNP delivery has been made. Here we compared two delivery strategies, electroporation and enveloped delivery vehicles (EDVs), to investigate the

Cas9 dosage requirements for genome editing. Using fluorescence correlation spectroscopy (FCS), we determined that >1300 Cas9 RNPs per nucleus are typically required for productive genome editing. EDV-mediated editing was >30-fold more efficient than electroporation, and editing occurs at least two-fold faster for EDV delivery at comparable total Cas9 RNP doses. We hypothesize that differences in efficacy between these methods result in part from the increased duration of RNP nuclear residence resulting from EDV delivery. Our results directly compare RNP delivery strategies, showing that packaged delivery could dramatically reduce the amount of CRISPR-Cas9 RNPs required for experimental or clinical genome editing.

2.1.1 Graphical Abstract

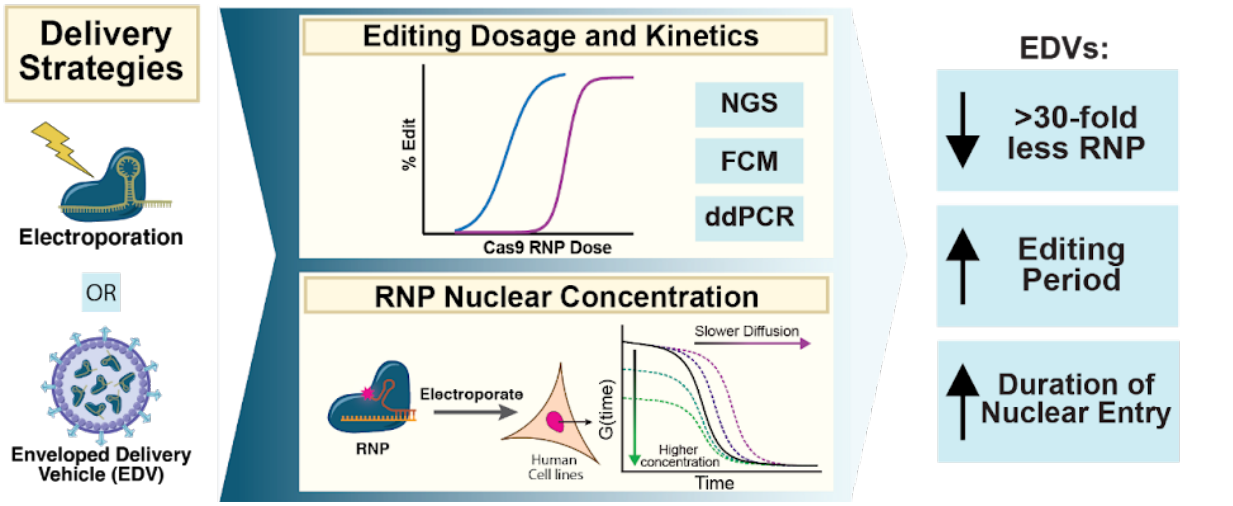

2.2 Introduction

CRISPR-based genome editing therapies have enormous potential to cure genetic diseases. Despite this promise, safe and effective delivery of genome editors remains a challenge for both therapeutic development and fundamental research [1,2]. Broadly speaking, genome editors can be delivered either as a nucleic acid, to be transcribed and/or translated in the target cell, or as an intact ribonucleoprotein complex (RNP) [1]. There are distinct advantages to delivering genome editors as RNPs, including shorter intracellular lifetimes that minimize off-target edits [3–5] and reduce immunogenicity [6–8]. Compared to mRNA delivery, RNP delivery may result in lower levels of toll-like receptor activation [6,9], and enable higher *in vivo* editing efficacy by bypassing *in situ* translation of mRNA [10] and protecting the guide RNA (gRNA) integrity due to Cas9 protein binding [5]. RNP delivery also avoids risks of random DNA integration posed by viral vectors, including lentivirus and adeno-associated virus (AAV) [11,12].

While delivery of proteins and RNA to the interior of cells remains a critical therapeutic challenge [13], extensive engineering efforts have generated multiple promising *ex vivo* and *in vivo* Cas9 RNP delivery strategies [1,2]. RNP electroporation is the most common strategy, currently used in several CRISPR genome editing therapies for blood disorders [14,15]. RNP electroporation is less cytotoxic than nucleic acid electroporation [16], is efficient in primary cells and has higher specificity than delivery systems that result in extended genome editor expression [3]. However, RNP electroporation requires an *ex vivo* approach, limiting its therapeutic utility. Furthermore, electroporation can impact cell viability [17] which increases the overall costs and production time frame for cell-based therapies [17]. Alternatively, enveloped delivery vehicles (EDVs), derived from retrovirus, offer a packaged approach to Cas9 RNP delivery which safeguards cell integrity by utilizing endogenous endocytic uptake for cell entry [18–23]. EDVs leverage intrinsic viral intracellular delivery capabilities while mitigating the risk of lentiviral genome integration or extended transgene expression [18,24,25]. EDVs use vesicular stomatitis virus glycoprotein, VSVG, for cellular uptake and endosomal escape, which typically exhibits broad cell tropism [12,18,19,24,26]. Recent work demonstrated that binding-deficient VSVG combined with antibody-derived targeting motifs enables cell-type specific Cas9 delivery both *ex vivo* and *in vivo* [24,27]. However, despite the promise of RNPs and EDVs, little is known about how much functional Cas9 RNP can be delivered in each case and how much is required for efficient editing in human cells [3,8,17,28].

To address these questions, we compared electroporation and EDVs for the delivery of S. *pyogenes* Cas9 RNPs to edit various human cell types. We determined the impact of delivery modality on the rate of DNA cleavage and repair. Using fluorescence correlation spectroscopy (FCS), we found that >1300 Cas9 RNPs per nucleus are required for editing in human cell lines. At comparable Cas9 RNP doses, EDVs are 30- to 50-fold more effective at editing, across multiple human cell types and target genome sequences. Furthermore, EDV delivery generates genome edits twice as fast as electroporation. We hypothesize that the observed differences in editing efficacy and rate result in part from differences in RNP versus EDV trafficking to the cell nucleus. Our results suggest that the Cas9 RNP dosage used for current *ex vivo* research and clinical genome editing could be substantially reduced by switching from electroporation to a packaged delivery strategy such as EDVs. These findings also reveal the importance of delivery modality for genome editing efficacy and pave the way for engineering optimal delivery methods to ensure maximal genome editing with minimal side effects.

2.3 Results

2.3.1 Several thousand Cas9 RNPs per cell nucleus are sufficient for editing human cell lines

To estimate the number of Cas9 RNP molecules per cell nucleus that are sufficient for editing, we used fluorescence correlation spectroscopy (FCS) to measure both the concentration and rate of diffusion of fluorescently labeled RNPs in cells (Fig. 2.1A) [29–31]. We incubated purified Cas9 protein with a dual guide RNA consisting of commercially available ATTO™ 550-labeled tracrRNA and a *B2M*-targeting crRNA (Supplemental Table 1). As we were most interested in quantifying the amount of intact RNP, we reasoned that fluorescently labeled guide RNA would provide a detectable shift in diffusion time between free RNA and the intact RNP in buffer (Fig. S1A, B) and in cells. We compared the concentration and diffusion rates of electroporated Cas9 pre-complexed with the labeled dual-guide RNA versus the labeled dual-guide RNA alone in HeLa cells (Fig. 2.1A). After 24 hours, fluorescent signal in nuclei was evaluated by FCS, with observed RNP diffusion time significantly higher than for dual-guide RNA alone (2.0 vs 1.0 ms, p-value =0.0004, Fig. 2.1B). The nuclear concentration of the RNP condition was higher than that observed for the dual-guide RNA only condition ($7.5x10^7$ Cas9 per cell, 25 vs. 19 nM, Fig. S2.1C), possibly due to both nuclear localization and RNA stabilization that results from Cas9 binding [32]. Two-component analyses of nuclear autocorrelation functions obtained by FCS provided best fits to the data and were used for all future nuclear delivery analyses (Fig. S2.1D, E).

Next, we quantified the nuclear concentration of Cas9 RNA containing a *B2M*-targeting, fluorescently labeled dual-guide RNA, across a range of dosages ($15x10^7$ to $0.24x10^7$ Cas9 per cell) in HeLa cells at 24 hrs (Fig. 2.1C, D). The RNP nuclear concentrations resulting from electroporation were linear across this dose range (R^2=0.96) ranging from 39 nM to 3 nM (Fig. 2.1C). Using published estimates of HeLa nuclear volume, ~690 μM^3 (34), we calculated the number of Cas9 molecules per nucleus to be 16,000-1200 molecules for this dose range (Fig. 2.1C, D; Supplemental Table 2), which corresponds to ~0.01% of total Cas9 per cell.

We wondered whether electroporation delivery efficiency varies substantially by cell type. Measurement of Cas9 RNP nuclear concentrations in two additional cell lines, HEK293T and U2OS, at two doses ($7.5x10^7$ and $0.94x10^7$ Cas9 per cell) revealed similar values to those measured in HeLa cells (Fig. 2.1E). This suggests that Cas9 RNP delivery efficiency by electroporation in multiple cell types is similar and thus the large RNP dose difference required for editing in different cell types may be due to differences in epigenetic landscape or DNA repair mechanisms [33,34].

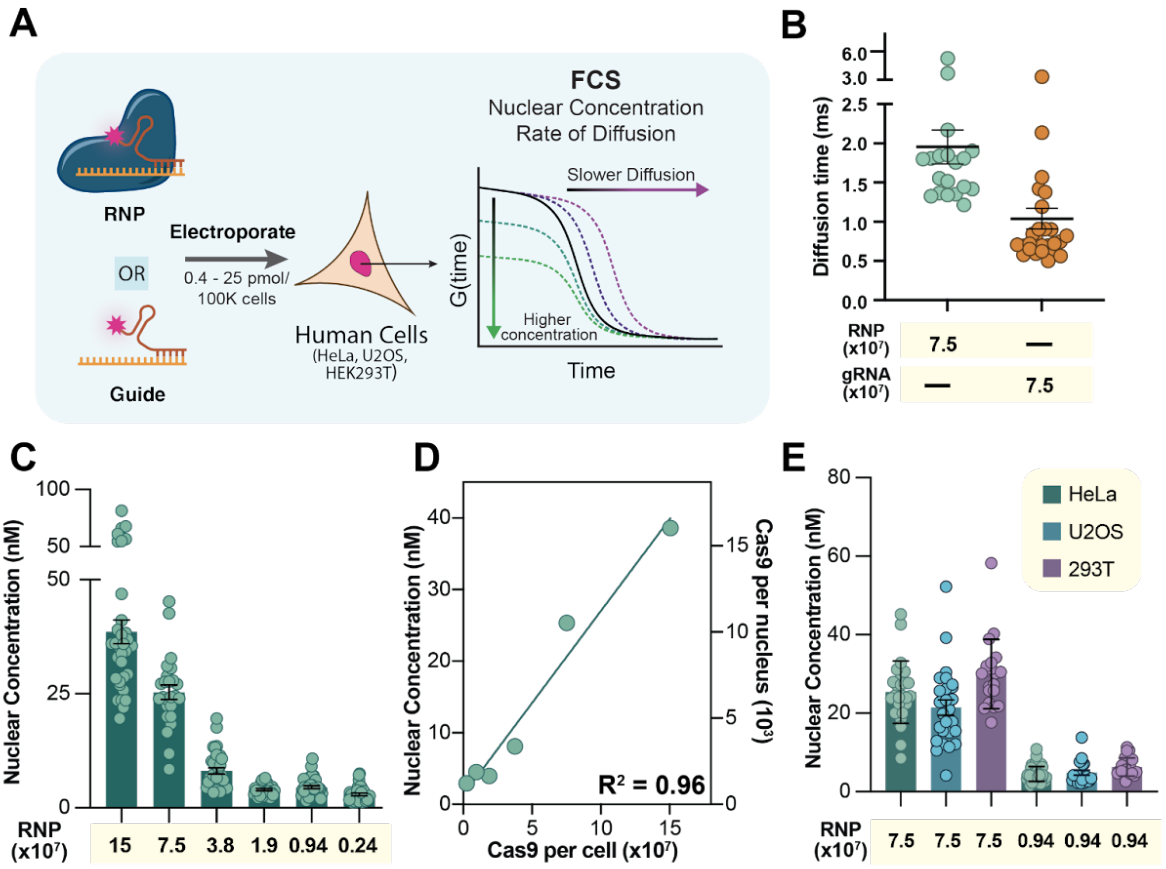

Figure 2.1: Quantifying Cas9 RNP nuclear concentration delivered by electroporation with fluorescence correlation spectroscopy (FCS)

A) Experimental schematic of workflow to quantify the Cas9 RNP nuclear concentration required for editing. B) Diffusion time of Cas9 RNP or gRNA, in Cas9 per cell, delivered in Hela cells and measured at 24 hrs (2.0 vs 1.0 ms, p-value =0.0004) Each point represents the average diffusion time in an individual cell modeled with a two-component diffusion fitting (Fig. S1). FCS diffusion times provided in ms, n>25 for each FCS condition with at least two biological replicates each (mean ± SEM). C) FCS analysis of HeLa cells electroporated with the Cas9 RNP. Nuclear concentration of Cas9 RNP as a function of dosage (in Cas9 per cell). Each point represents the concentration in an individual cell. FCS values provided in nM, n>25 for each FCS condition with at least two biological replicates each (mean ± SEM). All concentration values and diffusion times were derived by fitting FCS traces with a two-component 3D diffusion equation (see Methods for more detail). D) (Left Axis) Average nuclear concentration of Cas9 RNP versus dosage shows a strong linear correlation. (R^2 = 0.96). (Right Axis) Estimated number of Cas9 per nucleus from nuclear concentration values calculated by FCS and volume of HeLa nucleus (690 μM^3) [35]. E) FCS analysis of nuclear concentration for HeLa, U2OS, and HEK293T cells. FCS values provided in nM, n>20 for each FCS condition with at least two biological replicates each (mean ± SEM). Exact values for FCS, including experimental and biological replicates, mean, and SEM are reported in Supplemental Table 2.

2.3.2 EDVs dramatically reduce the amount of Cas9 RNP needed for genome editing

To determine how much functional Cas9 RNP is required for efficient editing in human cells, we first determined how much total Cas9 protein is needed for editing when delivered by electroporation or EDV into HEK293T or HeLa cells (Fig. 2.2A; Fig. S2.2). For electroporation, the dosage that resulted in half maximal editing (EC50) of the B2M gene was $2.4x10^6$ and $7.3x10^6$ Cas9 per cell in HEK293T and HeLa cells, respectively (Fig. 2.2B). For EDV delivery, the EC50 was $5.7x10^4$ and $1.5x10^5$ Cas9 per cell in HEK293T and HeLa cells, respectively (Fig. 2.2B). These values correspond to 42- and 50-fold reductions in required Cas9 dose for HEK293T and HeLa cells, respectively, for EDV-mediated RNP delivery compared to electroporation.

Extensive work has shown that the choice of ~~s~~gRNA strongly impacts the activity and specificity of Cas9[36,37], but it remains unknown the degree to which the ~~s~~gRNA impacts the Cas9 RNP dosage required for editing. We compared doses required for editing using four different guide RNAs targeting *B2M*, *VEGFA*, CCR*5* and *EMX1* and found that the amount of Cas9 required for editing varied by greater than 100-fold depending on guide choice (Fig. 2.2C, 2D).

We wondered whether these differences in required RNP dosage by these ~~s~~gRNAs were due to differences between the *B2M*, *VEGFA*, *CCR5* and *EMX1* loci. Therefore, to minimize the impact of potential differences in chromatin state, we generated a panel of nine gRNAs targeting a ~200-bp window in the *B2M* locus and compared the dosages required for *B2M* knockout in HEK293T and HeLa cells (Fig. 2.2E; Fig. S2.3). Different gRNAs resulted in substantial differences (>100 fold) between RNP doses required for editing using either electroporation or EDVs. For electroporation and EDVs respectively, the EC50 values across ~~s~~gRNAs were highly correlated between cell lines (R^2 = 0.78, R^2 = 0.83) (Fig. S2.4A, B). Interestingly however, the gRNA trends were only loosely correlated across delivery modalities (R^2 = 0.55, Fig. S2.4C) and there was no correlation between individual gRNAs' maximum editing levels and dosage requirements (R^2 =0.01, R^2 =0.08, Fig. S2.4D, E).

To remain functional in human cells Cas9 must remain guide-complexed and retain biochemical cleavage activity. Typically, ~20-40% of purified Cas9 is active *in vitro*[38–40]. Across three gRNAs, our in-house purified Cas9 averaged 30% activity (Fig. S5), but we wondered whether EDV packaging impacts the activity of encapsulated Cas9 RNPs. By Cas9 and p24 ELISA, we determined that each EDV packages 273 +/- 52.5 Cas9 molecules (Fig. S2.2, Fig. S2.6A, see Methods). Next, we quantified the maximum percent of Cas9 protein in EDVs that could be complexed with sgRNA by measuring the Cas9 protein and sgRNA concentrations using Cas9 ELISA and RT-qPCR, respectively (Fig. S6B). Across five independent batches of EDVs, only

8.3 +/- 1.7 sgRNA molecules were measured for every 100 molecules of Cas9 protein (Fig. S6B).

We first tested whether sgRNA availability limits the Cas9 cleavage functionality in EDVs. Cas9 packaged in EDVs with or without sgRNA was introduced into cells that were also transfected with a plasmid expressing a *B2M*-targeting sgRNA (Fig. S6C). However, this additional guide RNA supplementation failed to result in measurable improvement in editing efficacy (Fig. S6C). We next tested whether the Cas9 protein in EDVs is degraded or unfolded, which could render it incapable of guide RNA binding. Using Western blotting, we determined that most Cas9 in EDVs remains uncleaved from the lentiviral polyprotein Gag or is degraded in EDVs, and that only 35% of the Cas9 is intact (Fig. S6D). Together with previous results showing that Cas9 protein alone readily denatures at 37°C[41], this finding suggests that the vast majority of Cas9 in EDVs is not functional. Furthermore, we conclude that the per-molecule difference in RNP delivery efficiency between EDVs and electroporation is substantially greater than the >30-fold difference measured in editing assays (Fig. 2.2).

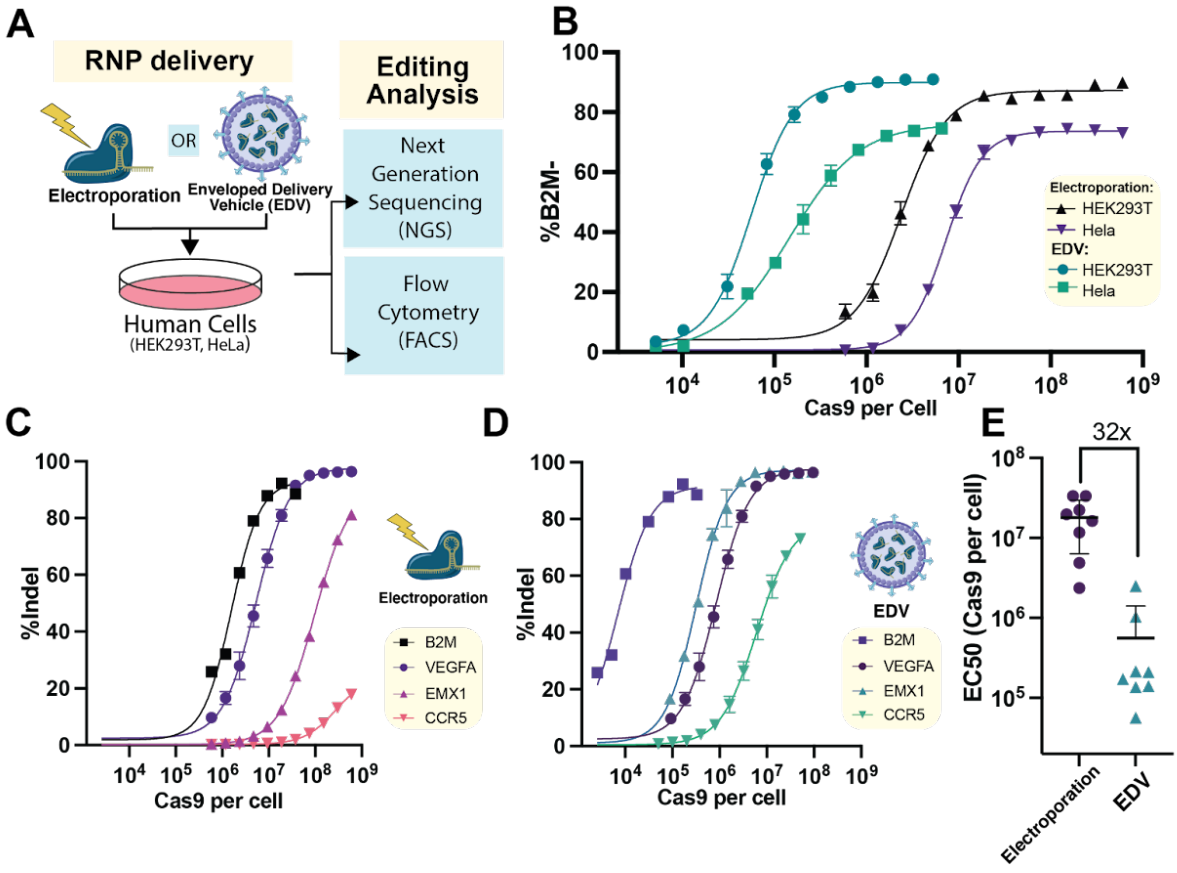

Figure 2.2: Assessing dosage requirements of Cas9 RNP delivered by electroporation and EDVs

(A) Experimental schematic of workflow to quantify the Cas9 RNP doses required for editing by electroporation and EDVs. **(B)** To assess Cas9 RNP dosage required for editing in HEK293T, Hela, Jurkats, and T cells were treated with varying doses of B2M-targeting Cas9 by electroporation and EDVs. Analysis was performed by flow cytometry 4 days post treatment to assess B2M knockdown. **(C)** Electroporated and **(D)** EDV delivery of Cas9 RNP targeting the B2M, VEGFA, EMX1 and CCR5 loci in HEK293T cells. Analysis was performed by next generation sequencing (NGS) 4 days post treatment to assess indels. **(E)** Comparison of required RNP doses delivered by electroporation and EDV for 9 different B2M guides in HEK293T (p-value = 0.0003, Mann Whitney Test). Analysis was performed by flow cytometry 4 days post treatment to assess B2M KO. n=3 technical replicates were used in all experiments. Datapoints represent the mean with error bars displaying SD. RNP dose curves were modeled (Prism v10) as sigmoidal (4PL, X is concentration).

2.3.3 EDV-mediated Cas9 RNP delivery results in rapid DNA cleavage and repair

The efficiency of genome editing depends on the integrated amount and duration of functional Cas9 RNP residing in the cell nucleus. To gain insight into the rate and duration of Cas9 RNP activity as a function of delivery modality, we treated cells with a range of saturating dosages (defined as that required for 90% maximal editing) of *B2M*-targeting RNP delivered by either electroporation or EDVs (Fig. 2.3A). Cells were harvested over the course of 54 hours post-treatment and analyzed using digital droplet PCR (ddPCR) and next generation sequencing (NGS) to measure double-strand DNA breaks (DSBs) and genome edits, respectively (Fig. 2.3A, B). Electroporation permeabilizes mammalian cells using electric pulses lasting a few microseconds to induce pore formation in the plasma membrane. These pores reseal within seconds to minutes, however, limiting the time in which RNPs can access the cell interior [42]. Consistent with this transient delivery window, at all RNP amounts tested, electroporation resulted in the majority of observed DSBs occurring within two hours post delivery (Fig. 2.3C). The highest and lowest ($6x10^7$ and $0.75x10^7$ Cas9 per cell) RNP doses resulted in similar maximum concurrent DSBs (64% versus 54%, respectively) (Fig. 2.3C).

We initially hypothesized that EDVs delivery would take longer than electroporation because EDV endocytosis requires fusion with endosomes to deliver RNPs into the cytosol. Interestingly, at a high RNP dose ($5.3x10^7$ Cas9 per cell), EDV-mediated RNP delivery occurred as quickly as electroporation, resulting in most DSBs occurring within two hours (Fig. 2.3D). These data show that the minimal time frame for EDV-mediated Cas9 RNP intracellular delivery, nuclear localization and genome target cleavage occurs within two hours, despite requiring additional delivery steps. Notably, for EDVs the timeframe for DSB formation was substantially more dose dependent, with the lowest doses of Cas9 delivered by EDV requiring 12 hours to reach the maximum level of DSBs (49%) (Fig. 2.3D). Importantly, this shows that it is possible to control and tune the rate of editing with the concentration of EDV.

In the absence of a DNA donor template, DSBs are typically resolved through non-homologous end joining (NHEJ). It remains unclear whether the time frame for DNA repair is impacted by delivery mode, particularly because delivery can perturb cellular metabolism and viability [17,42]. At high RNP doses ($6x10^7$ and $5.3x10^7$ Cas9 per cell), both strategies result in similar timeframes for DSB formation, but EDV delivery generated genome edits twice as fast (Fig. 2.3E-H; Fig. S2.7). At these same doses, half maximal editing for electroporation and EDVs occurred by 8.8 and 4.6 hours, respectively (Fig. 2.3E, F; Fig. S2.7). For electroporation, genome editing occurred within a similar timeframe for all doses, with the maximum rate of editing occurring in the 6-8 hour window (Fig. 2.3G). Conversely, the rate of editing for EDVs was highly dose dependent (Fig. 2.3H). At the earliest time point (one hour), the rate of genome edits was three times higher for EDVs than for electroporation at comparable doses, 10.6 vs 3.2 %edits/hour, respectively (Fig. 2.3G, H; Fig. S2.7). Combined, these results suggest that EDVs can continue to deliver functional RNPs into the nucleus over a prolonged time period.

One advantage of RNP delivery is increased editing specificity resulting from its transient activity within the cell. Therefore, we investigated whether the extended RNP delivery time by EDVs impacted editing specificity compared to electroporation. Using targeted deep sequencing, we compared editing specificity for two guides, targeting *VEGFA* and *EMX1*, at their on-target site and previously validated guide-seq off-target sites[43]. We titrated RNP doses delivered by electroporation and EDV, and compared the editing specificity by calculating the ratio of measured on-target editing compared to off-target editing. Consistent with previous research[3–5], RNP delivery by either strategy resulted in improved editing specificity compared to extended lentiviral expression (Fig. S2.8). Nuclease activity at mismatched off-target sequences is kinetically slower than at fully matched complementary on-target sequences[44]. Analogously, for both electroporation and EDV delivery, on-target editing occurred at substantially lower RNP dosages than off-target edits (Fig. S2.8A-D). Importantly, editing specificity was highly dependent on RNP dosage, with specificity dramatically decreasing in slight excess of doses required for half maximal on-target editing (Fig. S2.8A-D). For example, at RNP doses sufficient for 50% on-target editing at the EMX1 loci, the on:off-target ratio was 7.7 and 6.9 for electroporation and EDVs, respectively. At four-fold excess of these dosages, resulting in 80.9 and 83.8% editing, the on:off-target ratio was 15.3 and 3.6 for electroporation and EDVs, respectively (Fig. S8E,F).

Interestingly, EDV delivery did lead to decreased specificity at both target sites compared to electroporation. For VEGFA, the maximum on:off-target ratio was 8.5 and 7.3 for electroporation and EDV, respectively (Fig. S2.8E,F). For EMX1, the specificity difference between delivery modalities was more pronounced, with a maximum on:off-target ratio of 15.8 and 8.0 for electroporation and EDVs,

respectively (Fig. S2.8E,F). We hypothesize that the difference in specificity between these two RNP delivery strategies may result from increased EDV persistence in the cell.

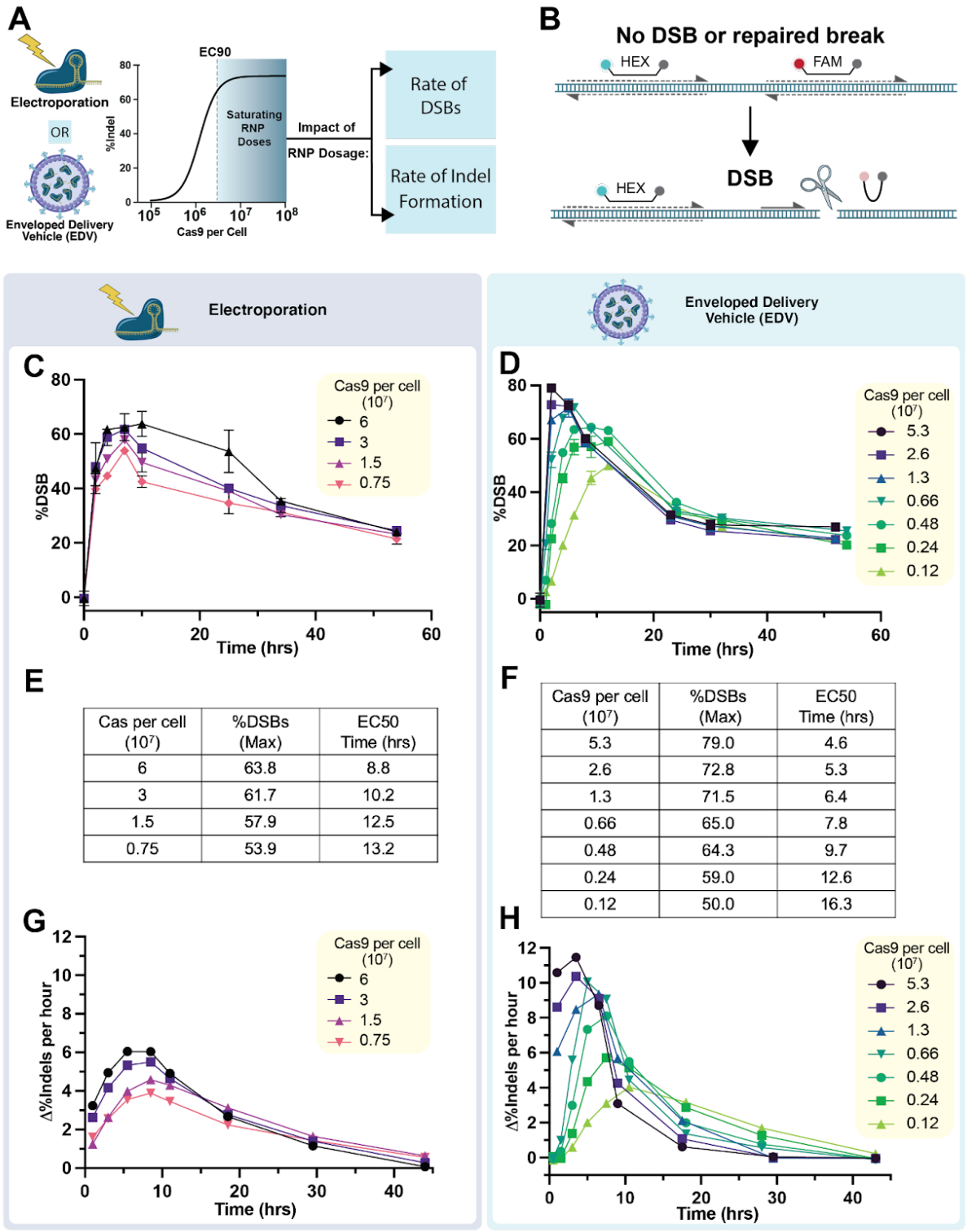

Cas per cell (10^7)	%DSBs (Max)	EC50 Time (hrs)
6	63.8	8.8
3	61.7	10.2
1.5	57.9	12.5
0.75	53.9	13.2

Cas9 per cell (10^7)	%DSBs (Max)	EC50 Time (hrs)
5.3	79.0	4.6
2.6	72.8	5.3
1.3	71.5	6.4
0.66	65.0	7.8
0.48	64.3	9.7
0.24	59.0	12.6
0.12	50.0	16.3

Figure 2.3: Kinetics of double stranded breaks and DNA repair resulting from delivery by RNP electroporation and EDVs

(A) Schematic overview of time course experiment comparing the impact of saturating, defined as doses at or exceeding levels for 90% of the maximum editing (>EC90), doses of Cas9 RNP delivered by electroporation and EDVs on the rate of double stranded breaks (DSBs) and consequent indel repair detected by NGS. **(B)** Experimental setup of the digital droplet PCR used to quantitatively detect DSBs. A HEX probe spans the first amplicon which is centromere proximal to the break site. A second FAM probe anneals to the second amplicon, which is lost upon DSB or chromosome loss. DSBs caused by **(C)** electroporation and **(D)** EDV delivery of Cas9 RNP targeting the B2M locus over a 54 hour time frame. Tables comparing the maximum percentage of synchronous DSBs and timeframe for half maximal editing (EC50) resulting from delivery of *B2M*-targeting RNP in HEK293T by **(E)** electroporation and **(F)** EDV delivery. Rate of indel formation caused by **(G)** electroporation and **(H)** EDV delivery of *B2M*-targeting RNP in HEK293T cells measured by NGS (Raw NGS time courses in Supplemental figure 7). All doses are at levels that meet or exceed the amount necessary for 90% maximal editing. n=3 technical replicates were used in all experiments. Datapoints represent the mean with error bars displaying SD.

2.3.4 EDV delivery results in extended nuclear accumulation of Cas9 RNPs over time

We hypothesized that the difference in genome editing kinetics observed using electroporation versus EDV-mediated Cas9 RNP delivery may correspond to the length of time that Cas9 RNPs reside in the nucleus. We hypothesized that EDVs could continue to deliver Cas9 RNPs to the nucleus over an extended time frame, whereas electroporation would result in decreasing levels of nuclear Cas9 following initial delivery. To quantify electroporated Cas9 RNPs as a function of time, we used FCS to measure the nuclear concentration of Cas9 RNP in HeLa cells at 12, 24, 36, 48, and 72 hours following electroporation (Fig. 2.4A). Following electroporation ($7.5x10^7$ Cas9 per cell), nuclear RNP concentrations did not vary from 12 to 36 hours but dropped by more than 75% by 48 hours (Fig. 2.4A; Supplemental Table 2). We used confocal microscopy to visualize the electroporated Cas9 RNPs in HeLa cells at these time points and validated the results by quantifying relative nuclear concentrations of Cas9 using fixed confocal microscopy (Fig. 2.4B; Fig. S2.9A, see Methods). The electroporated Cas9 exhibited punctate staining, which can be indicative of aggregation, endosomal entrapment or other forms of intracellular sequestering[29,30,45]. To determine if a significant proportion of electroporated RNP remained trapped in endosomes we stained for Rab5a and LAMP1, an early stage endosomal and lysosomal marker, and found minimal evidence for Cas9 colocalization inside endosomes or the lysosome (Fig. S2.9B-E). In addition, gRNA spacer sequence had no measurable impact on nuclear concentrations following electroporation with Cas9 complexed with a high- or poor- performing gRNA (Fig. S2.9F). Consistent with our editing time course (Fig. 3), the nuclear concentration of Cas9 delivered by EDVs continued to increase for up to 32 hours after delivery (Fig. 2.4C, D, Fig. S2.10A). Interestingly, for EDV delivery, Cas9 appeared to also accumulate around the nuclear envelope which was not observed for electroporation (Fig. 2.4B, Fig. S2.10B-C, Supplemental Table 3). This may be due to the nuclear

export signals present on the uncleaved Gag-Cas9 construct that facilitates EDV packaging (Fig. S2.6, S2.10B-C)[24,46] causing some of the Cas9 to accumulate around the nuclear envelope.

Collectively, these results together with insights from previous studies support a model for how EDV delivery impacts the rate and mode of Cas9 RNP delivery (Fig. 4E). The earliest detectable genome editing occurred within two hours for all EDV doses studied (Fig. 3), demonstrating that Cas9 RNP nuclear entry occurs quickly following delivery. EDVs adsorb quickly to the cell membrane[47] and remain associated even after cell washing. Over time, these EDVs undergo endosomal uptake and escape mediated by VSV-G on the EDV surface[47]. Cas9 RNP encapsulation by EDVs appears to extend RNP half-life in the nucleus, possibly by impacting Cas9 degradation mechanisms.

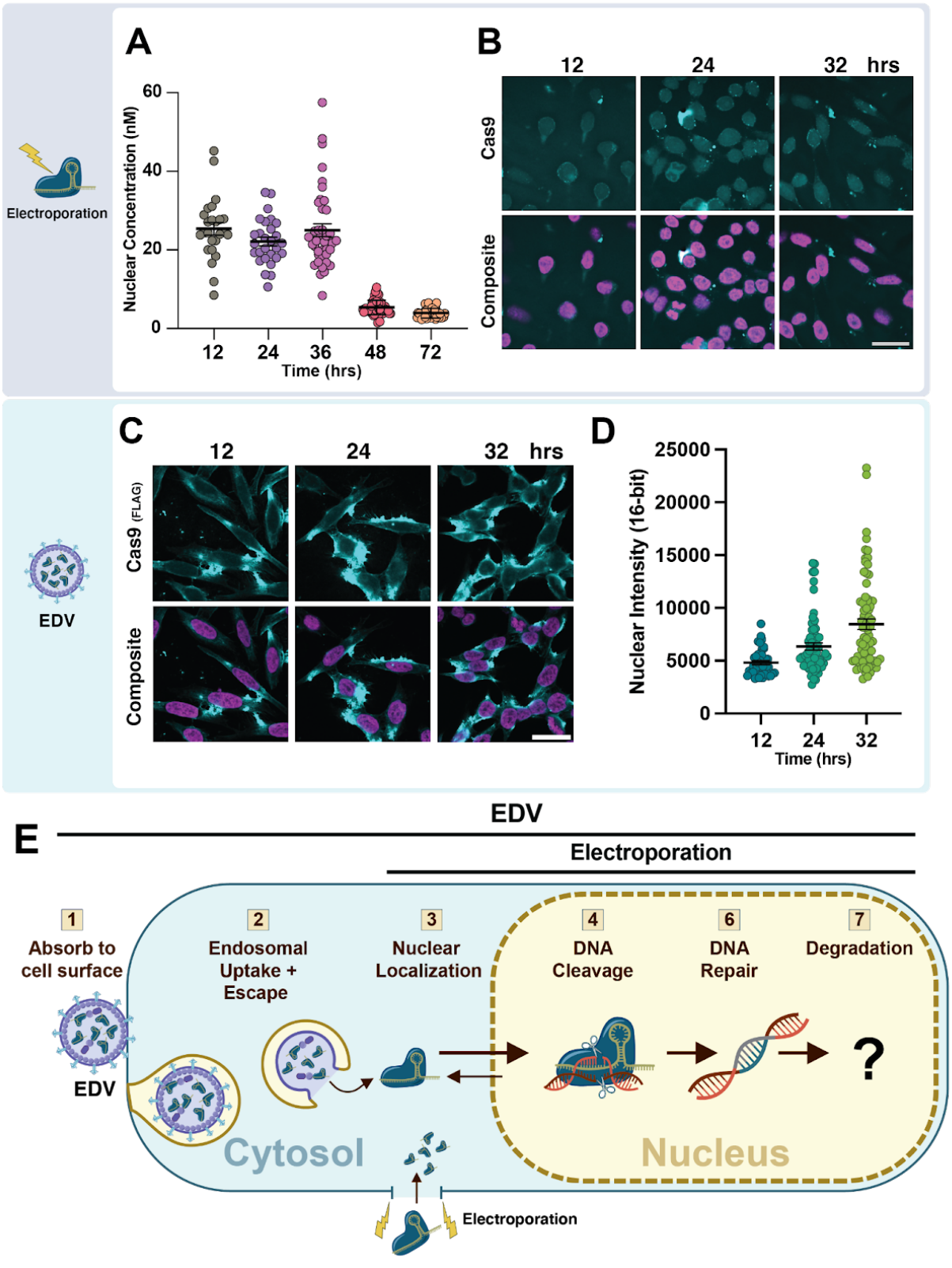
A
B
Electroporation
Nuclear Concentration (nM)
60
40
20
0
12
24
36
48
72
Time (hrs)
12
24
32 hrs
Cas9
Composite
C
D
EDV
Cas9 (FLAG)
Composite
12
24
32 hrs
Nuclear Intensity (16-bit)
25000
20000
15000
10000
5000
0
12
24
32
Time (hrs)
E
EDV
Electroporation
1
Absorb to cell surface
2
Endosomal Uptake + Escape
3
Nuclear Localization
4
DNA Cleavage
6
DNA Repair
7
Degradation
EDV
?
Cytosol
Nucleus
Electroporation

Figure 2.4: Comparison of nuclear localization and concentration of Cas9 delivered by electroporation and EDVs as function of time

(A) Quantification of the nuclear concentration of Cas9 RNP in HeLa cells by fluorescence correlation spectroscopy (FCS) at 12, 24, 36, 48, and 72 hours post-electroporation ($7.5x10^7$ Cas9 per cell). Each point represents the concentration in an individual cell. FCS values provided in nM, n>25 for each FCS condition with at least two biological replicates each (mean ± SEM). All concentration values and diffusion times were derived by fitting FCS traces with a two-component 3D diffusion equation (see Methods). Representative fixed confocal images of HeLa cells stained for Cas9 (top) and composite image of Cas9 overlaid with nuclear counterstain (SYTOX™ Deep Red Nucleic Acid Stain) showing the nuclear intensity of Cas9 at 12, 24, and 36 hours following **(B)** electroporation ($1.2x10^8$ Cas9 per cell) and **(C)** EDV treatment (~$3.0x10^6$ Cas9 per cell). Scale bar is 25 uM. **(D)** Relative quantification of median nuclear intensity of Cas9 delivered by EDV at 12, 24 and 36 hours (see Methods). Intensity on 16-bit scale (0 to 65536). Each data point represents an individual nuclei n> 40 (mean ± SEM). **(E)** Schematic overview of Cas9 delivery by EDVs and Electroporation.

2.3.5 Attempts to quantify EDV-mediated Cas9 delivery with fluorescence correlation spectroscopy

Note: Portions of the results and figure (Fig. 2.5) were modified with permission from Maddie Zoltek, a co-author and collaborator.

Given the >30-fold RNP delivery improvement by EDV compared to electroporation, we sought to quantify the concentration of Cas9 that reached the nucleus when delivered with EDVs. We hypothesized that the nuclear concentration of Cas9 following EDV delivery would be equal or greater than electroporation at analogous doses sufficient for editing because a substantial proportion of Cas9 in EDV is degraded or not guide-complexed (Fig. S2.6). RNPs are produced and packaged into EDVs by producer cells (see Methods for details) so the synthetic ATTO-550 cr:tracrRNA could not be used directly. Instead, we generated SpyCas9 fused mGreenLantern[48], a monomeric GFP variant, to track and quantify EDV-mediated delivery (Fig. 2.5A-D). The purified fusion delivered as RNP by electroporation or EDVs edited comparably to the 2xNLS SpyCas9 (Fig. 2.5B,D). The amount of Cas9 in Cas9-GFP EDVs was determined by Cas9 ELISA (Fig. S2.2). We then incubated a defined amount of Cas9-containing EDVs into HeLa cells for 24 hrs. After the incubation, the cells were washed twice with DPBS and evaluated by FCS (Fig. 2.5).

Unfortunately, FCS analysis of HeLa nuclei containing Cas9-GFP delivered by EDVs revealed irregular fluorescence behavior that convoluted data interpretation. Firstly, FCS measurements performed on non-EDV-treated cells detected significant background fluorescence probably due to autofluorescence, which is more common for fluorophores in the green fluorescent protein range[49]. Autofluorescence originates from organic molecules in cells and tissues, including flavins, NADH, and other organic molecules with polycyclic hydrocarbons that delocalize electrons, and are capable of absorbing photons at the wavelength used to excite GFP. FCS autofluorescence can be detected as a non-correlating species that contributes fluorescence intensity without

producing an autocorrelation function (ACF). During a measurement, this background can artificially lower the amplitude of the ACF for the fluorophore being analyzed and therefore must be rigorously subtracted from all acquired data. Although there are established equations for this subtraction,[39,40] the FCS data from EDV-treated cells suffered an additional limitation.

An FCS measurement in a single nucleus is generally performed by positioning the laser in the nucleus, acquiring ten autocorrelation traces, and using the average of these traces for autocorrelation fitting and analysis. During measurement of Cas9-GFP, we observed that the fluorescence intensity for the last measurement was consistently lower than that of the first (Fig. 2.5). Although some variation is expected, the fluorescence intensity should roughly overlap throughout the ten measurements (Fig. 2.5). The observed depletion in intensity is typical of photobleaching, which has been previously reported for this GFP variant (mGreenLantern).[41] Though photobleaching is not typically prohibitive for FCS measurements, the diffusion time of the Cas9-GFP fusion was extremely slow, due to its large size and DNA binding interactions. In addition, Cas9 may remain inside of EDVs (which are 100-120 nm[18,24]), or remain attached to the GAG polyprotein responsible for packaging (Fig. S2.6). Slow diffusion times prevent diffusion of photobleached molecules out of the focal volume, magnifying their effect. Therefore, the amplitude of the ACFs decreased throughout the duration of the FCS traces in a single cell, with the last trace measurably lower in amplitude than the first (Fig. 2.5C). This is indicative of decreasing signal-to-noise levels and is not observed for previous FCS measurements of Cas9 labeled with ATTO™ 550 (Fig. 2.1; Fig. 2.2). It is unclear whether this change in amplitude because of the photobleaching of GFP or background autofluorescence.[25,26,42,43] However, because the y-intercept of the ACF dictates the number of molecules detected during the measurement window, any artifacts may misrepresent the absolute concentrations of Cas9 measured in the nuclei.

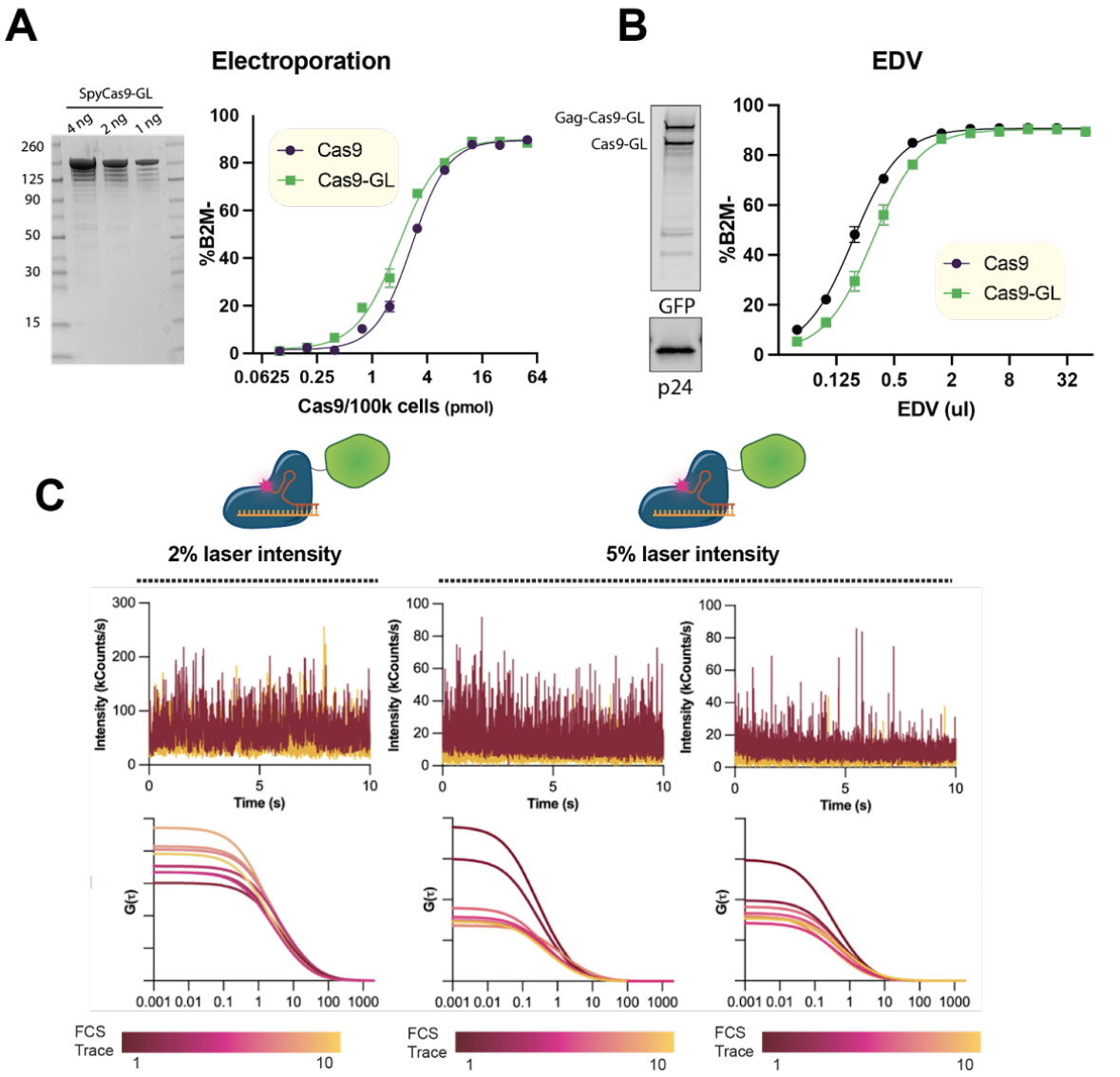

Figure 2.5. Establishing SpyCas9-GFP (mGreenlantern) fusion for proximity labeling of RNP delivery

(A) (left) Purified Cas9-GFP protein run on SDS-PAGE to illustrate purity (>95%) (see methods). (right) Dose titration of Cas9 (2xNLS (Macrolab)) and Cas9-GFP fusion with guide targeting *B2M* showing that purified Cas9-GFP fusion retains comparable editing activity following electroporation in HEK293T. Analysis was performed by flow cytometry 4 days post treatment to assess B2M knockdown **(B)** (left) Purified EDVs packaged with Cas9-GFP fusion detected with anti-GFP western blot. p24 is HIV capsid protein as viral loading control. (right) Dose titration of Cas9 (2xNLS (Macrolab)) and Cas9-GFP fusion with guide targeting *B2M* showing that purified Cas9-GFP fusion retains comparable editing activity following EDV-delivery in HEK293T. Analysis was performed by flow cytometry 4 days post treatment to assess B2M knockdown **(C)** Representative fluorescence intensity traces (top) and autocorrelation curves (bottom) obtained from cells treated with Cas9 EDVs. In all cases, both the overall fluorescence intensity and the amplitude of the autocorrelation function from

FCS decreases throughout the duration of the measurement. Laser intensities of **(C)** (left) 2% and (right) 5% were tested.

2.4 Discussion

Safe and effective delivery of CRISPR-Cas9 based genome editing enzymes has profound potential to advance both therapeutic development and fundamental research. Focusing on Cas9 RNP delivery, we compared electroporation and enveloped delivery vehicles (EDVs) for their ability to introduce sufficient RNPs into cells to mediate intended genome modifications. Our data show that a minimum of ~1300 Cas9 molecules per cell nucleus are required for half maximal genome editing across a range of different human cell lines. We also found that increasing genome editor lifetime in the nucleus is critical to minimize effective RNP concentration while maintaining editing efficacy. Recent work demonstrated that inhibiting Cas9 Keap1-mediated degradation enhanced epigenome editor performance[50]. Future research should investigate whether thermostable Cas9 variants, such as iGeoCas9[41], exhibit increased nuclear half-life, or for EDV delivery, allow for a larger proportion of RNPs to be functional.

We found that packaged delivery of Cas9 RNPs within EDVs resulted in continued RNP nuclear localization over a prolonged period (Fig. 4C, D). Similarly, other RNP delivery strategies, including related virus-like particles[19,22,23,51,52], lipid nanoparticles[41,53,54], and cell-penetrating peptides[17,55], may result in prolonged delivery windows compared to direct RNP electroporation. Importantly, these extended time windows could be leveraged for spatiotemporal control[26] or to impact DNA repair outcomes[17,26]. Furthermore, the delay between DSB and subsequent genome editing will likely be cell-type dependent, with longer repair times expected for clinically relevant post-mitotic cell types such as neurons and cardiomyocytes[26].

Improving nuclear localization efficiency of the Cas9 RNP is of paramount importance. Our study indicates that EDV delivery protects the Cas9 RNP and increases its delivery duration. For EDV delivery, there was noticeable accumulation of Cas9 around the nuclear envelope which suggests that nuclear localization may be limiting. This may be partially due to the nuclear export signals (NESs) added to the gag polyprotein to facilitate RNP packaging[19,24,51], and is consistent with recent EDV engineering demonstrating that adding additional nuclear localization signals (NLSs) to Cas9 can improve EDV-mediated editing efficiency by ~2-fold[46]. Interestingly, there appears to be an inherent tradeoff between requiring cytosolic localization for efficient EDV production, with additional NLSs reducing RNP packaging, and effective nuclear localization necessary for editing following EDV delivery[46]. For RNP electroporation, previous studies have also illustrated the importance of NLS optimization[17,46]. The optimal NLS configuration is different for other Type II and Type V Cas nucleases[56,57], such as Cas12a which contains putative NESs[58], and may also differ for fusion

constructs (i.e. base or prime editors). In addition, the impact of NLS tiling on cellular perturbation, editing specificity and half-life remains to be tested.

We show that understanding the impact of delivery modality on RNP intracellular trafficking, localization and genome editing efficacy can identify delivery bottlenecks that could be the focus of future engineering of improved RNP-based gene therapies. Our study examined the dosage requirements of nuclease active SpyCas9 in human cell lines. Future work should investigate the editor dosage requirements for other clinically-relevant cell types, as well as whether or how these requirements differ for other editing tools used for base, prime, and epigenome editing, to best preserve genomic and cellular integrity while efficiently achieving the desired genomic alterations.

2.5 Materials and Methods

2.5.1 Plasmid construction

Restriction enzymes used in this study were purchased from New England Biolabs (NEB). Plasmids were constructed using NEBuilder HiFi DNA Assembly Master Mix (NEB) with PCR products and backbone restriction digests. For guide plasmid cloning, protospacer oligos were annealed and then inserted using BsmBI golden gate assembly into the optimized Gag-Cas9 (Gag-3xNES-2xNLS-Cas9-U6-sgRNA) and PsPax-U6-sgRNA plasmids as previously reported [24]. Oligos encoding the sgRNA spacers (IDT), and all other oligos used in this study, are outlined in Supplementary table 3.

Cloning and DNA preparations were performed in MultiShot StripWell Mach1 (ThermoFisher). All plasmids used in tissue culture were prepared with Qiagen Plasmid Maxi Kit (Qiagen). All plasmids were sequence confirmed prior to use (Plasmidsaurus, UC Berkeley DNA Sequencing Facility).

2.5.2 Tissue culture

Lenti-X (Takara Biosciences), HEK293T, U2OS, and HeLa cells were obtained and authenticated by the UC Berkeley Cell Culture facility. Lenti-X, HEK293T, U2OS and HeLa cell lines were cultured in DMEM (Fisher Scientific) supplemented with 100 U/ml Penicillin-Streptomycin (Thermofisher), and 10% (v/v) fetal bovine serum (FBS) and passaged with Trypsin-EDTA (0.25%, Phenol Red, Fisher Scientific).

2.5.3 RNP electroporation

sgRNA (IDT, Supplemental Table 1) were resuspended in IDT duplex buffer to 100 µM concentration. Cas9 RNPs were formed by combining the sgRNA and 40 µM Cas9-NLS (UC Berkeley QB3 MacroLab) at a molar ratio of 1.5:1 and incubating at room temperature for 10-15 min. Electroporation was performed using a 96-well

format 4D-nucleofector (Lonza) with 10^5 cells per well (unless otherwise specified). HEK293T cells were electroporated with the SF buffer and the CM-130 pulse code. HeLa cells were electroporated with SE buffer and the CN-114 pulse code. For cell lines, cells were immediately resuspended in pre-warmed media and transferred to culture plates.

2.5.4 EDV and Lentiviral production

Cas9-EDVs were produced as previously described [18,24]. Briefly, Cas9-EDVs were produced by seeding approximately 4 million Lenti-X cells (Takara Bio) into 10 cm tissue culture dishes (Corning) and transfecting the next day with 1 µg pCMV-VSV-G (Addgene plasmid #8454), 6.7 µg Gag-Cas9-U6-sgRNA, 3.3 µg psPax2-U6-sgRNA (Addgene plasmid #12260) using TransIT-LT1 (Mirus Bio) at a 3:1 TransIT-LT1:plasmid ratio. Two days post-transfection, Cas9-EDV-containing supernatants were harvested, passed through a 0.45 µm PES syringe filter (VWR) and concentrated with ultracentrifugation by laying EDV containing supernatant on top of 30% sucrose in 100 mM NaCl, 10 mM Tris-HCl (ph 7.5), 1 mM EDTA at 25,000 rpm with a SW28 rotor (Beckman Coulter) for 2 hrs at 4°C in polypropylene tubes (Beckman Coulter). Concentrated Cas9-EDVs were resuspended in Opti-MEM (Gibco) at a final concentration of 20x unless otherwise noted and frozen at -80 °C until use.

2.5.5 Fluorescence correlation spectroscopy

On the day of each FCS experiment, 300 uL of 10 – 100 nM AlexaFluor 594 hydrazide for electroporation experiments using ATTO™ 550 for Cas9 detection, both diluted into MilliQ, was added to one well of the 8-well microscopy dish and incubated at 37°C for at least 30 min. Immediately prior to measurements, a DNA stain, 300 nM Hoechst 33342, was incubated with the cells for 5 minutes to visualize nuclei. After nuclear dye incubation, cells were washed 2x with DPBS and incubated with pre-warmed DMEM for imaging.

The general procedures used for FCS have been described previously [45,59,60]. Experiments were performed with a STELLARIS 8 microscope (Leica Microsystems) with a Leica DMi8 CS scanhead, a HC Plan-Apo 63x/1.4NA water immersion objective, and a pulsed white-light laser (440 nm- 790 nm; 440 nm: > 1.1 mW; 488 nm: > 1.6 mW; 560 nm: > 2.0 mW; 630 nm: > 2.6 mW; 790 nm: > 3.5 mW, 78 MHz). All confocal imaging was performed using HyD S or HyD X detectors in counting mode, while FCS measurements were carried out using only a Hybrid HyD X detector in counting mode. All microscopy experiments were performed at 37°C (monitored using Oko-Touch) and 5% CO_2 in a blacked out cage enclosure (Okolab). Before each experiment, the correction collar of the objective was adjusted by maximizing the counts per molecule for the AlexaFluor 594 hydrazide dye standard; minor fluctuations in the correction

collar are expected based on the variable thickness of the glass-bottom microscopy dishes (LabTek™). After correction collar adjustment, ten five-second autocorrelation traces were obtained from the well containing dye standard to calculate the focal volume of the microscope (see Analysis of FCS Data for more detail). AlexaFluor 594 was measured using the same settings as ATTO™ 550.

For electroporation experiments, ATTO™ 550 was excited at 553 nm with an emission window of 570 - 660 nm, and Hoescht 33342 was excited at 405 nm with an emission window of 432 – 509 nm. Laser intensity for ATTO™ 550 was determined using *in vitro* samples of each respective protein and guide and determining the maximal laser intensity for which the observed counts per molecule (CPM) remained within a linear range. The pinhole S5 of the laser was set to 1 AU. A confocal microscopy image of the cells was used to position the crosshairs of the microscope laser in the nucleus of 10-15 cells within the frame. All FCS measurements consisted of ten ten-second traces. A minimum of 30 cells per condition were measured for each biological replicate, and a minimum of two biological replicates were collected for each condition.

The expected diffusion time ($_{diff}$) for ATTO™ 550-Cas9 RNP was obtained by measuring *in vitro* autocorrelation traces for 400 nM solutions of RNP, annealed ATTO™ 550-tracrRNA:crRNA, or ATTO™ 550-tracrRNA alone in DMEM media (25 mM Hepes, no phenol red) at 37°C (Fig. S6). For each sample, ten ten-second autocorrelation traces using the settings described above were measured per point, and three points were obtained per sample.Given the distribution of τ_{diff} values measured for free RNA in buffer versus in cells, we employed a lower τ_{diff} filter of 0.5 ms for Cas9 RNP delivery experiments to avoid fluorescent signal contributed by free RNA. These data were fitted using eq (1) below to derive the average diffusion time (τ_{diff}).

2.5.6 Analysis of FCS Data

Autocorrelation traces obtained from FCS measurements were analyzed using a custom MATLAB script.[59,60] To extract quantitative information from *in cellula* data, the effective confocal volume of the microscope must be known. This value was determined using eqs 1-3 by and the *in vitro* autocorrelation traces for the AlexaFluor 594 hydrazide standard measured at the start of each experiment, which have known diffusion coefficients in water. [61,62].These traces were fitted to a 3D diffusion equation (eq 1):

$$G(\tau) = 1N1(1+_{diff})1+(s2\tau diff) \qquad (1)$$

where N = the average number of molecules detected in the focal volume (V_{eff}), $_{diff}$ = the average diffusion time that a molecule requires to cross V_{eff}, and s = the structure factor (the ratio of the radial to axial dimensions of the focal volume). The structure factor was measured to be 0.17 using the autocorrelation function of AlexaFluor 594 in

water at 25°C and fixed for all subsequent analysis. V_{eff} can be extracted from these data by inserting the $_{diff}$ value derived from eq (1) to calculate ω_1 in eq (2):

$$1 = 4 \cdot D \cdot \text{diff} \qquad (2)$$

where ω_1 = the lateral extension of the confocal volume and D = the known diffusion coefficient of the dye standard in water at 37°C. Note that diffusion coefficients at 25°C are typically reported in the literature and can be used to calculate the diffusion coefficient at 37°C using eq (3):

$$DT = D25°C \cdot t + 273.15t \cdot 2.985 \cdot 10\text{-}6\ \text{Pa} \cdot s \cdot \text{K-}1 \qquad (3)$$

where t = 37°C, D(25°C) for AlexaFluor 594 is $3.88 \cdot 10^{-6}$ cm^2/s and for AlexaFluor 488 is $4.14 \cdot 10^{-6}$ cm^2/s (ref.[47]), and η(t) is the viscosity of water at 37°C ($6.913 \cdot 10^{-4}$ Pa · s, ref.[30]). Using this formula, the diffusion coefficient of AlexaFluor 594 at 37° is $5.20 \cdot 10^{-6}$ cm^2/s and that of AlexaFluor 488 is $5.54 \cdot 10^{-6}$ cm^2/s.

V_{eff} can then be directly calculated from eq (2):

$$\text{Veff} = 32 \cdot (13) \cdot 1s \qquad (4)$$

The average V_{eff} for all experiments ranged from 0.25-0.4 fL.

To determine the appropriate fitting equation for data collected in cells, autocorrelation traces derived from *in cellula* measurements of HeLa cells treated with $0.24x10^7$ to $15x10^7$ Cas9 per cell were fitted using two equations. The first was a 3D anomalous diffusion equation used for previous FCS measurements of proteins in live cells (eq 5)[45]:

$$G = 1N \cdot 1(1 + {}_{diff})1 + s2(\text{diff}) + G(\infty) \qquad (5)$$

where N = the average number of molecules in the focal volume, $_{diff}$ = the average diffusion time that a molecule requires to cross V_{eff}, α = the anomalous diffusion coefficient, and s = the structure factor (0.17).

The second equation was a two-component diffusion equation previously applied to analysis of DNA-binding transcription factors by FCS.[60,63]. The equation incorporates both a rapidly and slowly diffusing component to account for biphasic autocorrelation functions. This equation is almost identical to a two-component diffusion equation used for previous single-molecule analysis of Cas9 in live cells, [64] except it incorporates an anomalous diffusion coefficient for the slow-diffusing fraction. [60] Since Cas9 binds DNA, we expected eq (6) to more accurately fit ACFs in live cells than eq 5:

$$G = 1N\ \ \text{Ffast} \cdot 11 + \text{diff1} \cdot 1 + s2\text{diff11} - \text{Ffast} \cdot 1(1 + (\text{diff2})1 + s2\text{diff2} \qquad (6)$$

where N = the average number of molecules in the focal volume, $_{diff1}$ = the average diffusion time for the rapidly-diffusing component, $_{diff2}$ = the average diffusion time for the slow-diffusing component, α = the anomalous diffusion coefficient, F_{fast} = the fraction of molecules that are rapidly diffusing, and s = the structure factor (0.17).

From the fittings, a set of parameters specific to individual measurements was obtained, including the diffusion time of the detected molecules (a single τ_{diff} for the 1-component fit or $_{diff1}$ and $_{diff2}$ for the 2-component fit), the fraction of molecules rapidly

diffusing (F_{fast}), the number of molecules detected in the focal volume, and a chi-square (χ^2) value to describe the goodness of fit. The χ^2 values were compared for the one-component vs two-component fits to determine that the two-component diffusion equation most accurately represents the data. All FCS data were therefore fitted by eq (6) and filtered as described previously [60] to remove measurements where $_{diff1}$ < 0.5 ms (indicative of free RNA), $_{diff1}$ > 10 ms (indicative of aggregation), α < 0.3, and χ^2 > 30. We also excluded fits for which a second component was not identified.

For all FCS curves that passed these thresholds, the concentration (C) of protein in the nucleus was then calculated using the value of N derived above in eq (7):

$$C = NNA \cdot Veff \qquad (7)$$

where N_A = Avogadro's number (6.023×10^{23} mol^{-1}). At least 20 concentration values from curves that passed all filters were used for each FCS condition.

The number of Cas9 molecules in the nucleus was calculated using the concentration obtained from eq (7) and a HeLa nuclear volume of $6.90 \cdot 10^{-13}$ L (ref.[38]) using eq (8):

$$Nnucleus = C \cdot 6.9 \cdot 10\text{-}13\ L \cdot NA \qquad (8)$$

where N_A = Avogadro's number (6.023×10^{23} mol^{-1}).

Finally, each concentration value derived from eq (7) had a corresponding F_{fast} value describing the fraction of this concentration that was rapidly diffusing. The concentration of DNA-bound Cas9 in the nucleus was then calculated using eq 9:

$$Cbound = 1Ffast \cdot C \qquad (9)$$

2.5.7 Cas9 Molecules per Nucleus Calculations

The number of Cas9 molecules per nucleus was calculated by multiplying the average volume of the HeLa nuclei, 690 μM^3 [35], by the nuclear concentration determined by FCS. To estimate the number of Cas9 RNPs per nucleus that are typically required for productive editing by nucleofection we first estimated the total Cas9 doses required for editing by electroporation by analyzing the Hela dose curves (Fig. S3B). The median Cas9 RNP dosage for half maximal (EC50) editing by electroporation was $6.4x10^7$ Cas9 per cell (Fig. S3B). The high efficiency B2M guide (Supplementary table 3) EC50 was $7.2x10^6$ Cas9 per cell in HeLa cells. Using the linear regression from the FCS electroporation dose titration (Fig. 2D, Supplementary Table 2), we calculated that this dosage would amount to nuclear concentration of 3.2 nM. Using Avogadro's number (6.023×10^{23} mol^{-1}), this amounts to ~1300 Cas9 RNP molecules per nucleus.

2.5.8 Western Blotting and densitometry

Samples were denatured by mixing with 5x Laemmli with 10% 2-mercaptoethanol and heating at 95°C for 3 minutes. Samples were run on 4%–20% SDS-PAGE gels (Bio-Rad) prior to transfer onto a methanol soaked polyvinylidene difluoride (PVDF,

Bio-Rad) membrane. PVDF membranes were blocked with 10% non-fat milk (Apex) in 1xPBS (GIBCO) with 0.1% Tween (Sigma) (PBS-T) for one hour at room temperature (~22-25°C). The solution was replaced with 0.1% non-fat milk in PBS-T and primary antibody dilution (Supplementary table 1) in 1% non-fat milk in PBS-T incubated at 4°C overnight. The following day, the solution was replaced with 1% non-fat milk in PBS-T and a secondary antibody dilution (Supplementary table 1) and gently shaken for 1 hour. Western blot membranes were washed with PBS-T three times, with 2-3 minutes wash steps, prior to imaging on a LI-COR OdysseyCLx. Fiji (previously imageJ) was used to quantify relative band intensity on western blots.

2.5.9 Quantification of Cas9 RNPs per EDV

The Cas9 ELISA kit (Cell BioLabs Inc.) and lenti-X p24 Rapid titer kit (Takara Biosciences) were used to quantify the cas9 and p24 in Cas9-EDVs, respectively. For cas9 and p24 measurements, Cas9-EDVs were diluted 20-2000 fold and 1000-100,000 fold, respectively. Both ELISA were done according to the manufacturer's protocol. Absorbance at 450 nm was measured by a plate reader (Biotek). The amount of Cas9 in the samples was determined by comparison to serial dilution to a cas9 standard (Cell Biolabs Inc.). The amount of p24 was determined by comparison to serial dilution to a p24 standard (Takara Biosciences). The number of p24 per EDV was approximated to be 2500 CA molecules per particle [65].

Cas9 from lyzed EDVs were measured by ELISA and validated against purified Cas9 from commercial (IDT, Cell Biolabs) and in-house sources (UC-Berkeley, Macrolab, QB3), quantified with photospectrometry (Fig. S2).

2.5.10 Quantitative RT-PCR of B2M sgRNA in EDVs

Quantitative RT-PCR was done as previously published[24]. Cas9-EDVs containing the sgRNA targeting the B2M gene were produced and concentrated as described above. RNA was extracted from 150 ul of Cas9-EDVs using the NucleoSpin RNA Virus Kit (Takara Bio) following the manufacturer's instructions. Quantitative RT-PCR was done with PrimeTimeTM One-Step RT-qPCR Master Mix (IDT) following the manufacturers instructions for the QuantStudio 6 Flex Real-Time PCR system (Thermo Fisher). The qPCR primers were custom ordered as a TaqMan Small RNA Assay to detect the B2M sgRNA (Supplementary Table 3)

2.5.11 In vitro cleavage assessment of Cas9 activity

Prior to use, double stranded DNA (dsDNA) substrate (Supplemental table 1) was annealed in 10 mM HEPES, 20 mM KCl, 1.5 mM $MgCl_2$ at 95 °C for 5 minutes and cooled at a rate of 1 C/min to 4C. The annealed substrate was run on 8% Native-PAGE and annealed band was excised, ground finely, and eluted in 5 ml of water overnight at 4C. Next day, this solution was filtered through a 0.22 uM filter,

concentrated with 3 kDa spin filter (Amicon), and ethanol precipitated. The dried pellet was resuspended with DEPC water, and concentration was determined by spectrophotometry.

Single guide targeting the spacer was complexed with Cas9 protein in 2:1 ratio for 15 minutes at 37C in 200 mM HEPES; 1M KCl; 100 mM MgCl2, 10% Glycerol, 5 mM DTT. Following complexation, the RNP was diluted and added in 1:1 stoichiometry to annealed dsDNA substrate (Supplemental table 1) at final concentrations of 100 nM. The cleavage reaction occurred at 37 °C for 2 hrs in 20 mM HEPES; 100 mM KCl; 10 mM MgCl2, 1% Glycerol, 0.5 mM DTT.

2.5.12 Next Generation Sequencing (NGS) to assess genome editing

Next-generation sequencing was used for detection of on-target genome editing in 293T cells. Genomic DNA was extracted using QuickExtract (Lucigen) as previously described [18]. Q5 high fidelity polymerase (NEB) was used to attach adapters to the Cas9-RNP target site amplicons (Supplemental table 1). The resulting PCR1 products were cleaned up using magnetic SPRI beds (UC Berkeley DNA Sequencing Facility). Library preparation and sequencing was performed by the Innovative Genomics Institute Next Generation Sequencing Core using MiSeq v2 (Illumina). Reads were analyzed with CRISPResso2 (http://crispresso.pinellolab.partners.org/login).

2.5.13 Digital Droplet quantitative PCR (ddPCR)

Cells were collected at day 4, unless otherwise stated in figures, following editing with electroporation or EDVs, and genomic DNA was extracted with QuickExtract DNA Extraction Solution (Lucigen).

For DSB detection, the ddPCR setup was similar to what has been previously described [66,67], with two ~200 bp amplicons for the *B2M* target gene (Supplementary Table 3). Amplicon 1 was located proximal to the centromere and utilized a 5' hexachlorofluorescein-labeled (HEX) oligonucleotide probe (PrimeTime qPCR probes, Zen double quencher, IDT). Amplicon 2 was located ~200 bp away from amplicon 1, and utilized a 5' 6-fluorescein-labeled (FAM) oligonucleotide probe (PrimeTime qPCR probes, Zen double quencher, IDT). Amplicon 1 served as a reference that should be unaffected by Cas9 genome editing and would signal whether *B2M* was in a given droplet. Amplicon 2 spanned the *B2M* target site, with the probe located ~50 bp from the cleavage site. If the target site was not repaired after Cas9 cleavage, or if the chromosome was lost[86], amplicon 2 would not be amplified and the FAM probe would be quenched. ddPCR reactions were assembled with ddPCR Supermix for Probes (No dUTP, Bio-Rad), 900 nM of each primer, 250 nM of each probe, and 15-30 ng gDNA.

Droplets were formed using a QX200 Droplet Generator (Bio-Rad) following the manufacturer's instructions prior to PCR. The next day, ddPCR droplets were analyzed on a QX200 Droplet Reader (Bio-Rad). Data was analyzed with the QX Manager Software (Bio-Rad), and thresholds were set manually based on wells with untreated reference samples. The percentage of DSBs was calculated based on droplets that had the reference amplicon 1 (HEX+) but did not produce the neighboring amplicon (FAM+) (equation below).

$$\%\mathrm{DSB} = 100 \text{ x } (1\text{-}([\mathrm{FAM}]/[\mathrm{HEX}]))$$

2.5.14 Immunofluorescent (IF) Imaging and Quantification

For imaging EDV delivery in HeLa cells, 400k cells were plated the evening prior in a 12 cm dish that had 18 mM coverslips precoated with poly-L-lysine (Sigma-Aldrich #P7886, 100 ug/ml in 75 mM NaCl, 50 mM $Na_2H_{20}B_4O_{17}$, pH 8.4) For EDV experiments, unless otherwise stated in figure legends, 350 ul of 20x concentrated EDV mixture were added to the cells in 1:1 mix with OptiMEM (final volume 700 ul). EDV containing media was swapped for prewarmed supplemented DMEM (see above) at ~4 hours. For imaging Cas9 delivered by electroporation, 3 million cells were electroporated with 600 pmol RNP ($1.2x10^8$ Cas9 per cell). Following delivery, at timepoints specified in the figures, cells were fixed with 4% PFA in 1xDPBS for 10 min (ThermoScientific #28908). For time course experiments, all cells were fixed and then stored in 1xDPBS until all samples were harvested, so that permeabilization and staining steps were done simultaneously. We then washed coverslips three times with 1×DPBS, and permeabilized samples with 0.2% Triton-X-100 in 1xDPBS for 10 minutes. Following permeabilization, samples were washed three times, and then blocked with Image-iT FX signal enhancer (Invitrogen). After this initial blocking step, samples were washed twice with 1xDPBS and then further blocked in 10% Goat Serum (ThermoFisher #50062Z) for 20-30 minutes. Then samples were incubated with primary antibodies (Supplementary table 1) diluted in 10% Goat Serum at 4C overnight. The following day, the coverslips were washed three times with 1xDPBS and incubated for 1 hour with secondary antibodies (Supplementary Table 3). For EDV confocal microscopy, secondary antibodies from tyramide signal superboost kits (ThermoFisher, Supplementary Table 3) were used following manufacturers instructions. The labeling reaction was done for 2 minutes for all EDV experiments. Samples were then washed three times and mounted with Prolong Diamond antifade mountant (Invitrogen). All slides were stored at -20 C for periods longer than 1 week. All fixed cell confocal microscopy was performed using the Zeiss LSM710 microscope (UC-Berkeley, Bioimaging Facility).

For quantification of relative nuclear intensity of Cas9 and colocalization analysis, all Z-stacks were obtained based off of half the wavelength of emission of the Cas9 associated fluorophore (Nyquist sampling) through the Z-plane of the HeLa

cells that were counterstained with SYTOX™ Deep Red Nucleic Acid Stain (1:2000, Invitrogen, #S11380). These images were deconvoluted using the default settings of Huygens Professional (v22.10) to reduce noise. For the colocalization analysis these images were thresholded using the Costes method[68] and for each image a Pearson's correlation was calculated. For the relative Cas9 nuclear intensity quantification, the entire nuclear counterstained region was outlined and the median nuclear intensity in the Cas9 channel was quantified using Imaris (v10.2). Any nuclei that were on the edges of the image, were actively dividing, or that could not be independently quantified due to their close proximity to other nuclei, were manually excluded from quantification.

2.5.15 Flow Cytometry

Cells were stained with anti-human B2M-PE (316306, Biolegend) in PBS containing 1% bovine serum albumin. An Attune NxT flow cytometer equipped with a 96-well autosampler (Thermo Fisher Scientific) was used for flow cytometry acquisition. Data analysis was performed using FlowJo v10 10.7.1 (FlowJo, LLC, Ashland OR).

2.5.16 Statistical analysis

Statistical analysis was performed using Prism v10 unless otherwise stated. Statistical details for experiments, including the values and definitions of the samples sizes and error bars are reported in the figure legends. Unless otherwise specified in figure legend, two sided t-tests were used for pairwise comparisons and ANOVA was used for multiple comparisons.

2.6 Data and materials availability

Flow cytometry, fluorescence correlation spectroscopy, unprocessed ddPCR data, quantified confocal Z-stacks and next generation sequencing (NGS) raw files are available upon request. All other data is in the main text or supplementary materials.

2.7 Acknowledgements

We appreciated useful discussions with Ross Wilson, Laura Hofman, Matthew Kan and Kai Chen. We thank Matthew Kan for assisting in setting up the ddPCR assay. H.K. was in part supported by the National Institutes of Health (NIH) Stem cell biological engineering training program (Grant no. T32GM098218). M.Z. was in part supported by the National Science Foundation (Grant no. 2203903) and the NIH (Grant no. R35GM134963). W.N .was supported by Natural Sciences and Engineering Research Council of Canada Postdoctoral Fellowship PDF-578176-2023. Microscopy research reported in this publication was supported in part by the NIH S10 program under the award number 1S10RR026866-01. The content is solely the responsibility of the authors and does not necessarily represent the official views of the National Institutes of Health.

2.8 Competing interest

The Regents of the University of California have patents issued and pending for CRISPR technologies on which J.A.D. is an inventor and delivery technologies on which J.A.D. and W.N. are co-inventors. J.A.D. is a cofounder of Azalea Therapeutics, Caribou Biosciences, Editas Medicine, Evercrisp, Scribe Therapeutics, Intellia Therapeutics, and Mammoth Biosciences. J.A.D. is a scientific advisory board member at Evercrisp, Caribou Biosciences, Intellia Therapeutics, Scribe Therapeutics, Mammoth Biosciences, The Column Group and Inari. She also is an advisor for Aditum Bio. J.A.D. is Chief Science Advisor to Sixth Street, a Director at Johnson & Johnson, Altos and Tempus, and has a research project sponsored by Apple Tree Partners. A.S has research projects sponsored by Novo Nordisk, Amgen, and Merck. All other authors have no competing interests.

2.9 Supplemental Materials

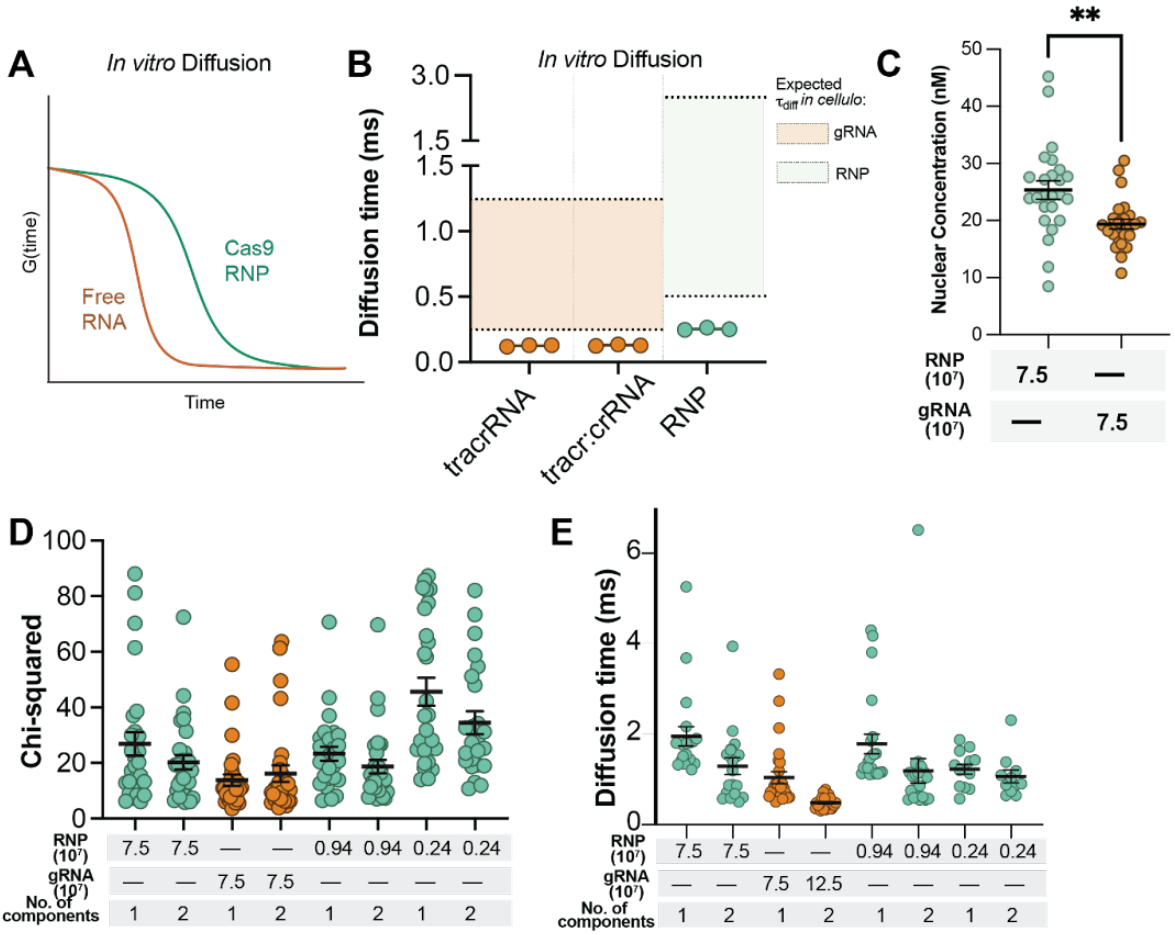

Supplemental Figure 2.1: Optimization of fitting parameters for measuring Cas9 RNP nuclear concentration by fluorescence correlation spectroscopy.
FCS measurements produce an autocorrelation function, which can be fit to derive both the concentration of delivered material and its diffusion time(s). **(A)** Example FCS traces for free

sgRNA versus an intact Cas9 RNP. The diffusion time is calculated as the inflection point of the autocorrelation function. **(B)** FCS traces were measured for tracrRNA, tracr:crRNA, and Cas9 RNP *in vitro* (right). Samples were prepared at a final concentration of 400 nM in DMEM. Each point represents the average diffusion time (t_{diff}) calculated from ten autocorrelation traces at that point. Average t_{diff} for tracrRNA = 0.126 ms, for sgRNA = 0.129 ms, and for Cas9 RNP = 0.253 ms. **(C)** HeLa cells were electroporated with fluorophore labeled gRNA (ATTO™ 550-tracrRNA:crB2M (IDT)) or with RNP pre-complexed 1:1 with fluorophore labeled guide
(7.5×10^7 cas9 per cell). FCS diffusion times provided in ms, n>25 for each FCS condition with at least two biological replicates each (mean ± SEM). **(D)** and **(E)** Comparison of one-component and two-component diffusion fitting equations for FCS data in cells. **(D)** Chi-square (c^2) values for autocorrelation curves fitted with one- or two-component diffusion equations plotted as a function of RNP or sgRNA dosage. Each point represents the c^2 for the fitting of an average autocorrelation curve (calculated as the mean autocorrelation function from ten individual traces) obtained from an individual cell. **(E)** Diffusion times for the autocorrelation curves fitted in **(D)**. For a one-component diffusion equation, only one diffusion time is produced. For a two-component diffusion equation, a fast diffusion and a slow diffusion time are both calculated; the fast diffusion time is plotted here. Each point corresponds to the t_{diff} derived from each fitted autocorrelation curve in **(D)**.

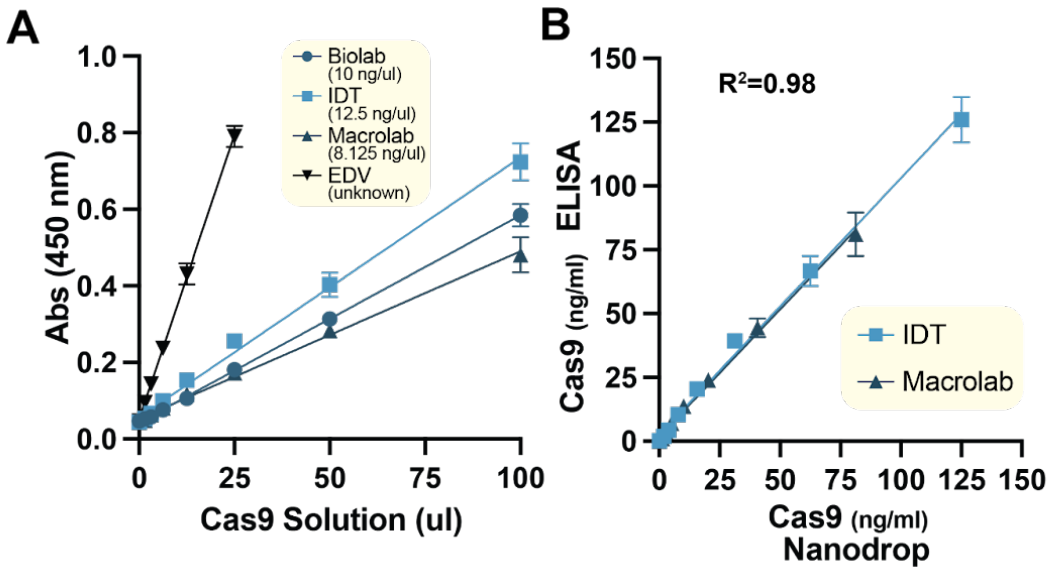

Supplemental Figure 2.2: Validation of ELISA for measuring Cas9 used for electroporation and in EDVs

A) Absorbance values from ELISA for Cas9 as purified RNP diluted 800-fold, from commercial (IDT) and in-house source (UC-Berkeley, Macrolab, QB3), and 20x concentrated EDVs prepared by ultracentrifugation diluted 4-fold (n=3). B) Absorbance values from ELISA used to quantify concentration of Cas9 in commercial (IDT) and in-house (UC-Berkeley, Macrolab, QB3) samples compared to reported concentrations calculated from photospectrometry (Nanodrop) (R^2=0.98, n=3).

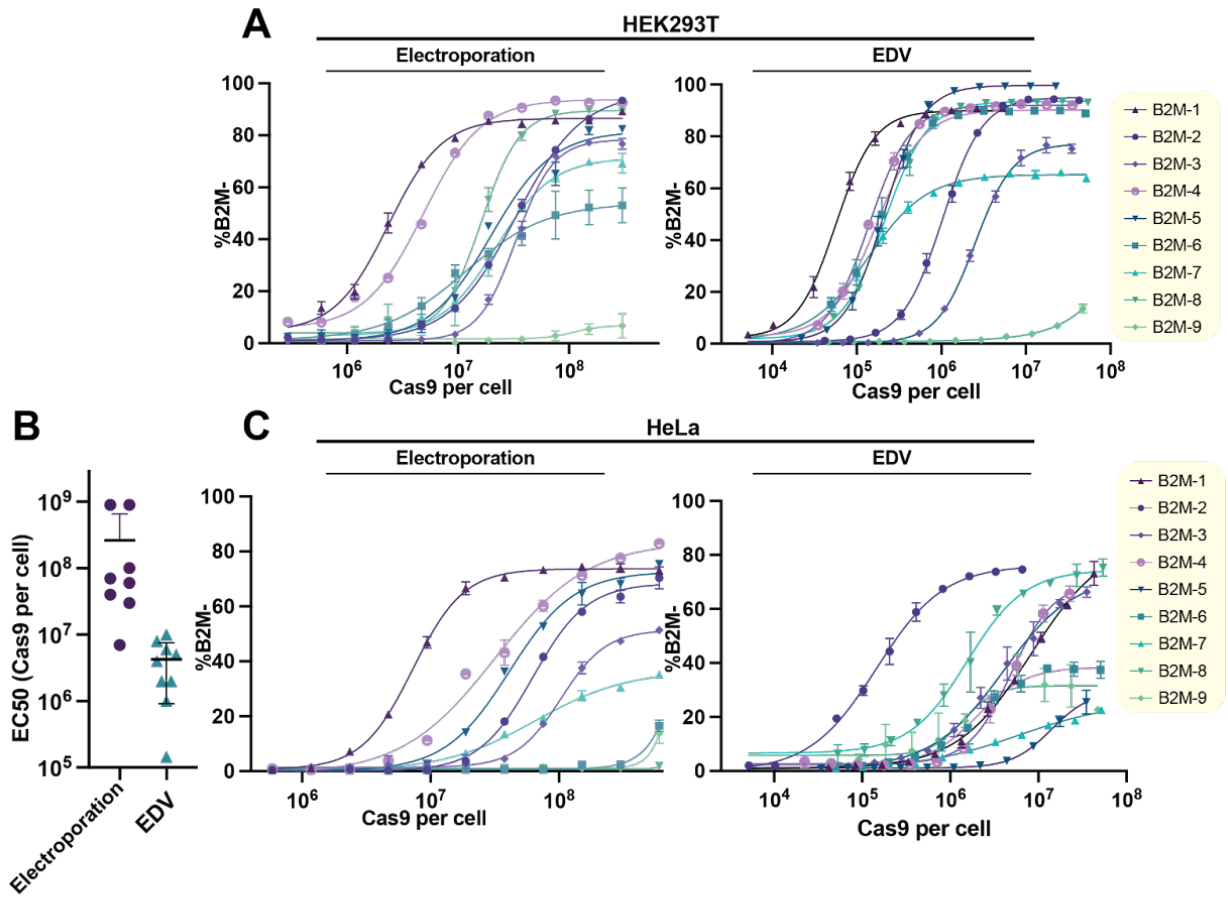

Supplemental Figure 2.3: Cas9 RNP doses required for editing by Electroporation and EDVs

(A) Comparison of required RNP doses delivered by electroporation and EDV for 9 different B2M guides in HeLa. Analysis was performed by flow cytometry 4 days post treatment to assess B2M KO. **(B)** HeLa cells treated with Cas9 RNP complexed with the same 9 guides delivered by (Left) electroporation and (Right) EDVs. Cells were analyzed by flow cytometry on day 4 (n=3). **(C)** HEK293T cells were treated with Cas9 RNP complexed with 9 different guides (Supplemental table 1) targeting B2M delivered by (Left) Electroporation and (Right) EDVs. Cells were analyzed by flow cytometry on day 4 (n=3). Datapoints represent the mean with error bars displaying SD. RNP dose curves were modeled (Prism v10) as sigmoidal (4PL, X is concentration).

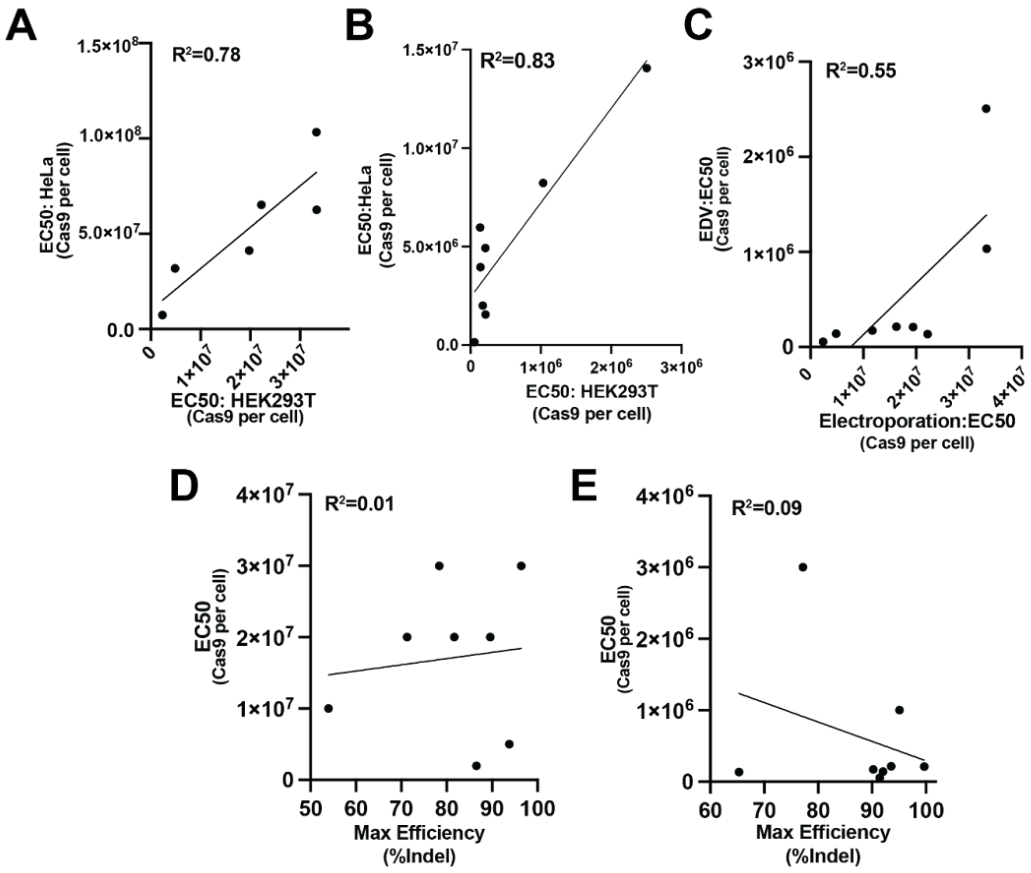

Supplemental Figure 2.4: Analyzing the linear relationships between RNP delivery modalities and guide RNA on editing dosage requirements

Correlation analysis of dosage required for half maximal editing (EC50) from Cas9 RNP delivered by **(A)** Electroporation and **(B)** EDVs in HEK293T (x-axis) and HeLa cells (y-axis).**(C)** Correlation analysis of dosage required for half maximal editing (EC50) from Cas9 RNP delivered by electroporation (x-axis) versus EDV (y-axis). Relationship between gRNA maximum editing efficiency (i.e. the top plateau of dosage curve) versus the dosage EC50 for **(D)** electroporation and **(E)** EDV in HEK293T cells. For correlation analyses, each value calculated from HEK293T HeLa dose curves (Supplemental Figure 3). n=3 technical replicates were used in all experiments.

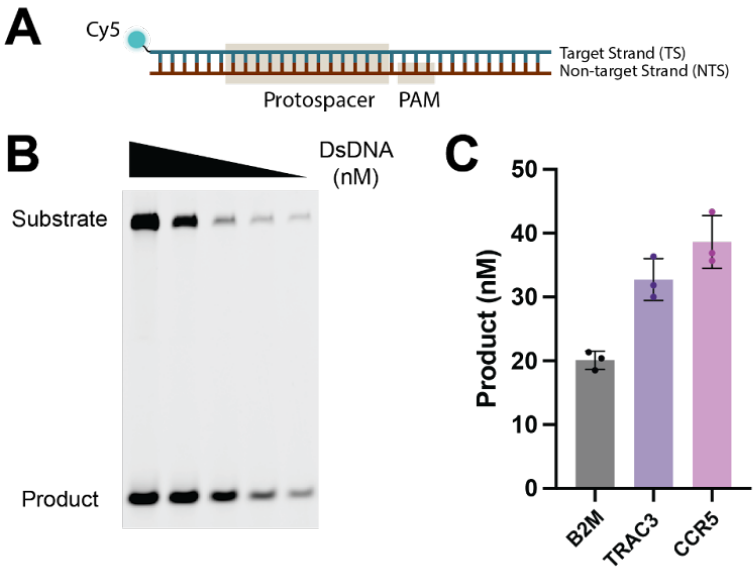

Supplemental Figure 2.5: In vitro cleavage assay to assess percent activity of purified Cas9

(A) Schematic of double-stranded DNA (DsDNA) substrate used for assessing the biochemical cleavage activity of purified Cas9 RNP, a single turnover enzyme [69], by active site titration. The Cy5 fluorophore label is on the 5' end of the target strand. **(B)** Representative gel showing 100 nM Cas9 RNP, complexed with TRAC3 guide, incubated with annealed DsDNA substrate with TRAC3 active site at titrated concentrations. Percent cleavage calculated by same method as [39] **(C)** Comparison of cleavage activity of in-house (UC-Berkeley, Macrolab, QB3) Cas9, complexed with respective sgRNA (IDT), targeting substrates with spacers from B2M, TRAC3, CCR5. n=3 technical replicates were used in all experiments. Datapoints represent the mean with error bars displaying SD. Oligos used are in Supplemental table 1.

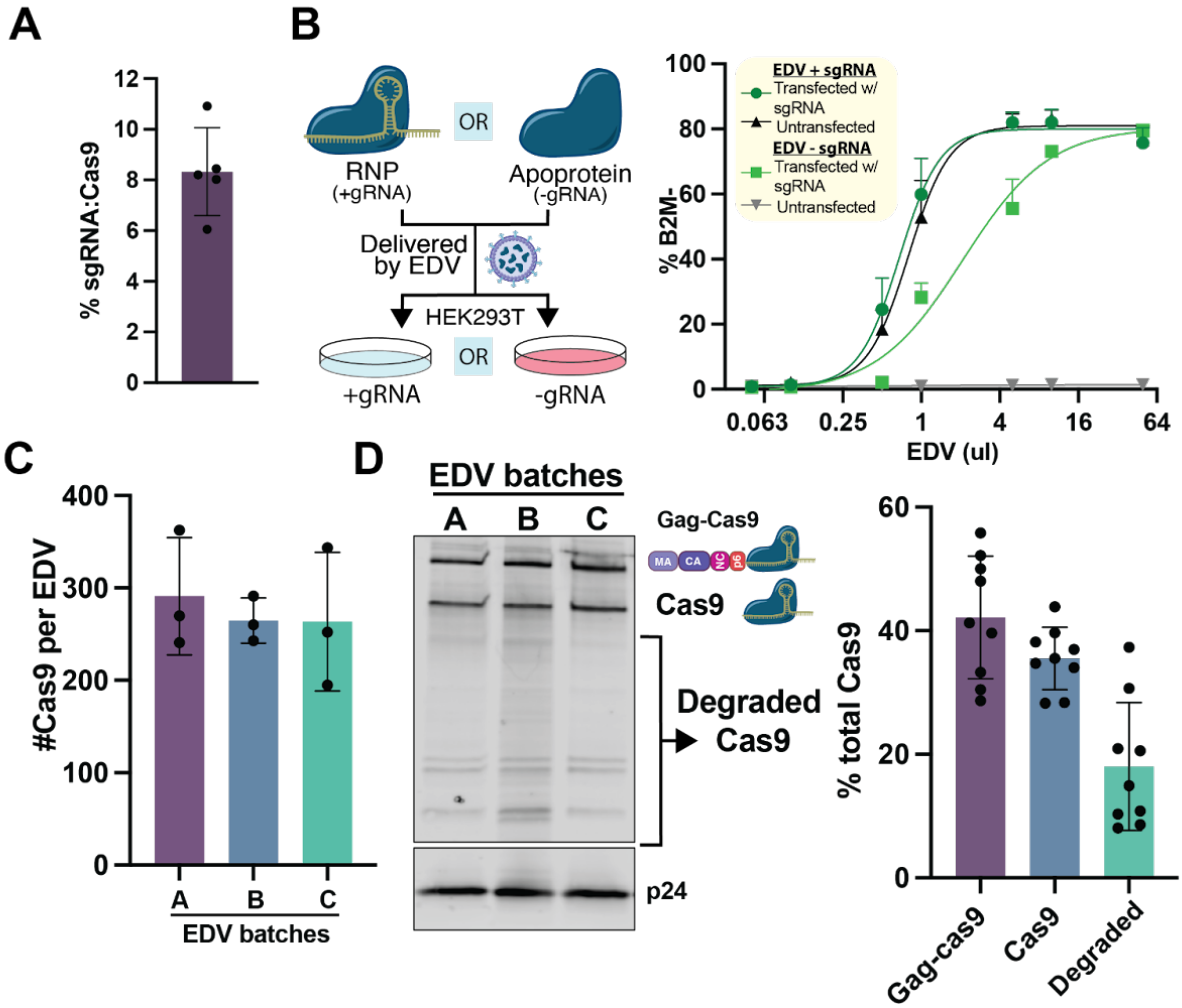

Supplemental Figure 2.6: Determining the percent of RNPs in EDVs that are functional **(A)** The percent of B2M sgRNA available relative to Cas9 protein molecules in EDVs (n=5 biological replicates, mean depicted from 3 technical replicates). The molecules of intact B2M sgRNA and Cas9 protein were determined by quantitative RT-PCR and Cas9 ELISA (n=5 biological replicates measured in triplicate), respectively. **(B)** Schematic of experimental setup to determine whether sgRNA is limiting editing potency of EDVs in cells. HEK293T cells, either untreated or transfected with U6-B2M-sgRNA expression plasmid, were treated with EDVs containing *B2M*-targeting Cas9 RNP or Cas9 apoprotein (n=3). **(C)** B2M knockout was assessed by flow cytometry four days post treatment with minimal difference between conditions where HEK293T cells expressed excess B2M-targeting gRNA versus delivery with EDVs containing *B2M*-targeting Cas9 RNP. **(D)** Quantification of the number of Cas9 molecules per EDV. p24, the capsid protein and a key structural component of EDVs and native HIV, and Cas9 were quantified by ELISA (n=3 biological replicates measured in triplicate). **(E)** Western blot of 20x ultracentrifuged concentrated EDVs for Cas9 and p24 (loading control). **(F)** Densitometry analysis of the percent of total cas9 in EDVs that remains uncleaved from gag-Cas9, free Cas9, and major Cas9 degradation products.

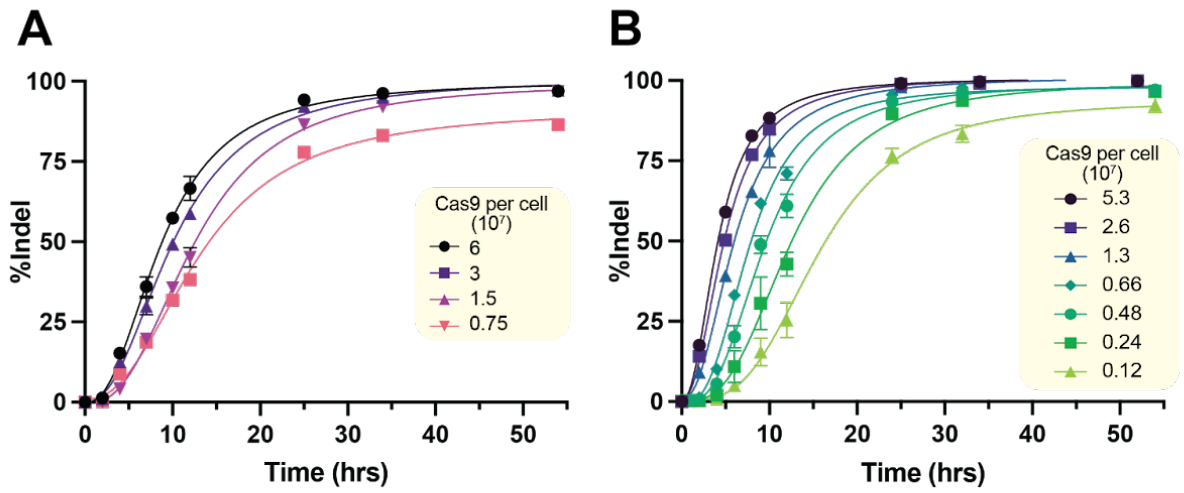

Supplemental Figure 2.7: Indels resulting from Cas9 delivery by electroporation and EDVs

(Relating to Figure 3) Indel formation caused by **(A)** electroporation and **(B)** EDV delivery of *B2M*-targeting RNP in HEK293T cells measured by NGS. All doses are at levels that meet or exceed the amount necessary for 90% maximal editing. The first derivative (rate of indel formation) of these curves is shown in Fig. 3G-H for electroporation and EDV delivery. n=3 technical replicates were used in all experiments. Datapoints represent the mean with error bars displaying SD.

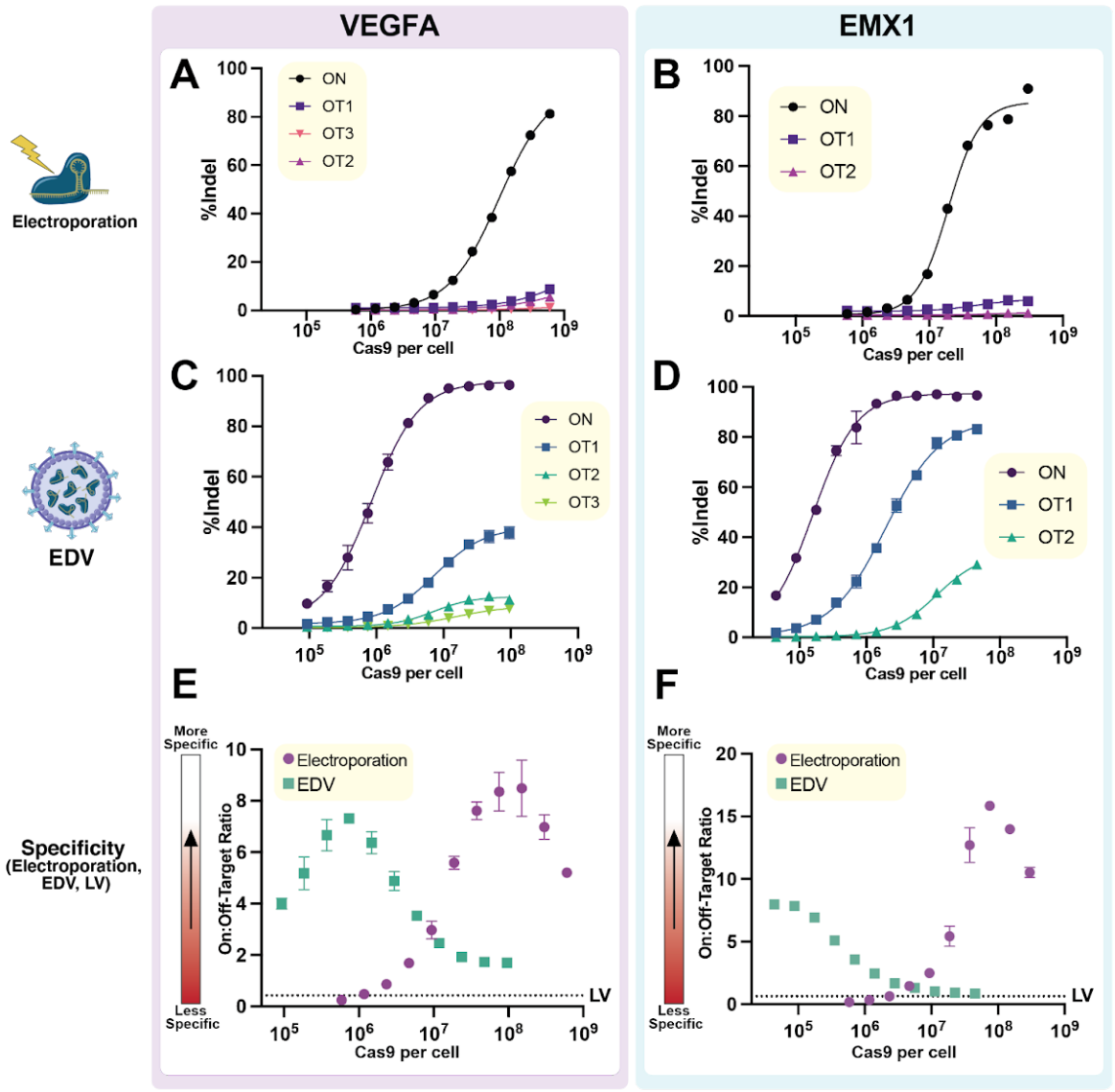

Supplementary Figure 8: Editing specificity resulting from delivery by RNP electroporation and EDVs

On-target and previously established [43] off targets were analyzed by targeted deep sequencing to compare relative editing specificity. Indels resulting from titrated RNP dosages delivered by electroporation targeting **(A)** VEGFA and **(B)** EMX1 at on-target and known off-target sites. Indels resulting from titrated RNP dosages delivered by EDVs targeting **(C)** VEGFA and **(D)** EMX1 at on-target and off-target sites (ON = on-target, OT = Off-target). Comparison of the ratio of on-target indel frequency to the combined off-target indels for lentivirus (LV) versus titrated RNP doses delivered by electroporation and EDVs targeting **(E)** VEGFA and **(F)** EMX1. n=3 technical replicates were used in all experiments. Datapoints represent the mean with error bars displaying SD. NGS primers used for target deep sequencing listed in Supplemental Table 1.

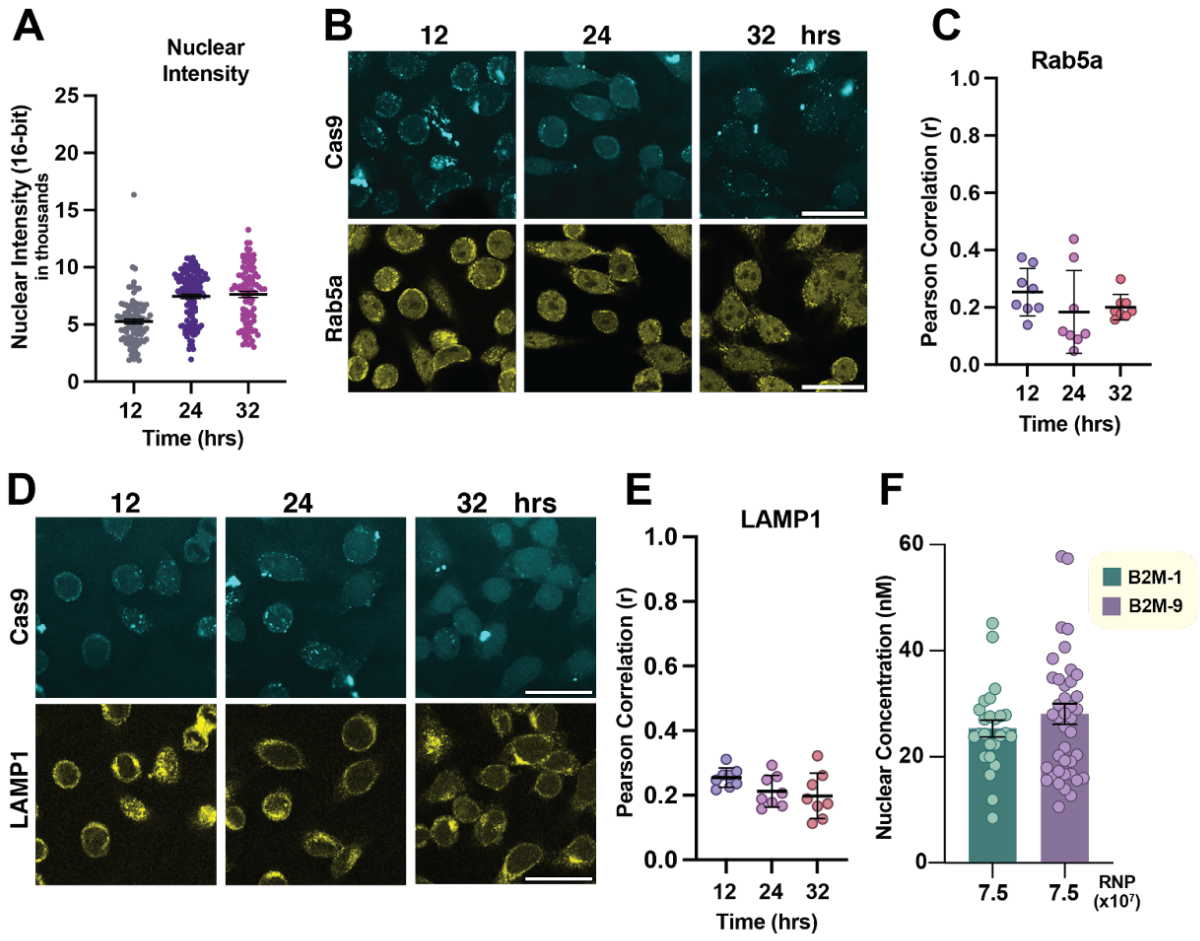

Supplemental Figure 9: Confocal microscopy for relative quantification of electroporated Cas9 RNP in nuclei and endosomes.

(A) Relative quantification of median nuclear intensity of Cas9 delivered by electroporation at 12, 24 and 32 hours in HeLa cells. (Representative images in Fig. 4B). Intensity on 16-bit scale (0 to 65536). Each data point represents an individual nuclei n> 94 (mean ± SEM). (see Methods for details). **(B)** Electroporated HeLa cells at 12, 24 and 32 hours stained to image Cas9 (Above) and Rab5a, an early endosome marker (Below). **(C)** Quantification of the colocalization of Cas9 and Rab5a at 12, 24 and 32 hours. **(D)** Electroporated HeLa cells at 12, 24 and 32 hours stained to image Cas9 (Above) and LAMP1, a lysosomal marker (Below). **(E)** Quantification of the colocalization of Cas9 and LAMP1 at 12, 24 and 32 hours. Each data point represents an independent z-stack (n=8 per time point) quantified with Pearson's correlation analysis (HuygensPro, see Methods for details). **(F)** Comparison of nuclear concentration of electroporated Cas9 ($7.5x10^7$) complexed with high- and poor-performing gRNA (Supplemental Table 1) 24 hours following electroporation by FCS.

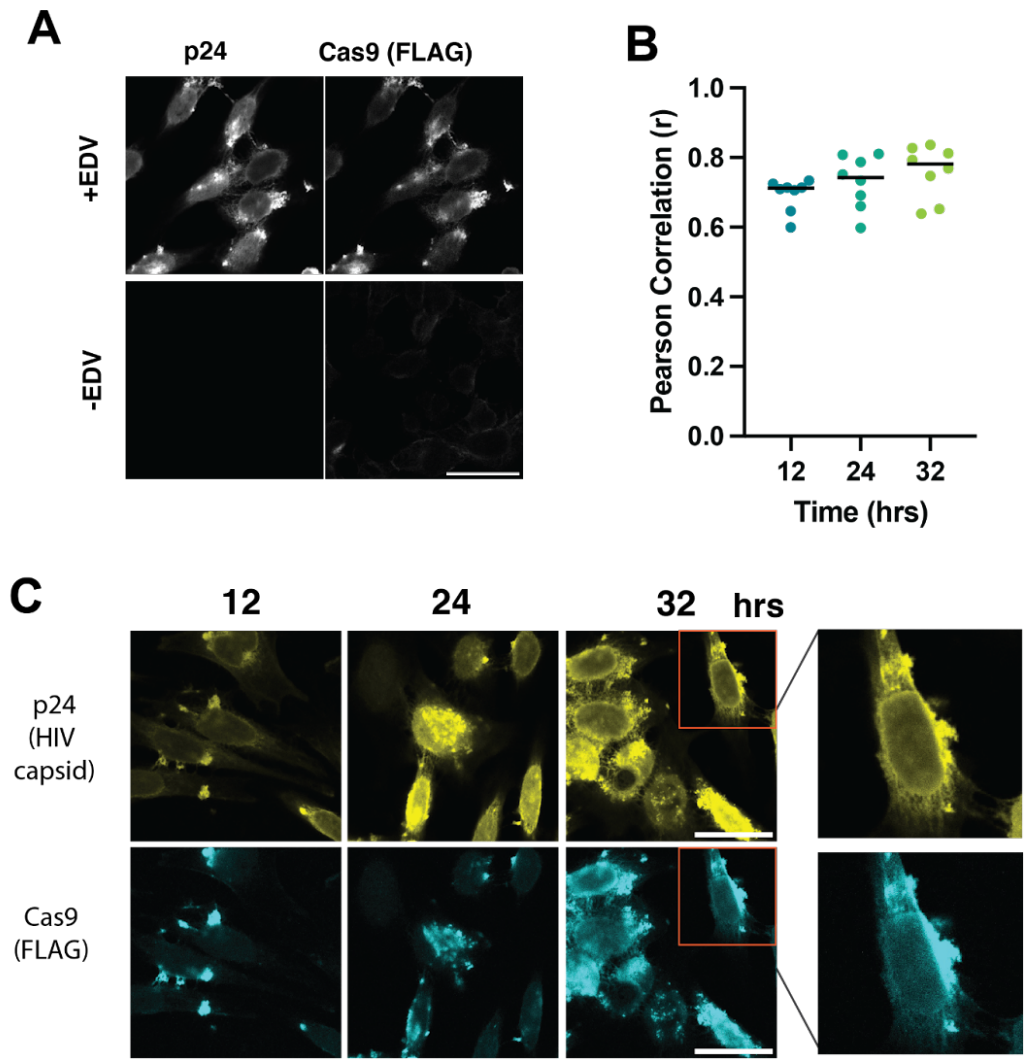

Supplemental Figure 10: Cas9 in EDV remains uncleaved from Gag, HIV structural polyprotein, in cells

(A) Validation of detection specificity for Cas9 and p24, a HIV capsid protein found in EDVs, stained in cells incubated with EDVs (350 ul 20x ultracentrifuged EDV, 1:1 dilution in OptiMEM) or OptiMEM media for 4 hours, then grown in supplemented DMEM until harvest at 32 hours (see Methods for details). Both EDV treated and untreated cells were stained with both primary and secondary antibodies (Supplemental Table 3). **(B)** Quantification of the colocalization of p24, a structural part of gag used in EDV packaging, and Cas9 at 12, 24 and 32 hours. Each data point represents an independent z-stack (n=8) quantified with Pearson's correlation analysis (HuygensPro, see Methods for details). **(C)** Representative images of EDV treated cells at 12, 24 and 32 hours stained to image p24 (Above) and Cas9 (Below), showing consistent colocalization of Cas9 and Gag.

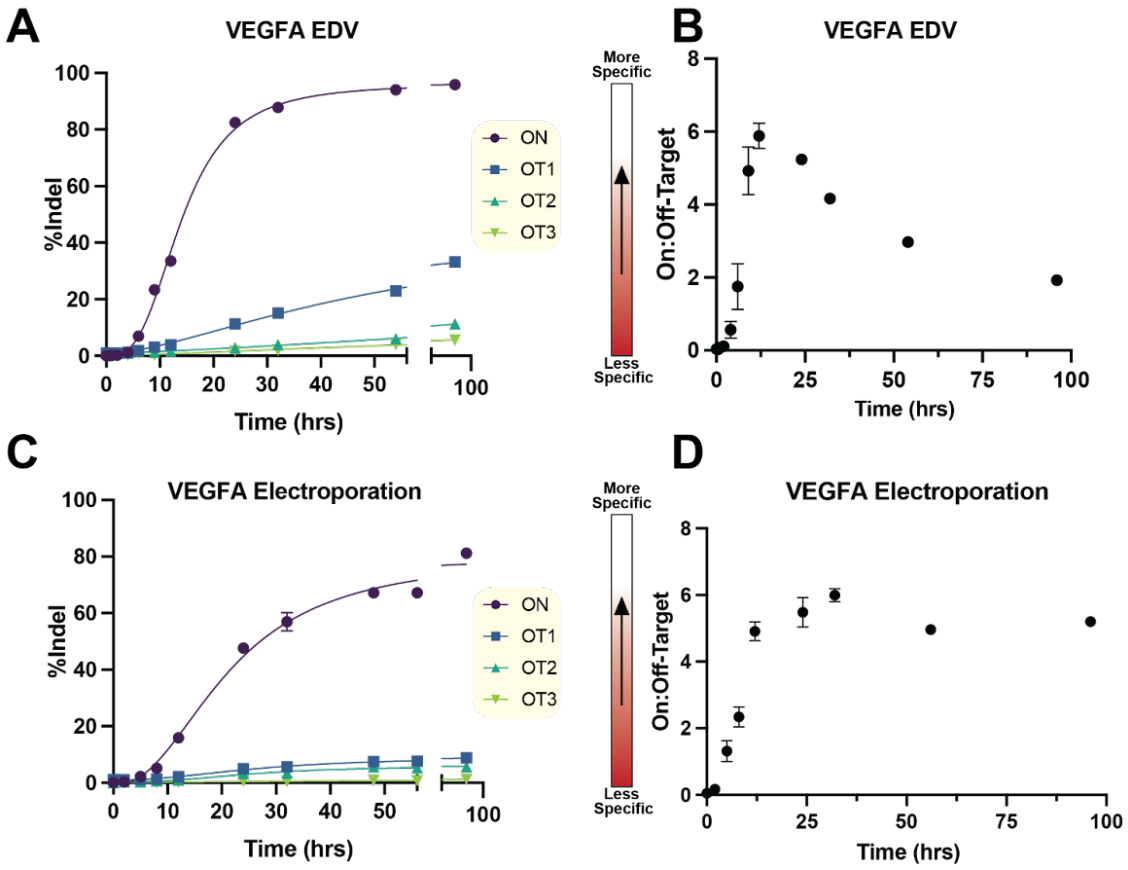

Supplemental Figure 11: Time Course of RNP Editing Specificity delivered by Electroporation and EDV

On-target and previously established [43] off targets were analyzed by targeted deep sequencing to compare relative editing specificity. **(A)** Indels RNP dosages delivered by EDV targeting VEGFA and at on-target and known off-target sites (25 ul of 20x EDV, 3.96 pmol/100k cells, 2.38×10^7 Cas9 per cell). **(B)** Comparison of the ratio of on-target indel frequency to the combined off-target indels over time for EDV delivery. **(C)** Indels RNP dosages delivered by electroporation targeting VEGFA and at on-target and known off-target sites (100 pmol/100k cells, 6.02×10^8 Cas9 per cell) **(D)** Comparison of the ratio of on-target indel frequency to the combined off-target indels over time for electroporation delivery.

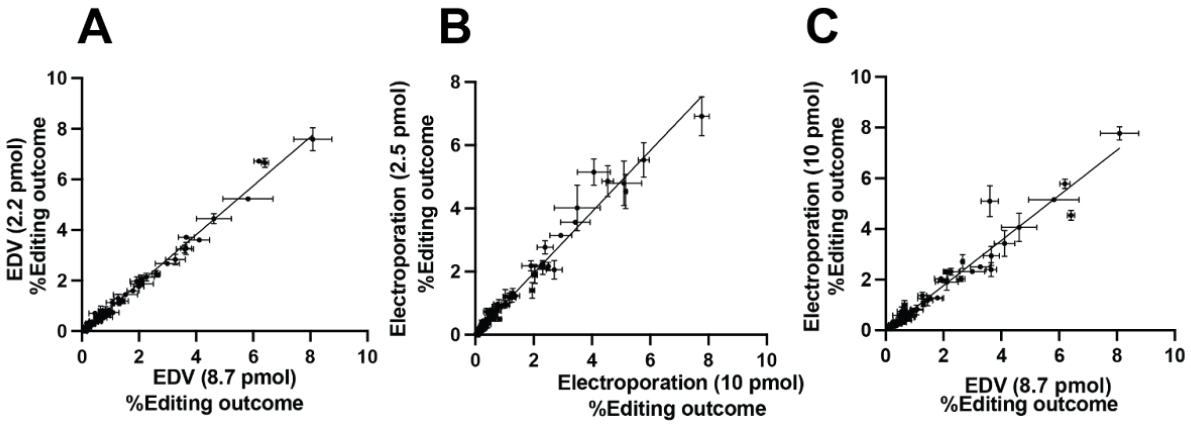

Supplemental Figure 12: Comparison of editing outcomes resulting from Cas9 RNP delivery by electroporation and EDV

Analysis of specific DNA editing repair outcomes resulting from editing dose curves depicted comparing the impact of saturating doses, at or exceeding levels for 90% of the maximum editing (>EC90), of Cas9 RNP targeting B2M delivered by electroporation and EDVs detected by NGS. Analysis was done with HEK293T cells collected at 54 hrs with indel analysis done with CRISPResso2 allele frequency tables [70].

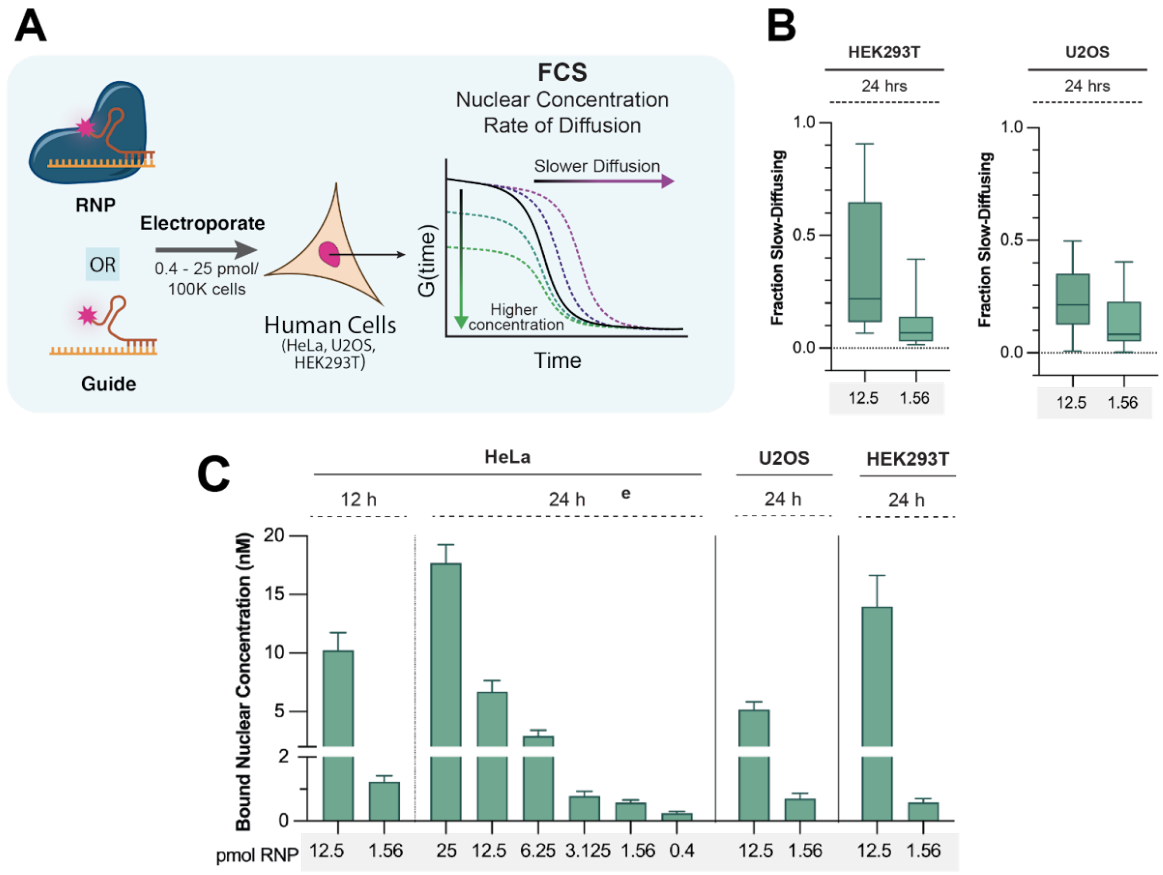

Supplemental Figure 13: Assessing the slow diffusing proportion of Cas9 RNP in HeLa, HEK293T, and U2OS cells.

(A) Human cells were electroporated with fluorophore labeled gRNA (ATTO™ 550-tracrRNA:crB2M (IDT)) or with RNP pre-complexed 1:1 with fluorophore labeled guide. FCS diffusion times provided in ms, n>25 for each FCS condition with at least two biological replicates each (mean ± SEM). HeLa, HEK293T or U2OS cells were electroporated with purified Cas9 complexed (12.5 or 1.56 pmol/100k cells) with fluorophore-labeled B2M guide for 24 hrs before FCS analysis. All concentration values and diffusion times were derived by fitting FCS traces with a two-component 3D diffusion equation (see Methods for more detail). **(B)** FCS analysis of fraction slowly diffusing for (left) HEK293T and (right) U2OS cells. **(E)** Bound nuclear concentration was calculated by multiplying the nuclear concentration of RNP in an individual cell by the fraction slowly diffusing in that same cell. Concentrations are reported for HeLa, U2OS, and HEK293T cells. For FCS values, including experimental and biological replicates, see Supplementary table 2. (Parts of this figure were adapted with permission from Madeline Zoltek).

Supplementary Table 2.1: Oligo sequences

Protospacer	Gene target	fwd oligo	reverse oligo	Source publication	NGS fwd	NGS rev
TAGCTGTGCTCGCGCTACTC	B2M-1	caccTAGCTGTGCTCGCGCTACTC	aaacGAGTAGCGCGAGCACAGCTA	10.1016/j.celrep.2021.109207	GCTCTTCCGATCTagctgacagcattcgggc	GCTCTTCCGATCTgaagtcacggagcgagagag
GAGTCCGAGCAGAAGAAGA	EMX1	caccGAGTCCGAGCAGAAGAAGAA	aaacTCTTCTTCTGCTCGGACTC	10.1038/nbt.4066	GCTCTTCCGATCTCCGGAGGACAAAGTACAAACGGC	GCTCTTCCGATCTAAGCAGCACTCTGCCCTCGTG
GGTGAGTGAGTGTGTGCGTG	VEGFA3	caccGGTGAGTGAGTGTGTGCGTG	aaacCACGCACACACTCACTCACC	10.1038/nbt.4066	GCTCTTCCGATCTCTGGGTGAATGGAGCGAGCAG	GCTCTTCCGATCTGGAAGGCGGAGAGCCGGACA
CTTCAAGAGCAACAGTGCTG	TRAC3	caccCTTCAAGAGCAACAGTGCTG	aaacCAGCACTGTTGCTCTTGAAG	10.1016/j.cell.2023.08.041	GCTCTTCCGATCTTGCCTATTCACCGATTTT	GCTCTTCCGATCTATGCAAAGTCAGATTTGTTG
GGTACCTATCGATTGTCAGG	CCR5sp11	caccGGTACCTATCGATTGTCAGG	aaacCCTGACAATCGATAGGTACC	10.1038/nbt.4066	GCTCTTCCGATCTCTTCTGGGCTCACTATGCTGC	GCTCTTCCGATCTGGTGACCGTCCTGGCTTTTA

Additional B2M sequence. B2M-1 used as default unless otherwise stated.

Protospacer	Target	Foward oligo	Reverse oligo
GAGTAGCGCGAGCACAGCTA	B2M-1	caccGAGTAGCGCGAGCACAGCTA	aaacTAGCTGTGCTCGCGCTACTC
ACTCTCTCTTTCTGGCCTGG	B2M-2	caccACTCTCTCTTTCTGGCCTGG	aaacCCAGGCCAGAAAGAGAGAGT
gCTCGCGCTACTCTCTCTTTC	B2M-3	caccgCTCGCGCTACTCTCTCTTTC	aaacGAAAGAGAGAGTAGCGCGAGc

GGCCACGGAGCGAG ACATCT	B2M -4	caccGGCCACGGAGCG AGACATCT	aaacAGATGTCTCGCTC CGTGGCC
AGGGTAGGAGAGAC TCACGC	B2M -5	caccAGGGTAGGAGAG ACTCACGC	aaacGCGTGAGTCTCT CCTACCCT
ACTCACGCTGGATAG CCTCC	B2M -6	caccACTCACGCTGGAT AGCCTCC	aaacGGAGGCTATCCA GCGTGAGT
CGCGAGCACAGCTA AGGCCA	B2M -7	caccCGCGAGCACAGC TAAGGCCA	aaacTGGCCTTAGCTGT GCTCGCG
GGCCGAGATGTCTC GCTCCG	B2M -8	caccGGCCGAGATGTCT CGCTCCG	aaacCGGAGCGAGACA TCTCGGCC
GCTACTCTCTCTTTC TGGCC	B2M -9	caccGCTACTCTCTCTT TCTGGCC	aaacGGCCAGAAAGAG AGAGTAGC

Anneal dsDNA substates used for in vitro cleavage assay.

Protospacer	Gene target	fwd oligo	reverse oligo
TAGCTGTG CTCGCGCT ACTC	B2M	/5Cy5/gcgagtacgaccttagctgt gctcgcgctactcgctaatgtcatgca cgc	gcgtgcatgacattagcgagtagcg cgagcacagctaaggtcgtactcg c
GGTACCTAT CGATTGTCA GG	CCR5	/5Cy5/gcgagtacgaCCTCCT GACAATCGATAGGTACCg ctaatgtcatgcacgc	gcgtgcatgacattagcGGTAC CTATCGATTGTCAGGAG Gtcgtactcgc
CTTCAAGAG CAACAGTG CTG	TRAC3	/5Cy5/gcgagtacgaCCACAG CACTGTTGCTCTTGAAGg ctaatgtcatgcacgc	gcgtgcatgacattagcCTTCAA GAGCAACAGTGCTGTGG tcgtactcgc

Guide sequence and NGS primers used for targeted deep sequencing specificity analysis.

Protospacer	Target	Fwd primer	Rev Primer
GAGTCCGA GCAGAAGA AGAA	EMX1	GCTCTTCCGATCTCCGGAGGACAA AGTACAAACGGC	GCTCTTCCGATCTAAGCAGCAC TCTGCCCTCGTG
	OT1	GCTCTTCCGATCTCTTTTATACCAT CTTGGGGTTACAG	GCTCTTCCGATCTCTAGGAAA GATTAACAGAGAGTCTGAC
	OT2	GCTCTTCCGATCTCAATGTGCTTC AACCCATCACGGC	GCTCTTCCGATCTCCTCTACTTC ATTGTACTCAAGGTAAG

GGTGAGTG AGTGTGTGC GTG	VEGFA3	GCTCTTCCGATCTCTGGGTGAATG GAGCGAGCAG	GCTCTTCCGATCTGGAAGGCG GAGAGCCGGACA
	OT1	GCTCTTCCGATCTGAAGGGGAGG GGGAAGTCACC	GCTCTTCCGATCTCGTGCGTGC CGCCGTTGATC
	OT2	GCTCTTCCGATCTTCTGTCACCAC ACAGTTACCACC	GCTCTTCCGATCTGTAGTTGCC TGGGGATGGGGTATG
	OT3	GCTCTTCCGATCTCACCTGGCCCA TTTCTCCTTTGAGG	GCTCTTCCGATCTTGGGGACA GCATGTGCAAGCCACA

Supplementary Table 2.2: Summary Values for in cellula FCS Experiments

For all fluorescence correlation spectroscopy (FCS) measurements, *n-BR* refers to the number of biological replicates and *n-Cells* refers to the number of individual cell measurements that passed all final filtering criteria across all biological replicates. The "FCS Mean" corresponds to the average nuclear concentration in nM measured for that condition. The "FCS SEM" is the standard error of the mean for the corresponding nuclear concentration measurement. Unless otherwise specified, the dosage is reported in the number of cas9 molecules per cell ($x10^7$) and in picomoles of Cas9 ribonucleoprotein complex per 10^5 cells.

Cell Type	**Time (hrs)**	**Dosage (Cas9 $x10^7$ per cell)**	**Dosage (pmol/10^5 cells)**	***n* - BR**	***n* - FCS**	**FCS Mean**	**FCS SEM**
HeLa	12	7.5	12.5	2	28	22.1	1.10
HeLa	12	7.5	1.56	2	30	4.41	0.245
HeLa	24	15	25	2	33	38.6	2.58
HeLa	24	7.5	12.5	2	25	25.4	1.59
HeLa	24	7.5 (RNA only)	12.5 (RNA only)	2	26	19.4	0.843
HeLa	24	3.8	6.25	3	37	8.11	0.650
HeLa	24	1.9	3.125	2	28	3.98	0.243
HeLa	24	0.94	1.56	2	37	4.22	0.239
HeLa	24	0.24	0.4	2	34	2.94	0.287

HeLa	36	7.5	12.5	2	40	25.0	1.61
HeLa	36	0.94	1.56	2	42	4.12	0.191
U2OS	24	7.5	12.5	2	26	21.4	1.96
U2OS	24	0.94	1.56	2	21	6.86	2.10
HEK293T	24	7.5	12.5	2	20	30.0	1.98
HEK293T	24	0.94	1.56	2	20	6.28	0.521

Supplementary Table 2.3: Antibodies used for Western Blots and Immunofluorescence microscopy

Antibodies Used:
WB= Western Blot; IF = immunofluorescence; mAb = monoclonal Antibody; pAb = polyclonal antibody

Primary Antibodies:

Antibody target/strain:	Source/Isotype:	Dilution(s) used:	Figures:	Company and Catalog #
CRISPR-Cas9	Rabbit pAb	1:1000 (WB), 1:100 (IF)	Fig. 4B (IF)	Diagenode (#C15310258)
FLAG (DDDDK sequence)	Rabbit Mab (recombinant)	1:250 (IF), 1:2500 (WB)	Fig. 4C (IF), Fig. S6D (WB), Fig. S9A (IF)	Abcam (#ab205606)
HIV1 p24	Mouse Mab	1:250 (IF), 1:1000 (WB)	Fig. S6D (WB), Fig. S9A (IF)	Invitrogen (#MA1-71515)

Secondary Antibodies:

Antibody:	Dilution(s) used:	Figures:	Company and Catalog #

IRDye® 680RD Goat anti-Mouse IgG Secondary Antibody	1:2500 (WB)	Fig. S6D	Licor (Catalog # 926-68070)
IRDye® 800CW Goat anti-Rabbit IgG Secondary Antibody	1:2500 (WB)	Fig. S6D	Licor (Catalog # 926-32211)
Goat anti-Rabbit IgG (H+L) Highly Cross-Adsorbed Secondary Antibody, Alexa Fluor™ Plus 405	1:1000 (IF)	Fig. 4B	Invitrogen (Catalog # A48254)
Alexa Fluor™ 594 Tyramide SuperBoost™ Kit, goat anti-rabbit IgG	Used in accordance with manufacturer's instructions.	Fig. 4D, Fig. S9A	ThermoFisher (Catalog # B40944)
Alexa Fluor™ 488 Tyramide SuperBoost™ Kit, goat anti-mouse IgG	Used in accordance with manufacturer's instructions.	Fig. S9A	ThermoFisher (Catalog # B40941)

Counterstain:	Cellular Compartment:	Dilution(s) used:	Figures:	Company and Catalog #
SYTOX™ Deep Red Nucleic Acid Stain	Nucleus	1:2000 (IF)	Fig. 4B,C	Invitrogen (#S11380)

References

1. Raguram, A., Banskota, S. & Liu, D. R. Therapeutic in vivo delivery of gene editing agents. *Cell* **185**, 2806–2827 (2022).
2. Sinclair, F., Begum, A. A., Dai, C. C., Toth, I. & Moyle, P. M. Recent advances in the delivery and applications of nonviral CRISPR/Cas9 gene editing. *Drug Deliv. Transl. Res.* **13**, 1500–1519 (2023).
3. Jang, H.-K. *et al.* High-purity production and precise editing of DNA base editing ribonucleoproteins. *Sci Adv* **7**, (2021).
4. Cameron, P. *et al.* Mapping the genomic landscape of CRISPR-Cas9 cleavage. *Nat. Methods* **14**, 600–606 (2017).
5. Hendel, A. *et al.* Chemically modified guide RNAs enhance CRISPR-Cas genome editing in human primary cells. *Nat. Biotechnol.* **33**, 985–989 (2015).
6. Wienert, B., Shin, J., Zelin, E., Pestal, K. & Corn, J. E. In vitro-transcribed guide RNAs trigger an innate immune response via the RIG-I pathway. *PLoS Biol.* **16**, e2005840 (2018).

7. Kim, S. *et al.* CRISPR RNAs trigger innate immune responses in human cells. *Genome Res.* **28**, 367–373 (2018).
8. Charlesworth, C. T. *et al.* Identification of preexisting adaptive immunity to Cas9 proteins in humans. *Nat. Med.* **25**, 249–254 (2019).
9. van Haasteren, J., Li, J., Scheideler, O. J., Murthy, N. & Schaffer, D. V. The delivery challenge: fulfilling the promise of therapeutic genome editing. *Nat. Biotechnol.* **38**, 845–855 (2020).
10. Hou, X., Zaks, T., Langer, R. & Dong, Y. Lipid nanoparticles for mRNA delivery. *Nat. Rev. Mater.* **6**, 1078–1094 (2021).
11. Hanlon, K. S. *et al.* High levels of AAV vector integration into CRISPR-induced DNA breaks. *Nat. Commun.* **10**, 4439 (2019).
12. Espinoza, D. A. *et al.* Aberrant Clonal Hematopoiesis following Lentiviral Vector Transduction of HSPCs in a Rhesus Macaque. *Mol. Ther.* **27**, 1074–1086 (2019).
13. Porello, I. & Cellesi, F. Intracellular delivery of therapeutic proteins. New advancements and future directions. *Front. Bioeng. Biotechnol.* **11**, 1211798 (2023).
14. Frangoul, H. *et al.* CRISPR-Cas9 gene editing for sickle cell disease and β-thalassemia. *N. Engl. J. Med.* **384**, 252–260 (2021).
15. Hanna, R. *et al.* S264: Edit-301 shows promising preliminary safety and efficacy results in the phase i/ii clinical trial (Ruby) of patients with severe sickle cell disease using highly specific and efficient ascas12a enzyme. *HemaSphere* **7**, e05170e0 (2023).
16. Kim, S., Kim, D., Cho, S. W., Kim, J. & Kim, J.-S. Highly efficient RNA-guided genome editing in human cells via delivery of purified Cas9 ribonucleoproteins. *Genome Res.* **24**, 1012–1019 (2014).
17. Foss, D. V. *et al.* Peptide-mediated delivery of CRISPR enzymes for the efficient editing of primary human lymphocytes. *Nat Biomed Eng* **7**, 647–660 (2023).
18. Hamilton, J. R. *et al.* Targeted delivery of CRISPR-Cas9 and transgenes enables complex immune cell engineering. *Cell Rep.* **35**, 109207 (2021).
19. Banskota, S. *et al.* Engineered virus-like particles for efficient in vivo delivery of therapeutic proteins. *Cell* **185**, 250–265.e16 (2022).
20. Choi, J. G. *et al.* Lentivirus pre-packed with Cas9 protein for safer gene editing. *Gene Ther.* **23**, 627–633 (2016).
21. Mangeot, P. E. *et al.* Genome editing in primary cells and in vivo using viral-derived Nanoblades loaded with Cas9-sgRNA ribonucleoproteins. *Nat. Commun.* **10**, 45 (2019).
22. Indikova, I. & Indik, S. Highly efficient 'hit-and-run' genome editing with unconcentrated lentivectors carrying Vpr.Prot.Cas9 protein produced from RRE-containing transcripts. *Nucleic Acids Res.* **48**, 8178–8187 (2020).
23. Haldrup, J. *et al.* Engineered lentivirus-derived nanoparticles (LVNPs) for delivery of CRISPR/Cas ribonucleoprotein complexes supporting base editing, prime editing and in vivo gene modification. *Nucleic Acids Res.* **51**, 10059–10074 (2023).

24. Hamilton, J. R. *et al.* In vivo human T cell engineering with enveloped delivery vehicles. *Nat. Biotechnol.* (2024) doi:10.1038/s41587-023-02085-z.
25. Johnson, N. M. *et al.* HIV-based lentiviral vectors: origin and sequence differences. *Mol. Ther. Methods Clin. Dev.* **21**, 451–465 (2021).
26. Ramadoss, G. N. *et al.* Neuronal DNA repair reveals strategies to influence CRISPR editing outcomes. *bioRxivorg* (2024) doi:10.1101/2024.06.25.600517.
27. Strebinger, D. *et al.* Cell type-specific delivery by modular envelope design. *Nat. Commun.* **14**, 5141 (2023).
28. Leibowitz, M. L. *et al.* Chromothripsis as an on-target consequence of CRISPR-Cas9 genome editing. *Nat. Genet.* **53**, 895–905 (2021).
29. Kim, S. A., Heinze, K. G. & Schwille, P. Fluorescence correlation spectroscopy in living cells. *Nat. Methods* **4**, 963–973 (2007).
30. Elson, E. L. Fluorescence correlation spectroscopy: past, present, future. *Biophys. J.* **101**, 2855–2870 (2011).
31. Schwille, P. Fluorescence correlation spectroscopy and its potential for intracellular applications. *Cell Biochem. Biophys.* **34**, 383–408 (2001).
32. Moon, S. B., Kim, D. Y., Ko, J.-H., Kim, J.-S. & Kim, Y.-S. Improving CRISPR genome editing by engineering guide RNAs. *Trends Biotechnol.* **37**, 870–881 (2019).
33. Lazzarotto, C. R. *et al.* CHANGE-seq reveals genetic and epigenetic effects on CRISPR-Cas9 genome-wide activity. *Nat. Biotechnol.* **38**, 1317–1327 (2020).
34. Wu, X. *et al.* Genome-wide binding of the CRISPR endonuclease Cas9 in mammalian cells. *Nat. Biotechnol.* **32**, 670–676 (2014).
35. Monier, K., Armas, J. C., Etteldorf, S., Ghazal, P. & Sullivan, K. F. Annexation of the interchromosomal space during viral infection. *Nat. Cell Biol.* **2**, 661–665 (2000).
36. Doench, J. G. *et al.* Optimized sgRNA design to maximize activity and minimize off-target effects of CRISPR-Cas9. *Nat. Biotechnol.* **34**, 184–191 (2016).
37. Moreno-Mateos, M. A. *et al.* CRISPRscan: designing highly efficient sgRNAs for CRISPR-Cas9 targeting in vivo. *Nat. Methods* **12**, 982–988 (2015).
38. Liu, M.-S. *et al.* Engineered CRISPR/Cas9 enzymes improve discrimination by slowing DNA cleavage to allow release of off-target DNA. *Nat. Commun.* **11**, 3576 (2020).
39. Gong, S., Yu, H. H., Johnson, K. A. & Taylor, D. W. DNA Unwinding Is the Primary Determinant of CRISPR-Cas9 Activity. *Cell Rep.* **22**, 359–371 (2018).
40. Shi, H. *et al.* Rapid two-step target capture ensures efficient CRISPR-Cas9-guided genome editing. *bioRxiv* 2024.10.01.616117 (2024) doi:10.1101/2024.10.01.616117.
41. Chen, K. *et al.* Lung and liver editing by lipid nanoparticle delivery of a stable CRISPR-Cas9 RNP. *bioRxivorg* (2023) doi:10.1101/2023.11.15.566339.

42. Kotnik, T., Rems, L., Tarek, M. & Miklavčič, D. Membrane electroporation and electropermeabilization: Mechanisms and models. *Annu. Rev. Biophys.* **48**, 63–91 (2019).
43. Casini, A. *et al.* A highly specific SpCas9 variant is identified by in vivo screening in yeast. *Nat. Biotechnol.* **36**, 265–271 (2018).
44. Pacesa, M. *et al.* Structural basis for Cas9 off-target activity. *Cell* **185**, 4067–4081.e21 (2022).
45. Knox, S. L. *et al.* Chapter Twenty-One - Quantification of protein delivery in live cells using fluorescence correlation spectroscopy. in *Methods in Enzymology* (ed. Chenoweth, D. M.) vol. 641 477–505 (Academic Press, 2020).
46. Ngo, W. *et al.* Mechanism-guided engineering of a minimal biological particle for genome editing. *bioRxivorg* (2024) doi:10.1101/2024.07.23.604809.
47. Ci, Y., Yang, Y., Xu, C. & Shi, L. Vesicular stomatitis virus G protein transmembrane region is crucial for the hemi-fusion to full fusion transition. *Sci. Rep.* **8**, 10669 (2018).
48. Campbell, B. C. *et al.* mGreenLantern: a bright monomeric fluorescent protein with rapid expression and cell filling properties for neuronal imaging. *Proc. Natl. Acad. Sci. U. S. A.* **117**, 30710–30721 (2020).
49. Karpishin, T. Reducing tissue autofluorescence: Innovations in immunofluorescent analysis boost signal-to-noise ratios: : Innovations in immunofluorescent analysis boost signal-to-noise ratios. *Biotechniques* **64**, 131–131 (2018).
50. Chen, J. *et al.* Engineered Cas9 variants bypass Keap1-mediated degradation in human cells and enhance epigenome editing efficiency. *Nucleic Acids Res.* gkae761 (2024).
51. An, M. *et al.* Engineered virus-like particles for transient delivery of prime editor ribonucleoprotein complexes in vivo. *Nat. Biotechnol.* 1–12 (2024).
52. Lu, Z. *et al.* Lentiviral capsid-mediated Streptococcus pyogenes Cas9 ribonucleoprotein delivery for efficient and safe multiplex genome editing. *CRISPR J.* **4**, 914–928 (2021).
53. Wei, T., Cheng, Q., Min, Y.-L., Olson, E. N. & Siegwart, D. J. Systemic nanoparticle delivery of CRISPR-Cas9 ribonucleoproteins for effective tissue specific genome editing. *Nat. Commun.* **11**, 3232 (2020).
54. Wang, M. *et al.* Efficient delivery of genome-editing proteins using bioreducible lipid nanoparticles. *Proc. Natl. Acad. Sci. U. S. A.* **113**, 2868–2873 (2016).
55. Zhang, Z. *et al.* Efficient engineering of human and mouse primary cells using peptide-assisted genome editing. *Nat. Biotechnol.* (2023) doi:10.1038/s41587-023-01756-1.
56. Tsukamoto, T., Mizuta, H., Sakai, E., Sakurai, F. & Mizuguchi, H. Evaluation of the correlation between nuclear localization levels and genome editing efficiencies of Cas12a fused with nuclear localization signals. *J. Pharm. Sci.* (2024) doi:10.1016/j.xphs.2024.10.029.
57. Luk, K. *et al.* Optimization of nuclear localization signal composition improves CRISPR-Cas12a editing rates in human primary cells. *GEN Biotechnol.* **1**, 271–284 (2022).

58. Gier, R. A. *et al.* High-performance CRISPR-Cas12a genome editing for combinatorial genetic screening. *Nat. Commun.* **11**, 3455 (2020).
59. Zoltek, M. *et al.* HOPS-Dependent Endosomal Escape Demands Protein Unfolding. *ACS Cent Sci* **10**, 860–870 (2024).
60. Zhang, X. *et al.* Dose-Dependent Nuclear Delivery and Transcriptional Repression with a Cell-Penetrant MeCP2. *ACS Cent Sci* **9**, 277–288 (2023).
61. Steinauer, A. *et al.* HOPS-dependent endosomal fusion required for efficient cytosolic delivery of therapeutic peptides and small proteins. *Proc. Natl. Acad. Sci. U. S. A.* **116**, 512–521 (2019).
62. Petrov, E. P. & Schwille, P. State of the art and novel trends in fluorescence correlation spectroscopy. in *Springer Series on Fluorescence* 145–197 (Springer Berlin Heidelberg, Berlin, Heidelberg, 2008).
63. Kaur, G. *et al.* Probing transcription factor diffusion dynamics in the living mammalian embryo with photoactivatable fluorescence correlation spectroscopy. *Nat. Commun.* **4**, 1637 (2013).
64. Knight, S. C. *et al.* Dynamics of CRISPR-Cas9 genome interrogation in living cells. *Science* **350**, 823–826 (2015).
65. Cimarelli, A. & Darlix, J.-L. Biomedicine and Diseases: Review¶Assembling the human immunodeficiency virus type 1. *Cell. Mol. Life Sci.* **59**, 1166–1184 (2002).
66. Tsuchida, C. A. *et al.* Mitigation of chromosome loss in clinical CRISPR-Cas9-engineered T cells. *Cell* **186**, 4567–4582.e20 (2023).
67. Rose, J. C. *et al.* Rapidly inducible Cas9 and DSB-ddPCR to probe editing kinetics. *Nat. Methods* **14**, 891–896 (2017).
68. Dunn, K. W., Kamocka, M. M. & McDonald, J. H. A practical guide to evaluating colocalization in biological microscopy. *Am. J. Physiol. Cell Physiol.* **300**, C723–42 (2011).
69. Sternberg, S. H., Redding, S., Jinek, M., Greene, E. C. & Doudna, J. A. DNA interrogation by the CRISPR RNA-guided endonuclease Cas9. *Nature* **507**, 62–67 (2014).
70. Clement, K. *et al.* CRISPResso2 provides accurate and rapid genome editing sequence analysis. *Nat. Biotechnol.* **37**, 224–226 (2019).

CHAPTER THREE

Spatiotemporal profiling of the impact of CRISPR RNP delivery modality on intracellular Uptake

3.1 Abstract

Intracellular protein delivery is critical to the development of novel therapies and fundamental research. For gene therapies, delivering CRISPR ribonucleoproteins (RNPs), rather than DNA or RNA, can result in comparable editing while mitigating undesirable clinical outcomes, such as off-target editing and increased immunogenicity, that can arise from extended gene editor expression. However, robust protein delivery, particularly *in vivo*, remains challenging, largely because endosomal entrapment leads to cargo being degraded without achieving any therapeutic function. *Ex vivo* electroporation disrupts the cell membrane offering direct access to the cytosol, enabling efficient nuclear entry but also triggering significant cell damage and death. Alternative delivery strategies, including enveloped delivery vehicles (EDVs) and cell-penetrating peptides delivered *in trans* (PERC), trigger endocytosis which can safeguard cell integrity but requires subsequent endosomal escape prior to nuclear localization. To identify prominent delivery bottlenecks and commonalities, we utilized spatiotemporally resolved proteomics to compare RNP delivery by electroporation, EDVs, and PERC, in HEK293T and T-cells. This workflow uncovered cell-type differences in uptake for EDVs and PERC. Regardless of delivery strategy, Cas9 associates with endogenous RNA binding proteins and localizes to the nucleoli prior to degradation. This method enables flexible comparison of Cas9 RNP delivery strategies, and the impact of cell-type on uptake mechanism.

3.2 Introduction

CRISPR gene therapies have enormous potential to cure disease with underlying genetic etiologies; however, safe and effective delivery of gene editors, especially *in vivo*, remains a limiting obstacle. Delivering RNP, rather than nucleic acid, reduces the time period that gene editors reside in the cells, minimizing undesirable clinical outcomes from off-target edits[1] or immune response[2–5]. In contrast to mRNA strategies, RNP delivery bypasses the need for *in situ* translation of mRNA[6] and protects the guide RNA (gRNA) due to the high affinity binding of the Cas9 protein[7] which may enable higher in vivo editing efficacy in difficult to edit cell types, and result in lower levels of toll-like receptor activation[2,8]. RNP delivery fundamentally avoids risks of random DNA integration posed by viral delivery strategies, including lentivirus[9] and adeno-associated virus (AAV)[10].

The idealized goal of RNP-delivery is to deliver only sufficient RNP into every target cell to mediate the intended genome modifications. Higher levels of dosing, particularly *in vivo*, increases the risk of adverse effects, resulting from the immune response to the RNP[4] or vehicle, off-target editing[11], or cytotoxicity[12,13]. While progress has been made on both delivery and endosomal escape[14,15], effective intracellular protein delivery, particularly in the strictly dosage-limited context of *in vivo* therapies, remains a challenge. Therefore, reducing the gene editor dose necessary for

therapeutic effect, both systemically and in individual cells, is paramount to improve the safety and efficacy of emerging gene therapies.

Enormous engineering efforts have led to the development of many promising RNP delivery strategies[16]. RNP electroporation is the most commonly used protein-based delivery strategy, with multiple clinical therapies[17] utilizing it for treatment of hematopoietic indications[18]. RNP electroporation is less cytotoxic than nucleic acid electroporation[19], is effective in many primary cell types[18,20,21], and has a better safety profile than delivery systems that result in extended gene editor expression[1]. However, RNP electroporation requires an *ex vivo* approach, limiting its utility in many therapeutic applications. Furthermore, electroporation can impact cell viability and metabolism[22], which increases manufacturing costs for cell-based therapies[22]. Recently it has been shown that fusion of TAT, a peptide from HIV which is shown to promote cellular adsorption and endocytosis[23,24], fused to the endosomolytic peptide, HA2 from influenza[25], allows for highly efficient delivery of RNPs when delivered *in trans*[22,26] to activated T-cells. However, it is unclear how generalizable this emerging approach is to other cell-types or *in vivo*. EDVs, derived from human immunodeficiency virus (HIV), have the structural components of HIV, but package SpyCas9 RNPs[27–30]. EDVs, leverage the advantages of lentivirus, while mitigating the risk of lentiviral genome integration or extended transgene expression.

Despite extensive development of RNP-based gene therapies, and substantial evidence that gene editor dose is intrinsically linked to its therapeutic safety profile[1,4], little is known about the intracellular pharmacokinetics of RNPs. To date, numerous native and engineered Cas9 variants have been identified[31,32]. However, these bacterial systems are not naturally present in human cells, and how these CRISPR gene editors are processed and subsequently degraded is poorly understood. Degradation of foreign proteins is intimately associated with their immunogenicity[33,34], and understanding of Cas9 degradation could facilitate engineering of variants with reduced immunogenicity, which may allow for repeat dosing strategies. In addition, recent work[35] showed that extending protein half-life may improve the efficacy of Cas9 fusion editors, such as epigenome editors. Elucidation of Cas9 degradation pathways could facilitate engineering of longer-lived Cas9, allowing for similar therapeutic editing at substantially lower doses. RNPs must traffic to the nucleus to make a genome modification, but the impact of different delivery strategies on the timeframe and mechanisms of RNP nuclear entry and subsequent degradation remains enigmatic.

In this study, we utilize spatiotemporally resolved proteomics to quantify the impact of delivery modality on RNP intracellular trafficking and localization. APEX2[36] is a proximity labeling enzyme which, in the presence of exogenous biotin and H_2O_2, biotinylates endogenous proteins within a ~20 nM radius[36]. APEX2 labeling occurs in a brief time frame, less than a minute, enabling snapshots of the proteome that are restricted spatially and temporally[36]. Proximity labeling enzymes are typically expressed as a genetic fusion to a protein of interest[37,38], and previous reports have utilized expressed Cas9-APEX2 fusions to identify proteins involved at particular DNA regions[39,40]. However, Cas9 is not a native protein, and gene therapies require that Cas9 be delivered exogenously into cells. We developed Cas9-APEX2 RNPs that enable flexible, cell-type comparison of different RNP-based delivery strategies.

RNP delivery strategies that leverage active endosomal uptake into the cell, including EDV and PERC, exhibit dramatically different efficiencies depending on cell type. These differences are not explainable by differential expression of the receptors required for uptake. For example, PERC leverages the highly cationic TAT peptide for cell which is known to bind extensively to anionic proteoglycans, such as heparan sulfate proteoglycan (HSPG)[41]. These proteoglycans are highly overexpressed in many immortalized cell lines, including HEK293T, and scarcely present in T cells. Despite this, we found that PERC fails to work robustly in HEK293T and is nearly comparable to electroporation in T cells[22]. Similarly, VSV-G pseudotyped EDVs should require the low density lipoprotein receptor (LDLR) for efficient entry, yet editing efficiencies contradict what would be predicted from LDLR expression. LDLR is highly expressed in T cells, and hardly expressed in HEK293T, but we found that EDV delivery into HEK293T is dramatically more efficient than in T cells. To elucidate additional protein interactions involved in differential cell type delivery efficiency, we compared the spatiotemporal profile of HEK293T cells and activated T cells. We found that delivery of Cas9-APEX2 fusions allowed for specific enrichment of known interactors of HIV machinery involved in EDV delivery and TAT-HA2 peptide used in PERC delivery. PERC peptides still mediate RNP association with the cell membrane surface, but fail to be efficiently taken into the cell at an early time point (2 hours). Regardless of delivery strategy, following internalization Cas9 associates with endogenous RNA binding proteins and localizes to the nucleoli prior to degradation. This method enables investigation of the impact of delivery modality on RNP intracellular trafficking, and will identify prominent delivery bottlenecks and commonalities that will promote engineering of improved RNP-based gene therapies.

3.3 Results

3.3.1 Cas9-APEX2 ribonucleoproteins for genome editing and APEX2 proximity labeling

We have generated *S. pyogenes* Cas9 fused to APEX2[36] to enable spatiotemporally resolved proteomic analysis of protein-based intracellular delivery. Our SpyCas9-APEX2 fusion (Fig. S3.1) is an adaptation of the triNLS variant[22] which has multiple NLS motifs to allow for efficient RNP nuclear localization and editing when electroporated and also facilitate effective CPP delivery[22].

We confirmed that the APEX Spy-APEX2 fusion is able to mediate efficient biotinylation of endogenous proteins and edit efficiently when electroporated (Fig. 3.1B,C) or delivered by EDVs (Fig. 3.1D,E) or PERC (Fig. 3.1F,G) into human cells. APEX2-based proteomics utilizes biotin phenol (BP) and hydrogen peroxide to label nearby (<20 nM) tyrosine residues through an oxidative radical mechanism [36]. Previous work showed that the amount of Cas9 RNP required for editing differs substantially between RNP delivery modalities[42], with EDV delivery requiring approximately 30-fold less Cas9 protein for comparable editing efficiency in human cell lines.

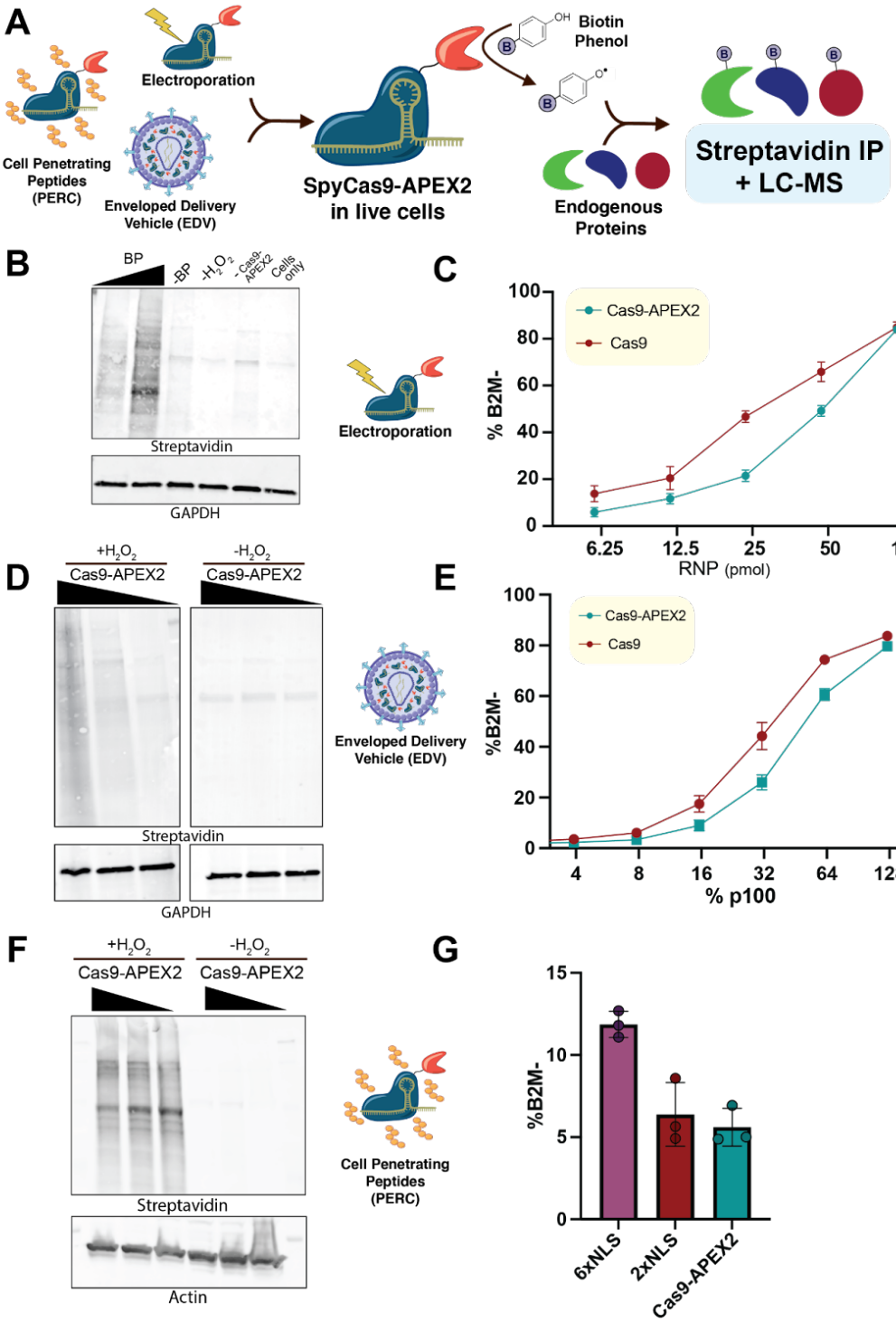
A
Electroporation
Cell Penetrating Peptides (PERC)
Enveloped Delivery Vehicle (EDV)
SpyCas9-APEX2 in live cells
Biotin Phenol
Endogenous Proteins
Streptavidin IP + LC-MS
B
BP
-BP
-H2O2
Cas9-APEX2
Cells only
Streptavidin
GAPDH
Electroporation
C
Cas9-APEX2
Cas9
% B2M-
RNP (pmol)
D
+H2O2
-H2O2
Cas9-APEX2
Streptavidin
GAPDH
Enveloped Delivery Vehicle (EDV)
E
Cas9-APEX2
Cas9
%B2M-
% p100
F
+H2O2
-H2O2
Cas9-APEX2
Streptavidin
Actin
Cell Penetrating Peptides (PERC)
G
%B2M-
6xNLS
2xNLS
Cas9-APEX2

Fig. 3.1 Establishing SpyCas9-APEX2 fusion for proximity labeling of RNP delivery

(A) Schematic of Spatiotemporal profiling of Cas9 RNP delivery by Electroporation, EDVs and PERC. In the presence of exogenous biotin phenol (BP) and H_2O_2 this fusion biotinylates endogenous proteins (~20 nm radius). **(B)** Conditional Biotinylation labeling reaction following electroporation of Cas9-APEX2. Biotinylation only occurs in presence of Cas9-APEX, BP and H_2O_2, and is more defined at higher BP concentrations (0.5 to 2.5 mM). **(C)** Dose titration of Cas9 and Cas9-APEX2 fusion with guide targeting *B2M* showing that purified Cas9-APEX2 fusion retains comparable editing activity following electroporation in HEK293T. Analysis was performed by flow cytometry 4 days post treatment to assess B2M knockdown. **(D)** Biotinylation by Cas9-APEX2 RNP delivered by EDVs in HEK293T. Biotinylation intensity is dose dependent by EDV dosage. **(E)** EDV Dose titration of Cas9 and Cas9-APEX2 fusion with guide targeting *B2M* in HEK293T. Analysis was performed by flow cytometry 4 days post treatment to assess B2M knockdown. **(F)** Biotinylation by Cas9-APEX2 RNP delivered by PERC in HEK293T. Cas9-APEX2 complexed gB2M (1:1.5) and then incubated with 20-fold excess HA2-TAT peptide prior to application on cells. **(G)** PERC dose titration of Cas9 and Cas9-APEX2 fusion with guide targeting *B2M* in HEK293T. Analysis was performed by flow cytometry 4 days post treatment to assess B2M knockdown. n=3 technical replicates were used in all dose titration experiments. Datapoints represent the mean with error bars displaying SD.

3.3.2 RNP delivery modality specific quantitative proteomics

We hypothesized that by comparing the spatiotemporal profile enriched in HEK293T and activated T cells that we could identify what cellular interactions underlie the cell-type discrepancies in delivery efficiency (Fig. 3.2A). Briefly, HEK293T or activated T cells were either treated with Cas9-APEX2 RNPs delivered by electroporation, EDVs or PERC or left untreated. After 90 minutes, both RNP treated and control cells were incubated in 2.5 mM BP for ~45 minutes and then activated with 1 mM H_2O_2 for one minute. Following the biotinylation reaction, streptavidin magnetic beads were used to enrich biotinylated proteins from cell lysates. Western blot analysis of the input cell lysate and eluate confirmed that the biotinylated proteins were successfully enriched (Fig. S3.2) for the experimental samples. Next, we digested the protein bound to the beads with trypsin to generate peptides for quantitative bottom-up proteomics, where peptides are analyzed by liquid chromatography tandem mass spectrometry (LC MS/MS). To facilitate deeper proteomic coverage and robust quantification, isolated and normalized peptides were labeled with the TMT-6plex, with both the experimental and control conditions being analyzed in triplicate. For the electroporation samples, we identified a total of 3503 and 2194 proteins in the HEK293T and T cells, respectively (Supplementary table 1). For the EDV samples, we identified a total of 1081and 1582 proteins in the HEK293T and T cells, respectively. The biotinylation fingerprint for Cas9-APEX2 was typically fainter than that of the electroporation and PERC blots (Fig. 3.1) consistent with the fact that less total Cas9-APEX2 per cell is required for editing by EDVs than electroporation[42]. For PERC, we identified a total of 3594 and 2039 proteins in the HEK293T and T cells, respectively (Supplementary table 1).

To our knowledge, our study is the first to utilize a proximity labeler delivered exogenously to study interactions involved in intracellular uptake. To validate that our Cas9-APEX2 fusions were labeling endogenous proteins involved in delivery we first

looked at the degree of enrichment of previously validated HIV protein interactions which are involved in EDV delivery. The structural components of EDVs[27,43] are derived from HIV which has been extensively studied. In particular, gag polyprotein used to package Cas9 into EDVs has extensive interactions with human host cell machinery, particularly around the nucleus, and impacts many aspects of RNA regulation, including RNA export, chromatin remodeling, splicing and transcription[44]. A region of the HIV gag polyprotein, TAT, interacts extensively with many cellular proteins[41,45], and is implicated in enhancing transcription initiation by promoting assembly of the RNA polymerase II assembly by recruiting various transcription factors[46]. Lastly, VSV-G has a well understood fusion mechanism, binding to LDL-R on the cell surface, and then mediating fusion following endosomal acidification[47]. Many of these proteins, including HSPG2 and LDL-R and associated proteins, such as LRP4 and LRP6[48], were only identified in the Cas9-APEX2 treated cells. Consistent with recent work[42,49] showing that Cas9 delivered by EDVs results in substantial accumulation around the nuclear envelope, many nuclear pore proteins were hits, including NUP107, NUP207, NUP85 and importin-11[50].

Previous research identified 283 gag protein interactors[44] which represents approximately 1.4% of human proteins but more than 6.0% and 8.1% of the total enriched (>1 Experimental:Control) hits in our HEK EDV and T cell EDV data sets, which is a 4.3 and 5.8 fold enrichment (Fig. 2C,D). Similarly, known nuclear TAT peptide interactors represent 0.9% of human proteins, but 4.27% and 4.58% of enriched proteins in the HEK EDV and T-cell EDV datasets. This is notable, because this is an extremely minor difference in enriched protein enrichment, but editing by EDVs in activated T cells is substantially less efficient than in cell lines (Fig. S3.3).

For PERC, TAT interactors are highly enriched in the T-cells (10.4x) but only minorly enriched in the HEK (2.7x) data set (Fig. 3.2). This is consistent with the relatively low efficiency of PERC-mediated editing (5-12%) compared to the efficiency in T-cells, which is nearly comparable to electroporation.

One caveat of APEX2 labeling is that it labels both direct and indirect proteins, leading to a large number of protein identifications. Many of the TAT and GAG interaction partners identified are expressed in the nucleus, so we sought to confirm that their enrichment was not merely due to the nuclear localization of Cas9. Nucleoplasm proteins make up 34% of total proteins with known subcellular locations (6842/20161) and were only minorly enriched in the HEK EDV (>1 Experimental:Control) pulldown (41.4%, 447/1080) and T-cell EDV datasets (39.2%, 621/1583).

TAT is extensively cationic[23,45] and binds to the membrane, particularly at anionic motifs on the cell surface, including proteoglycans. Therefore, we sought to confirm that the enrichment for HSPG and associated proteins was not due to overall membrane protein enrichment. Membrane proteins make up 11.9% of experimentally validated human proteins (2400/20161) and 9.5% of the T-cell PERC (>1 Experimental:Control) datasets. Combined, these results are indicative that the enrichment of TAT and GAG interactors is unlikely to be due to mere nuclear or membrane localization and that the Cas9-APEX2 fusion is enriching for previously validated protein interactions.

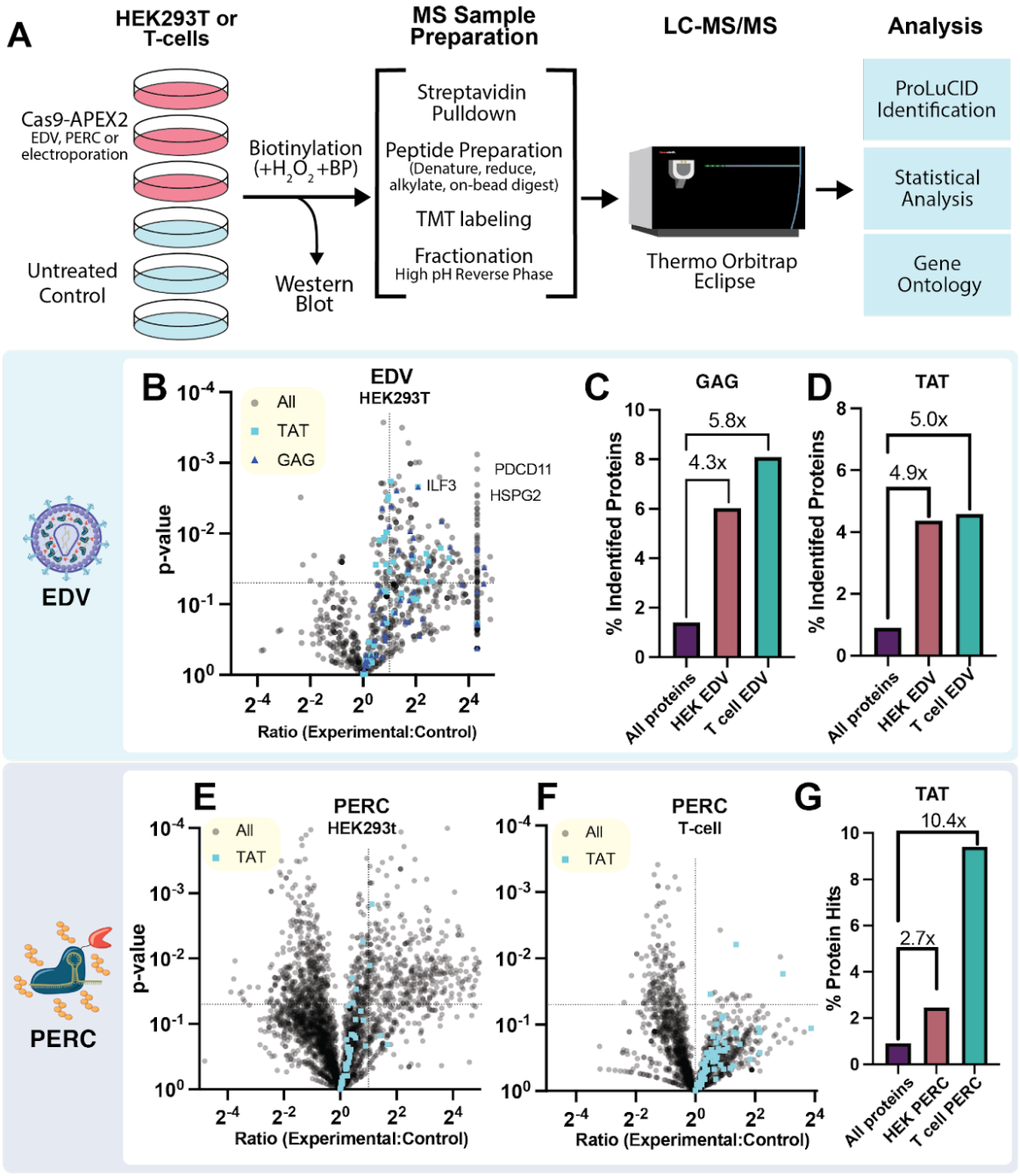

Fig. 3.2: SpyCas9-APEX2 fusion enriches RNP-delivery specific protein interactions.

(A) Schematic overview of proteomics workflow to identify protein interactions of Cas9 RNP following delivery by electroporation, EDVs, and PERC. Two hours following RNP delivery into HEK293T or T cells, SpyCas9-APEX2 treated and non-treated control cells were incubated with BP for 45 minutes and then treated with H2O2 to initiate biotinylation. Cell lysates were incubated with streptavidin to enrich for biotinylated protein, and thoroughly

washed prior to tryptic digestion. Peptides were TMT labeled and equally mixed prior to high pH reversed-phase fractionation. MS data was acquired by Thermo Eclipse LC MS/MS and processed using ProLuCID. **(B)** Volcano plot of proteins identified by proximity labeling MS (APEX2-MS) in HEK293T EDV. Previously identified HIV TAT[46] peptide and GAG[44] polyprotein interactions found in the enriched protein dataset (Experimental: Control intensity >1) are highlighted. **(C)** Previously identified GAG protein interactors are 1.4% of total human proteins (284 GAG[44] associated / 20161 human proteins[50]) are 6.0% and 8.1% of the proteins in the enriched HEK293T and activated T-cell EDV datasets. **(D)** Previously identified TAT peptide interactors are 0.9% of total human proteins (183 TAT associated / 20161 human proteins[50]) are 4.4% and 4.6% of the proteins in the enriched HEK293T and activated T-cell EDV datasets. **(E)** Volcano plot of proteins identified by proximity labeling MS (APEX2-MS) in HEK293T PERC. Previously identified HIV TAT[46] peptide interactions found in the enriched protein dataset (Experimental: Control intensity >1) are highlighted.

3.3.3 Enrichment of endogenous RNP structures

We sought to identify what endogenous cellular components Cas9 interacts with and how this is impacted by delivery mechanisms. For all 2-hour timepoints we analyzed the cellular components most enriched by gene ontology analysis (Webgestalt[51,52]). Intriguingly, 5 out of 6 datasets showed strong enrichment of endogenous RNPs and RNA binding proteins more generally (Fig. 3)[53].

The exception was the HEK PERC, with the majority of the hits involved in the external cell membrane (Fig. 3). This is consistent with the substantially lower editing performance of PERC mediated RNP delivery in HEK293T than in T-cells[22], and is suggestive that PERC delivered RNPs are not internalized at the 2 hour timepoint. In particular, cellular components associated with ribosomal biogenesis, including the nucleolus and pre-ribosome, were strongly enriched. In the absence of specific complementary sequences, viral RNA binding proteins are known to bind promiscuously to DNA. In addition, apoCas9 has a cationic internal region that facilitates complexation with its guide RNA. Therefore, we hypothesized that Cas9, either in RNP or apo form may bind promiscuously to RNA and end up localizing to the same regions as RNA binding proteins within the cell.

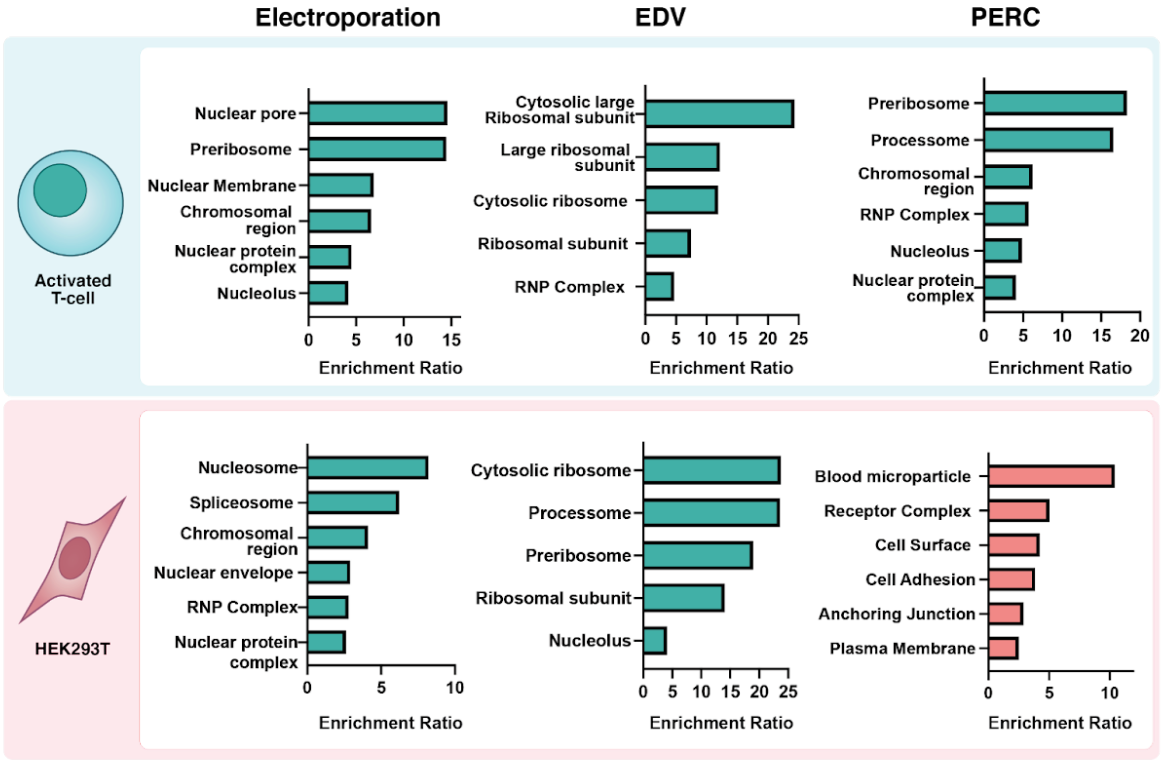

Fig. 3.3: Enrichment of RNA binding protein in proximity labeling mass spectrometry (APEX2-MS).

Gene ontology[51,52] analysis of cellular components 2-fold enriched* (Experimental:Control >2) in Cas9-APEX2 RNP delivered by electroporation, enveloped delivery vehicles (EDVs), and peptide mediated delivery (PERC) in activated T-cells (Top) and HEK293T (Bottom) two hours post-delivery. Analysis was done using over representation and comparing identified hits to all protein encoding genes to identify cellular components disproportionately enriched. (*T-cell EDV dataset cut-off was 1.5-fold enriched due to lower total identified hits).

3.3.4 Investigating the degradation mechanism of Cas9 RNPs

From our gene ontology analysis, we explored the hypothesis that Cas9 RNP localizes to the nucleoli prior to being degraded. Consistent with this hypothesis, proteins associated with the nuceloli, but not nucleoplasm or nuclear proteins more generally, were enriched in all datasets (Fig. 3.4A), except for the HEK PERC dataset. Next, we utilized a cell-based protein stability reporter that permits the translation of two fluorescent proteins from one mRNA transcript[54] separated by an internal ribosomal entry site (IRES). The first fluorescent protein, green fluorescent protein (GFP), is fused to our protein of interest (X), whereas the second, mCherry, serves as an internal control. When integrated into the genome of cells, mCherry and X-GFP proteins are produced at a constant rate[54] because they are derived from the same mRNA. Cellular perturbations that selectively deplete or stabilize the protein of interest will change the relative abundance of the X-GFP fusion, but not the mCherry control, leading to an alteration in the GFP/mCherry ratio[54]. We designed a SpyCas9-GFP, SauCas9, and GFP-only construct on a doxycycline-inducible promoter (pTRE3GS). Cells expressing the pTRE3GS-GFP-IRES-mCherry and pTRE3GS-

SpyCas9-IRES-mCherry constructs were treated with varying doses of doxycycline, which lead to an increase in fluorophore expression but, as predicted[54], an equivalent ratio of GFP/mCherry (Fig. S3.4).

To determine whether Cas9 localized to the nucleoli, we stained for nucleolin, a protein specifically found in the nucleoli[50]. For the Cas9-GFP fusion, but not GFP independently, there was puncta that co-localized with nucleolin. The precise mechanisms of nucleoli degradation are not clear[55], but are hypothesized to involve nucleophagy in which the nucleoli are moved outside of the nucleus prior to degradation by the autophagy lysosomal network.

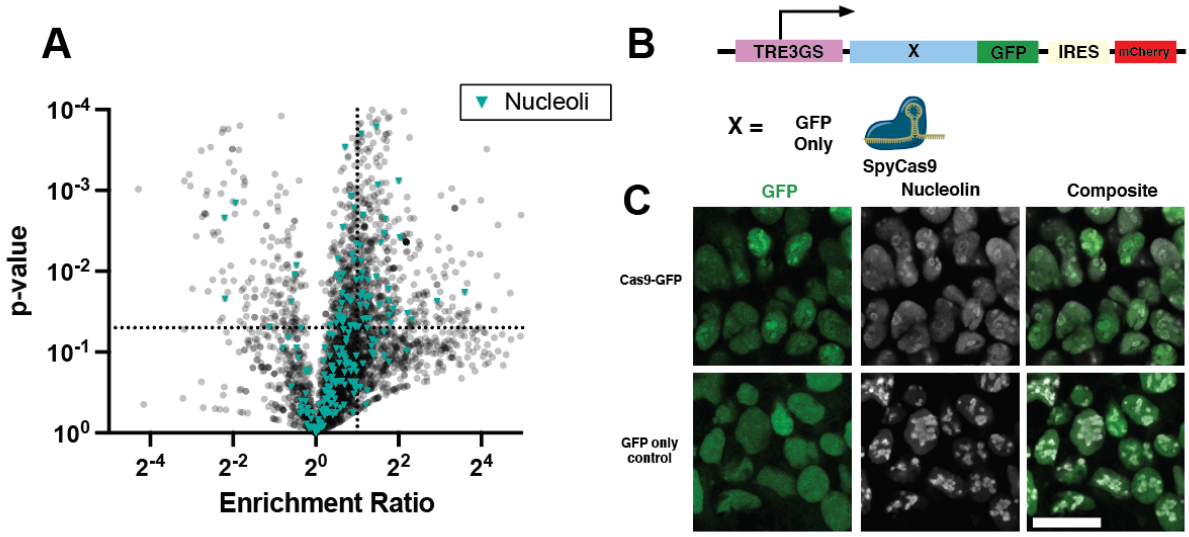

Fig. 3.4: Degrading Cas9 localizes to the nucleoli.
(A) Volcano plot of proteins identified by proximity labeling MS (APEX2-MS) in HEK293T electroporation at 2 hours. Nucleoli proteins[50] highlighted. (B) Schematic of the protein stability reporter established to study SpyCas9 degradation (C) Fixed cell confocal microscopy showing punctate staining of Cas9 fused to GFP, but not GFP expressed independently, within nucleoli. Nucleolin is a structural protein found in nucleoli and was used as nucleoli stain. (See Supplemental table 2)

Discussion

Most delivery vehicles require a specific receptor or ligand efficient intracellular uptake. However, many studies, on viral transduction[56–59], LNPs[60] and cell penetrating peptides[23,24], have shown that factors underlying cell-tropism are multi-faceted, and the expression of the cognate receptor/ligand is often only loosely correlated with uptake. In our study, we utilized a proximity labeler, APEX2[36], fused to SpyCas9 to probe the differential RNP uptake pathways resulting from delivery by electroporation, EDVs and PERC, in HEK293T and activated T-cells. For PERC, we found that Cas9-APEX2 bound readily to the HEK293T cell membrane, but failed to be meaningfully internalized at the two hour time point. For EDVs, which also have significantly different editing efficiency in immortalized cell lines and T-cells, the majority of enriched proteins were

RNA binding proteins present inside the cell. Previous research on lentivirus have found that cell type differences in viral delivery can stem from post-entry steps resulting from selective proteasomal degradation[59]. Unlike editing measurements, which are an endpoint readout used as a proxy for CRISPR genome editor delivery, spatiotemporal profiling can be used to gain mechanistic insight into what steps are limiting.

Engineering SpyCas9, or other CRISPR genome editors, with improved intracellular RNP stability may allow for similar editing to occur at substantially lower doses[42]. Recent work showed that increasing SpyCas9 stability, by inhibiting KEAP1-associated degradation, improved its performance in CRISPR screens and in epigenome editing[35]. We found that, regardless of RNP delivery strategy or cell type, Cas9 associates with endogenous RNA binding proteins, and localizes to the nucleoli prior to degradation. Using a protein stability reporter system[54], we found that SpyCas9 is more soluble in the nucleus, and accumulates less readily in the nucleoli than SauCas9, which may in part account for the difference in their editing ability[61–63]. CRISPR editors are the scaffold for numerous fusion editors[32], including epigenome[35], prime, and base editors. Future investigations on the degradation mechanism of CRISPR genome editors could facilitate the development of less immunogenic or longer-lived variants.

Methods

Plasmid construction

Restriction enzymes used in this study were purchased from New England Biolabs (NEB). Plasmids were constructed using NEBuilder HiFi DNA Assembly Master Mix (NEB) with PCR products and backbone restriction digests. For guide plasmid cloning, protospacer oligos were annealed and then inserted using BsmBI golden gate assembly as previously reported. Cloning and DNA preparations were performed in MultiShot StripWell Mach1 (ThermoFisher).

Tissue culture

Lenti-X, HEK293T, and HeLa cells were obtained and authenticated by the UC Berkeley Cell Culture facility. Cell lines were cultured in DMEM (Fisher Scientific) supplemented with 100 U/ml Penicillin-Streptomycin (Thermofisher), and passed with Trypsin-EDTA (0.25%, Phenol Red, Fisher Scientific). T-cells were isolated and cultured similarly as previously published[43]. Cryopreserved PBMCs (AllCells) were thawed and cultured in X-VIVO 15 (Lonza) supplemented with with 50 µM 2-mercaptoethanol (Gibco), 5% fetal bovine serum (VWR) and 10 mM *N*-acetyl L-cysteine (Sigma-Aldrich). To isolate T cells, PBMCs were incubated in 100 µg ml^{-1} DNase I solution (StemCell Technologies) at room temperature for 15 min and resuspended in EasySep Buffer (StemCell Technologies). DNAse treated suspensions were filtered through a 37 µm cell strainer (StemCell Technologies) and incubated for 5 min with EasySep Human T Cell Isolation Cocktail (StemCell Technologies). Then, EasySep RapidSpheres (StemCell Technologies) were used to separate T cells via an EasySep Magnet (StemCell Technologies). Dynabeads Human T-Activator CD3/CD28 (Gibco) and recombinant human 500 U ml^{-1} IL-2 (Peprotech), 4 ng ml^{-1} IL-7 (Peprotech) and 4 ng ml^{-1} IL-15 (Peprotech) were used to stimulate and activate T cells for 2 days before treatment. Pre-activated T cells were cultured in media containing 500 U ml^{-1} IL-2 (Peprotech).

RNP electroporation

B2M-targeting sgRNA (IDT, Supplemental Table XX) were resuspended in IDT duplex buffer to 100 µM. Cas9 RNPs were formed by combining the sgRNA and 40 µM Cas9-NLS (UC Berkeley QB3 MacroLab) at a molar ratio of 1.5:1 and incubating at room temperature for 10-15 min. Electroporation was performed using a 96-well format 4D-nucleofector (Lonza) with 150,000 cells per well (unless otherwise specified). HEK293T cells were electroporated with the SF buffer and the CM-130 pulse code. Cells were immediately resuspended in pre-warmed media and transferred to culture plates.For primary T-cells, cells were electroporated in P3 buffer with the EH-115 code and then resuspended in prewarmed media, incubated for 20 min and plated.

Peptide-enabled RNP delivery

A5K peptide (GLFEKIEGFIENGWEGMIDGWYGYGRKKRRQRR) were generated by solid phase synthesis (CPC Scientific, >95% purity). Peptides were either stored lyophilized at -20 C or as 10 mM stocks in DMSO at -80C with desiccant.

For peptide mediated delivery, Cas9 protein was dilute to 10 uM in RNP reconstitution buffer (20 mM HEPE pH 7.5 150 mM NaCl, 10% glycerol, and 2 mM $MgCl_2$). SgRNA (IDT) was diluted to 15 uM in reconstitution buffer. Then the diluted protein was slowly added to the diluted guide and incubated at room temperature for 5-10 min. Peptides (10 mM in 100% DMSO) were diluted in nuclease free water (Ambion) to 1 mM (90% water and 10% DMSO) and added to already complexed RNP, with a 20:1 stoichiometric ratio of peptide:RNP and incubated for an additional 5 min. The PERC master mix (peptide:RNP) was added dropwise directly to cells.

EDV production

Cas9-EDVs were produced similarly to previously described[27]. Briefly, Cas9-EDVs were produced by seeding 4 million Lenti-X cells (Takara Bio) into 10 cm tissue culture dishes (Corning) and transfecting the next day with 1 µg pCMV-VSV-G (Addgene plasmid #8454), 6.7 µg Gag-Cas9-U6-sgRNA, 3.3 µg psPax2-U6-sgRNA (Addgene plasmid #12260) using TransIT-LT1 (Mirus Bio) at a 3:1 TransIT-LT1:plasmid ratio. APEX2-Cas9-EDVs were produced in the same way, except with 6.7 ug of Gag-Cas9-APEX2-U6-sgRNA. Two days post-transfection (or media change), Cas9-EDV-containing supernatants were harvested, passed through a 0.45 µm PES syringe filter (VWR) and concentrated with either ultracentrifugation, for LC-MS, ELISA quantification (unless otherwise stated), and confocal experiments, or with Lenti-X concentrator (Takara Bio) for editing experiments. LentiX concentrator (Takara Bio) was used according to the manufacturer's instructions. For LC-MS experiments and confocal experiments, Cas9-APEX2-EDVs were concentrated with ultracentrifugation by laying EDV containing supernatant on top of 30% sucrose in 100 mM NaCl, 10 mM Tris-HCl (ph 7.5), 1 mM EDTA at 25,000 rpm with a SW28 or SW41 Ti rotor (Beckman Coulter) for 2 hrs at 4 C in polypropylene tubes (Beckman Coulter). Concentrated Cas9-EDVs were resuspended in Opti-MEM (Gibco) at a final concentration of 20x unless otherwise noted. Following concentration, the EDV pellet

was resuspended in OptiMEM reduced serum media (Gibco) and frozen at -80 C until use.

Western Blotting and densitometry

Samples were denatured by mixing with 5xLaemmli with 10% 2-mercaptoethanol and heating at 95°C for 3 minutes. Samples were run on 4%–20% SDS-PAGE gels (Bio-Rad) prior to transfer onto a methanol soaked polyvinylidene difluoride (PVDF, Bio-Rad) membrane. PVDF membranes were blocked with 10% non-fat milk (Apex) in 1xPBS (GIBCO) with 0.1% Tween (Sigma) (PBS-T) for one hour at room temperature (~22-25°C). The solution was replaced with 0.1% non-fat milk in PBS-T and primary antibody dilution (Supplementary table XX) in 1% non-fat milk in PBS-T incubated at 4°C overnight. The following day, the solution was replaced with 1% non-fat milk in PBS-T and a secondary antibody dilution (Supplementary table XX) and gently shaken for 1 hour. Western blot membranes were washed with PBS-T three times, with 2-3 minutes wash steps, prior to imaging on a LI-COR OdysseyCLx. Fiji (previously imageJ) was used to quantify relative band intensity on western blots.

Proximity Labeling and Streptavidin Pulldown for LC-MS/MS

Incubated 10 cm dishes (5 million HEK cells/dish) in 10 ml of 2.5 mM BP in cDMEM pre-warmed to 37 °C. After 30 minutes incubation at 37 C, add 50 uL of 200x H_2O_2 to a final concentration of 0.5 mM (9.7 mL DPBS and 100 uL 30% H_2O_2 to make 100 mM stock solution) for 1 min. Spread H_2O_2 evenly around the plate and swirled for even coverage. After 1 min, added 15 mL of our quencher solution. GENTLY remove wash, and add another 15 ml wash of quencher solution. Let this wash sit for 1 min.

After the three washes with the quencher solution, I took off the solution again, added 5 mL DPBS to the plate, took off the DPBS, spun down the quencher + DPBS washes (300 x g for 3 minutes), while trypsinizing the plate with 5 mL trypsin for 5 minutes. Quenched the trypsinization with 10 mL cDMEM. Took off the supernatant from the spun-down cell pellet and added the trypsinized cells to spin down one more time (300 x g for 3 minutes). After this spin, washed the cell pellet one last time with DPBS (300 x g for 3 minutes). Wash 5x total per plate with quencher solution. Keep the cell pellet in -80.

Pellets were lysed with fresh RIPA lysis buffer[36]. The protein concentration of whole cell lysate was determined using the 660 protein assay reagent (Pierce, #22660).

Streptavidin magnetic beads (300 ul) (Pierce # 88817) were washed twice with 1 ml of RIPA lysis buffer without. Beads were added to 1000 ug of whole cell lysate and bound overnight at 4C. Beads were washed similarly to previously published protocol[36]. Briefly, beads were washed twice with RIPA lysis without protease inhibitors, once with KCl, once with 2M urea in 10 mM HCl (ph 8.0), twice with RIPA, and two more times with PBS.

On-Bead Trypsin Digestion

Enriched proteins were digested and prepared for TMT LC-MS similar to previous publication[36,38]. Washed beads with enrichment proteins bound were resuspended in

PBS supplemented with 0.1% SDS (62.5 µL per 1 mg protein/sample). Dithiothreitol (DTT) (30 mg/mL stock in dH2O 3.2 uL per 1 mg protein/sample) and incubate at 65o for 20 min on shaker (600-800 rpm) to reduce all disulfide bonds.Add iodoacetamide (74mg/ml) stock in water, 3.2 µL per 1 mg of protein per sample) and incubate at 37C with agitation for 1 hr. Dilute the reaction with 1 mL PBS and collect beads by centrifugation at 1300 g for 4 min. Beads were washed 3 times with 1 mL of PBS with magnetic separation to remove the supernatant. The washed beads were resupsended in 27.5 ul of pre-mixed solution of the following of 100 mM triethylammonium bicarbonate (TEAB) solution supplemented with 100 mM CaCl2 and 0.5 ul of mass spectrometry grade trypsin (insert trypsin cat#). The beads were trypsinized overnight at 37 C with orbital shaking (600-800 rpm). The supernatant was transferred to fresh tubes by magnetic separation and washed an additional two times to elute remaining peptides. Peptide eluent was quantified and normalized to 50 mM TEAB and same final peptide quantity and concentration for TMT labeling (20-40 ug of peptide per sample).

TMT-based quantitative proteomic profiling

Individual samples were labeled with isobaric tags using TMTsixplex (Thermofisher) according to manufacturer's protocols. Tagged samples (20-40 ug per sample) were combined, dried in a SpeedVac, resuspended in 300 ul 0.1% TFA in H_2O and fractionated using high pH reverse phase peptide fractionation kit (Thermofisher) according to manufacturer's protocols. Fractions were dried with the SpeedVac and stored at -80 °C until resuspension. Fractions were resuspended with 50 ul 0.1% FA in H_2O and analyzed by LC-MS/MS as described below.

TMT-based quantitative proteomic profiling was done as previously described [66] with a Thermo Eclipse with LC MS/MS. MS data was processed used ProLuCID search methodology in IP2 v.3-v.5 (Integrated Proteomics Applications, Inc). Carbamidomethylation of cysteine was set as a fixed modification, methionine oxidation, and TMT-modification of N-termini and lysine residues were set as variable modifications. Reporter ion ratio calculations were performed using summed abundances with the most confident centroid selected from a 20 ppm window. Only peptide-to-spectrum matches that were unique assignments to the identified protein were considered for protein quantification. Differential abundance significance was estimated using ANOVA with Benjamini-Hochberg correction to determine p-values.

SpyCas9-APEX2 fusion construct expression and Purification

SpyCas9-APEX2 expression vector was transformed in Rosetta DE3 (Sigma-Aldrich) and plated onto LB agar plate supplemented with 50 ug/ml ampicillin. Next day, a colony was selected and grown overnight (~16 hrs) in 200 ml LB supplemented with 50 ug/ml Carbenicillin. This starter culture was grown at 37 C for 16 hrs overnight.

Next day, 4 2xYT flasks supplemented with 50 ug/ml were inoculated with 25 ml of starter culture and grown at 37 C at 140 rpm until an OD of 0.6-0.8. Flasks were left on ice for 30 minutes and then induced with 0.5 mM IPTG and grown at 16 °C, 140 rpm for 16-18 hrs.

After overnight expression, culture was pelleted for 30 minutes at 4,000 x *g* at 4°C. Pellets were resuspended in lysis buffer (50 mM HEPES, pH 7.0 500 mM NaCl

1 mM TCEP, 5% glycerol) (25 ml/flask) supplemented with Roche Complete Protease inhibitor tablets (~1 tab/50 ml), PMSF (0.1 mM), TCEP (1 mM), and DNAse (250 µL/50 mL). Resuspended pellets were sonicated on ice (5 minutes total - 10 seconds on, 15 seconds off, 5.5 power output) and then centrifuged at 35,000 x *g* for 45 minutes at 4 °C.

While the sonicated sample was spinning, the Ni-NTA column was prepared with 4 mL of a 50% Nickel resin resuspension (Qiagen) per liter of culture. The column was washed five times with 2 CVs (~12 mls) of wash buffer (50 mM HEPES, pH 7.0 500 mM NaCl 1 mM TCEP 10 mM imidazole 5% glycerol). After centrifugation, the supernatant was directly transferred onto the nickel columns and incubated with resin for 60 min at 4 °C while mixing gently. The flow-through was by gravity-flow and washed three times with 2 CVs wash buffer. Protein was eluted from the column 3 times with elution buffer (50 mM HEPES, pH 7.0 500 mM NaCl 1 mM TCEP 300 mM imidazole 5% glycerol) and pooled until dialysis.

For dialysis, the pooled eluent was injected into a pre-hydrated Slide-A-Lyser (10,000 MWCO, ThermoFisher) in 1L dialysis buffer (50 mM HEPES, pH 7.0 250 mM NaCl 1 mM TCEP 5% glycerol). The Slide-A-Lyzer was spun gently at 4 °C for 1 hr and then TEV protease was injected into the cassette (for 20 mg protein estimated from A280: 1 mg TEV), and left dialyzing overnight at 4 °C with gentle stirring.

The next morning, the dialyzed protein was spun for 45 minutes at 35,000 x *g*, 4 °C and filtered through a .22 µM Millex GP (Millipore) filter and Concentrated to a maximum volume of 5 mL. Next, we use a 5 mL HiTrap SP HP column (Laura's 4C) and an AKTA to purify the protein. The AKTA was washed with IEX buffer A (50 mM HEPES, pH 7.0 250 mM KCl 1 mM TCEP 5% glycerol) and the protein solution was manually injected into the column. The column was equilibrated with IEX buffer A for 1 column volume at 2.5 mL/min, and then washed with IEX buffer A for 1 column volume at 2.5 mL/min. The protein was eluted at 2.5 mL/min using a linear gradient elution starting with 100% IEX buffer A and ending with 100% IEX buffer B over 10 column volumes, with protein fractionated into 1 mL fractions. Following elution the fractions of pure protein were pooled and concentrated. Purity of the SpyCas9-APEX2 protein was confirmed by SDS-PAGE (Supplementary Figure 1).

Next Generation Sequencing to assess genome editing

Next-generation sequencing was used for detection of on-target genome editing in 293T cells. Genomic DNA was extracted using QuickExtract (Lucigen) as previously described[27]. Q5 high fidelity polymerase (NEB) was used to amplify the B2M Cas9-RNP target site using primers 5'- GCTCTTCCGATCTaagctgacagcattcgggc and 5'-GCTCTTCCGATCTgaagtcacggagcgagagag. The resulting PCR1 products were cleaned up using magnetic SPRI beds (UC Berkeley DNA Sequencing Facility). Library preparation and sequencing was performed by the Innovative Genomics Institute Next Generation Sequencing Core using iSeq Micro v2 (Illumina). Reads were analyzed with CRISPResso2 (http://crispresso.pinellolab.partners.org/login).

Flow Cytometry

Cells were stained with anti-human B2M-PE (316306, Biolegend) in PBS containing 1% bovine serum albumin. An Attune NxT flow cytometer equipped with a 96-well

autosampler (Thermo Fisher Scientific) was used for flow cytometry acquisition. Data analysis was performed using FlowJo v10 10.7.1 (FlowJo, LLC, Ashland OR).

Immunofluorescent (IF) Staining and Imaging

18 mM slides were fixed with 4% PFA in 1xDPBS for 10 min. For time course experiments, all cells were fixed and then stored in 1xDPBS until all samples were harvested, so that permeabilization and staining steps were done simultaneously. We then washed coverslips three times with 1×PBS, and permeabilized samples with 0.2% Triton-X-100 in 1xDPBS for 10 minutes. Following permeabilization, samples were washed three times, and then blocked with Image-iT FX signal enhancer (Invitrogen). After this initial blocking step, samples were washed twice with 1xDPBS and then further blocked in 10% Goat Serum (ThermoFisher #50062Z) for 20-30 minutes. Then samples were incubated with primary antibodies (Supplementary table 2) diluted in 10% Goat Serum at 4C overnight. The following day, the coverslips were washed three times with 1xDPBS and incubated for 1 hour with secondary antibodies (Supplementary table 2). For confocal microscopy, secondary antibodies from tyramide signal superboost kits (Thermofisher, Supplementary Table 2) were used following manufacturers instructions. The labeling reaction was done for 2 minutes for all EDV experiments. Samples were then washed three times and mounted with Prolong Diamond antifade mountant (Invitrogen). All slides were stored at -20 C for periods longer than 1 week.

Statistical analysis

Statistical analysis was performed using Prism v10 unless otherwise stated. Statistical details for experiments, including the values and definitions of the samples sizes and error bars are reported in the figure legends.

Acknowledgements

We appreciated useful discussions with Ross Wilson, Matthew Kan, Chenglong Xia, Katarzyna (Kasia) Soczek and Kai Chen. H.K. was in part supported by the National Institutes of Health (NIH) Stem cell biological engineering training program (Grant no. T32GM098218). Microscopy research reported in this publication was supported in part by the NIH S10 program under the award number 1S10RR026866-01. The content is solely the responsibility of the authors and does not necessarily represent the official views of the National Institutes of Health.

Data and materials availability

Flow cytometry and raw image files are available upon request. All other data is in the main text or supplementary materials.

Competing interest

The Regents of the University of California have patents issued and pending for CRISPR technologies on which J.A.D. is an inventor and delivery technologies on which J.A.D. and W.N. are co-inventors. J.A.D. is a cofounder of Azalea Therapeutics,

Caribou Biosciences, Editas Medicine, Evercrisp, Scribe Therapeutics, Intellia Therapeutics, and Mammoth Biosciences. J.A.D. is a scientific advisory board member at Evercrisp, Caribou Biosciences, Intellia Therapeutics, Scribe Therapeutics, Mammoth Biosciences, The Column Group and Inari. She also is an advisor for Aditum Bio. J.A.D. is Chief Science Advisor to Sixth Street, a Director at Johnson & Johnson, Altos and Tempus, and has a research project sponsored by Apple Tree Partners. A.S has research projects sponsored by Novo Nordisk, Amgen, and Merck. All other authors have no competing interests.

Supplementary Figures

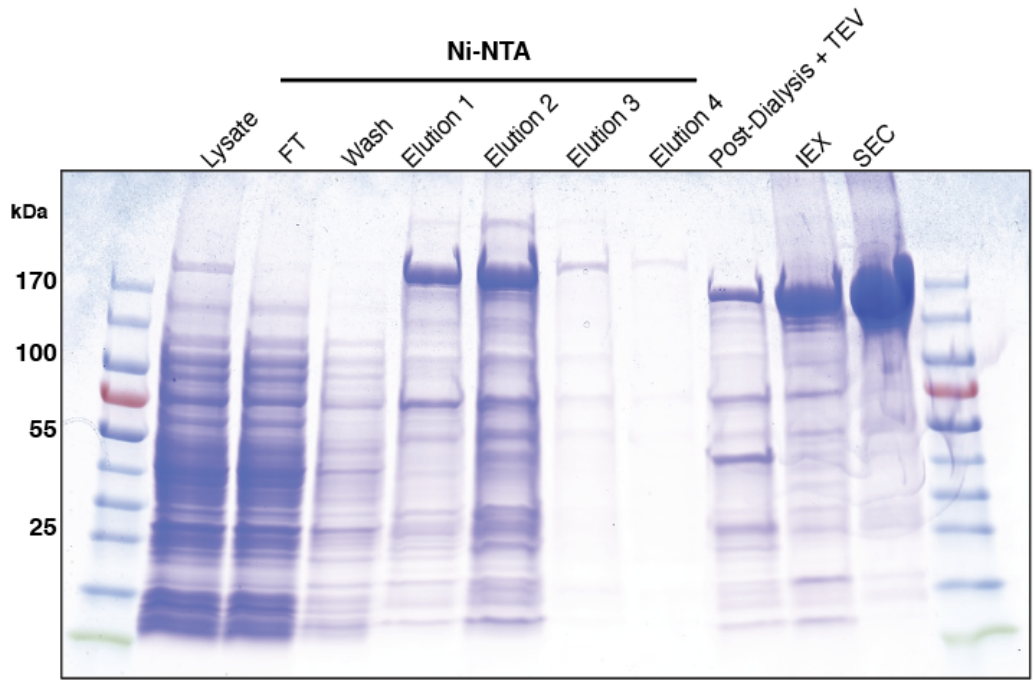

Supplementary Figure 3.1: Expression and Purification of Cas9-APEX2 from E. coli

Each lane corresponds to a step in the recombinant protein purification process. First, induced cells are lysed and mixed with Ni-NTA resin. The His-tagged Cas9-APEX2 is bound to the Ni-NTA beads while non-tagged proteins are in the flowthrough. Cas9-APEX2 is eluted four times (Ni-NTA elution 1-4) with an imidazole containing buffer. Tev protease is used to cleave the affinity tags from Cas9-APEX2 (Post-TEV cleavage) and before the protein undergoes ion exchange chromatography (post-IEX) and size exclusion chromatography (Post-SEC) to yield a pure final product (>95% pure by HPLC).

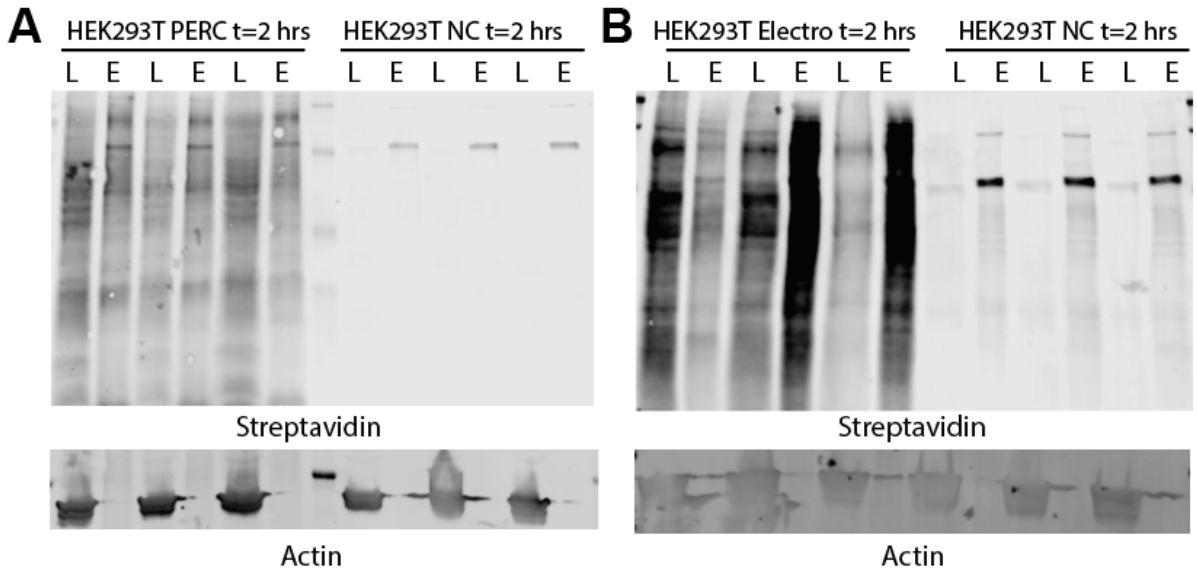

Supplementary Figure 3.2: Enrichment of endogenous proximity labeled protein by Streptavidin bead enrichment prior to APEX2-MS.

Confirmation of proximity labeling by Cas9-APEX2 fusion and enrichment by western blot prior to proximity labeling mass spectrometry (APEX2-MS). L = normalized whole cell lysate E = Bead elution after washing[36]. **(A)** Experimental cells treated with Cas9-APEX2 delivered by PERC (Right) and control untreated (negative control (NC)) HEK293T cells (Left) in triplicate. (B) Experimental cells treated with Cas9-APEX2 delivered by electroporation (Right) and control untreated (negative control (NC)) HEK293T cells (Left) in triplicate. The bands visible in the negative control samples are known endogenously biotinylated proteins[36].

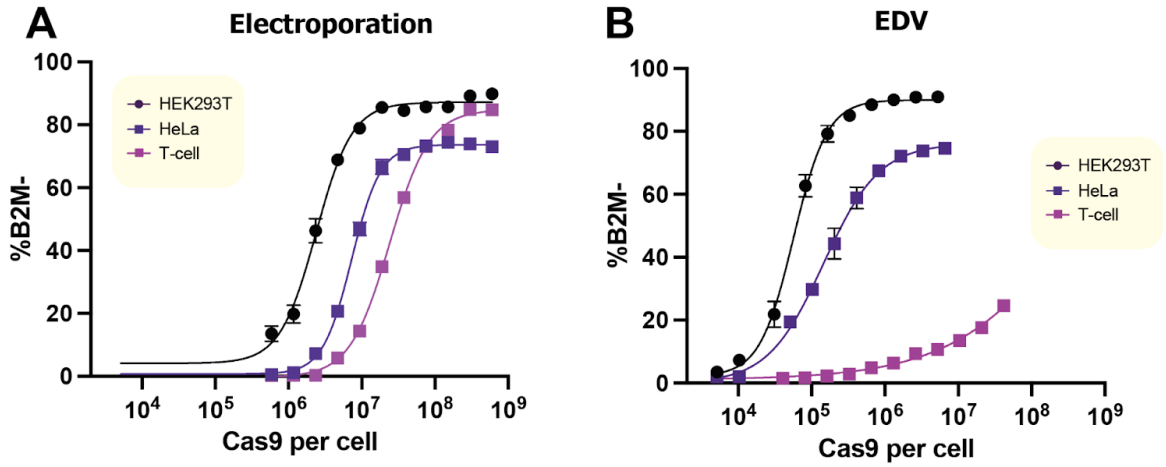

Supplementary Figure 3.3: Comparison of editing efficiency by Electroporation and EDVs by Cell-type.

To assess Cas9 RNP dosage required for editing in HEK293T, HeLa, and T cells were treated with varying doses of B2M-targeting Cas9 by **(A)** electroporation and **(B)** EDVs.

Analysis was performed by flow cytometry 4 days post treatment to assess B2M knockdown. Datapoints represent the mean with error bars displaying SD. RNP dose curves were modeled (Prism v10) as sigmoidal (4PL, X is concentration).

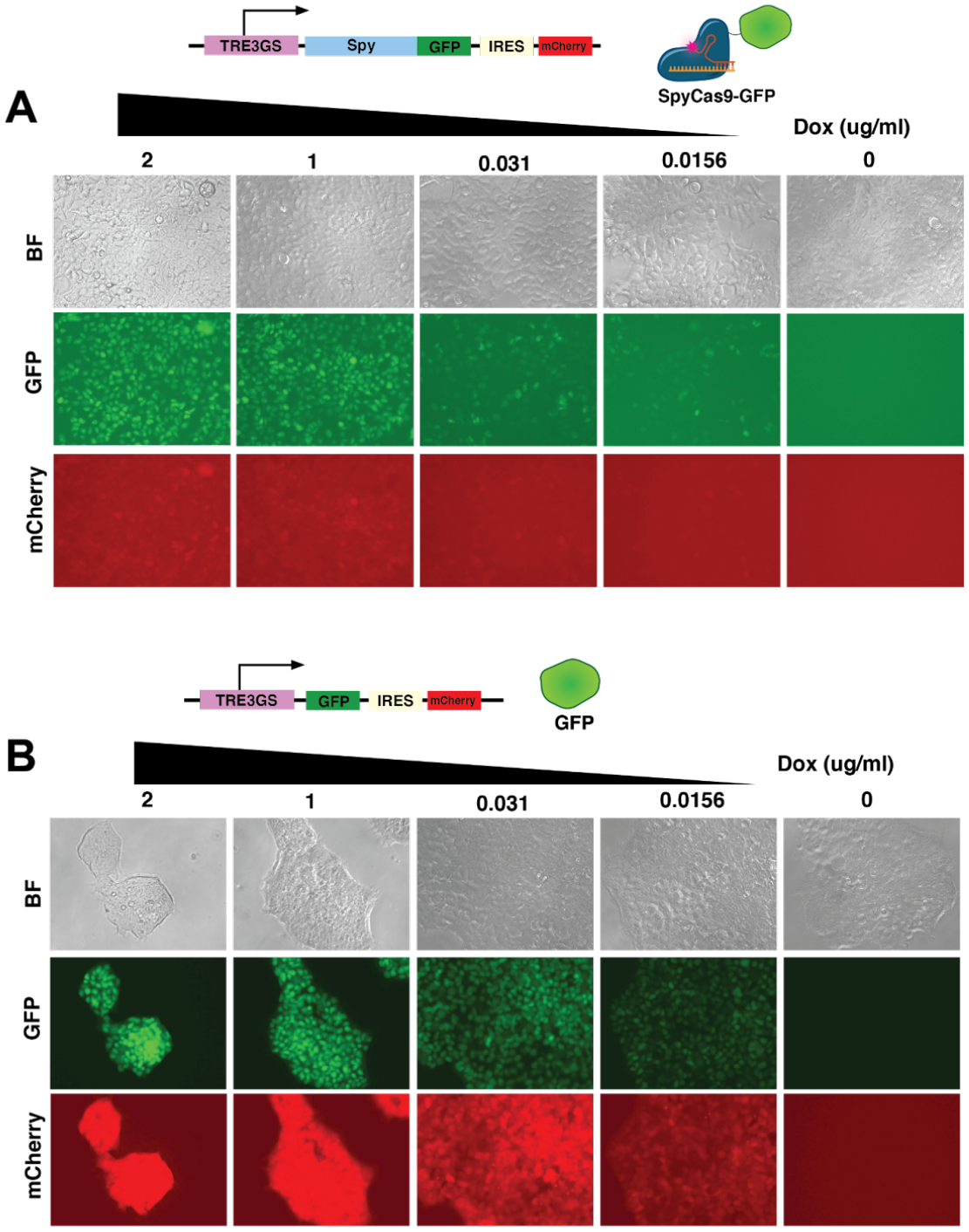

Supplementary Figure 3.4: Establishing a doxycycline-inducible Cas9 protein stability reporter.

(A) Dose response of pTRE3GS-SpyCas9-GFP-IRES-mCherry monoclonal cell line to titrated doses of doxycycline. **(A)** Dose response of pTRE3GS-GFP-IRES-mCherry monoclonal cell line to titrated doses of doxycycline. Cells incubated with doxycycline for 48 hours prior to imaging.

Supplementary Table 1

General summary of LC-MS results at 24 hour time point by RNP delivery modality (electroporation, PERC and EDV).

Delivery Method	Cell Type	Total #	# experimentally enriched	# statistically significant
Electroporation	HEK293T	3503	2799	950
	T cell	2194	1177	381
PERC	HEK293T	3594	1576	1028
	T cell	2039	883	185
EDV	HEK293T	1081	479	231
	T cell	1582	617	52

Supplementary Table 2

Antibodies Used:
IF = ImmunoFluorescence; WB= Western Blot; FC= Flow cytometry; mAb = monoclonal Antibody; pAb = polyclonal antibody

Primary Antibodies:

Antibody target/strain:	Source/Isotype:	Dilution(s) used:	Company and Catalog #
CRISPR-Cas9 (7A9-3A3)	Mouse mAb	1:350 (IF)	Novus Biologicals

			(#NBP2-36440)
CRISPR-Cas9	Rabbit pAb	1:1000 (WB)	Diagenode (#C15310258)
LAMP1 (D2D11)	**Rabbit mAb**	1:100 (IF)	Cell Signaling Technology (#9091)
RAB5A (2E8B11)	Mouse mAb	1:100 (IF)	eBioscience (# 14-9711-82)
Anti-GAPDH [6C5]	Mouse mAb	1:2500 (WB)	Abcam (#ab8245)
Beta Actin	Mouse Mab	1:2500 (WB)	Proteintech (#60008)
IRDye® 800CW Streptavidin	NA	1:1000-1:10,000 (WB)	Licor (#926-32230)
FLAG (DDDDK sequence) [EPR20018-251]	Rabbit Mab (recombinant)	1:250 (IF)	Abcam (ab205606)
HIV1 p24 (**Catalog # MA1-71515)**	Mouse Mab	1:500 (IF)	Invitrogen (**# MA1-71515)**

Secondary Antibodies:

Antibody:	Dilution(s) used:	Company and Catalog #
Goat anti-Rabbit IgG (H+L) Highly Cross-Adsorbed Secondary Antibody, Alexa Fluor™ Plus 405	1:1000 (IF)	Invitrogen (Catalog # **A48254)**
Goat anti-Mouse IgG (H+L) Highly Cross-Adsorbed Secondary Antibody, Alexa Fluor™ Plus 488	1:1000 (IF)	Invitrogen (**Catalog # A32723)**

Goat anti-Rabbit IgG (H+L) Highly Cross-Adsorbed Secondary Antibody, Alexa Fluor™ Plus 488	1:1000 (IF)	Invitrogen (**Catalog # A32723)**
Goat anti-Rabbit IgG (H+L) Highly Cross-Adsorbed Secondary Antibody, Alexa Fluor™ 555	1:1000 (IF)	**Invitrogen (Catalog # A48255)**

Counterstain:	Cellular Compartment:	Dilution(s) used:	Company and Catalog #
SYTOX™ Deep Red Nucleic Acid Stain	Nucleus	1:2000 (IF)	**Invitrogen (#S11380)**
Alexa Fluor™ 633 Phalloidin	Actin (cytoskeleton)	1:2000 (IF)	Invitrogen (#A22284)

References

1. Jang, H.-K. *et al.* High-purity production and precise editing of DNA base editing ribonucleoproteins. *Sci Adv* **7**, (2021).
2. Wienert, B., Shin, J., Zelin, E., Pestal, K. & Corn, J. E. In vitro-transcribed guide RNAs trigger an innate immune response via the RIG-I pathway. *PLoS Biol.* **16**, e2005840 (2018).
3. Kim, S. *et al.* CRISPR RNAs trigger innate immune responses in human cells. *Genome Res.* **28**, 367–373 (2018).
4. Charlesworth, C. T. *et al.* Identification of preexisting adaptive immunity to Cas9 proteins in humans. *Nat. Med.* **25**, 249–254 (2019).
5. Bulcha, J. T., Wang, Y., Ma, H., Tai, P. W. L. & Gao, G. Viral vector platforms within the gene therapy landscape. *Signal Transduct Target Ther* **6**, 53 (2021).
6. Hou, X., Zaks, T., Langer, R. & Dong, Y. Lipid nanoparticles for mRNA delivery. *Nat. Rev. Mater.* **6**, 1078–1094 (2021).
7. Hendel, A. *et al.* Chemically modified guide RNAs enhance CRISPR-Cas genome editing in human primary cells. *Nat. Biotechnol.* **33**, 985–989 (2015).
8. van Haasteren, J., Li, J., Scheideler, O. J., Murthy, N. & Schaffer, D. V. The delivery challenge: fulfilling the promise of therapeutic genome editing. *Nat. Biotechnol.* **38**, 845–855 (2020).
9. Espinoza, D. A. *et al.* Aberrant Clonal Hematopoiesis following Lentiviral Vector Transduction of HSPCs in a Rhesus Macaque. *Mol. Ther.* **27**, 1074–1086 (2019).

10. Hanlon, K. S. *et al.* High levels of AAV vector integration into CRISPR-induced DNA breaks. *Nat. Commun.* **10**, 4439 (2019).
11. Leibowitz, M. L. *et al.* Chromothripsis as an on-target consequence of CRISPR-Cas9 genome editing. *Nat. Genet.* **53**, 895–905 (2021).
12. Ihry, R. J. *et al.* p53 inhibits CRISPR-Cas9 engineering in human pluripotent stem cells. *Nat. Med.* **24**, 939–946 (2018).
13. Haapaniemi, E., Botla, S., Persson, J., Schmierer, B. & Taipale, J. CRISPR-Cas9 genome editing induces a p53-mediated DNA damage response. *Nat. Med.* **24**, 927–930 (2018).
14. Bruce, V. J. & McNaughton, B. R. Inside Job: Methods for Delivering Proteins to the Interior of Mammalian Cells. *Cell Chem Biol* **24**, 924–934 (2017).
15. Porello, I. & Cellesi, F. Intracellular delivery of therapeutic proteins. New advancements and future directions. *Front. Bioeng. Biotechnol.* **11**, 1211798 (2023).
16. Wilson, R. C. & Gilbert, L. A. The Promise and Challenge of In Vivo Delivery for Genome Therapeutics. *ACS Chem. Biol.* **13**, 376–382 (2018).
17. Sharma, G., Sharma, A. R., Bhattacharya, M., Lee, S.-S. & Chakraborty, C. CRISPR-Cas9: A preclinical and clinical perspective for the treatment of human diseases. *Mol. Ther.* **29**, 571–586 (2021).
18. Frangoul, H. *et al.* CRISPR-Cas9 gene editing for sickle cell disease and β-thalassemia. *N. Engl. J. Med.* **384**, 252–260 (2021).
19. Kim, S., Kim, D., Cho, S. W., Kim, J. & Kim, J.-S. Highly efficient RNA-guided genome editing in human cells via delivery of purified Cas9 ribonucleoproteins. *Genome Res.* **24**, 1012–1019 (2014).
20. Jacobi, A. M. *et al.* Simplified CRISPR tools for efficient genome editing and streamlined protocols for their delivery into mammalian cells and mouse zygotes. *Methods* **121-122**, 16–28 (2017).
21. Shapiro, J. *et al.* Increasing CRISPR efficiency and measuring its specificity in HSPCs using a clinically relevant system. *Mol. Ther. Methods Clin. Dev.* **17**, 1097–1107 (2020).
22. Foss, D. V. *et al.* Peptide-mediated delivery of CRISPR enzymes for the efficient editing of primary human lymphocytes. *Nat Biomed Eng* **7**, 647–660 (2023).
23. Ruseska, I. & Zimmer, A. Internalization mechanisms of cell-penetrating peptides. *Beilstein J. Nanotechnol.* **11**, 101–123 (2020).
24. Kalafatovic, D. & Giralt, E. Cell-Penetrating Peptides: Design Strategies beyond Primary Structure and Amphipathicity. *Molecules* **22**, (2017).
25. Han, X., Bushweller, J. H., Cafiso, D. S. & Tamm, L. K. Membrane structure and fusion-triggering conformational change of the fusion domain from influenza hemagglutinin. *Nat. Struct. Biol.* **8**, 715–720 (2001).
26. Zhang, Z. *et al.* Efficient engineering of human and mouse primary cells using peptide-assisted genome editing. *Nat. Biotechnol.* (2023) doi:10.1038/s41587-023-01756-1.
27. Hamilton, J. R. *et al.* Targeted delivery of CRISPR-Cas9 and transgenes enables complex immune cell engineering. *Cell Rep.* **35**, 109207 (2021).

28. Haldrup, J. *et al.* Engineered lentivirus-derived nanoparticles (LVNPs) for delivery of CRISPR/Cas ribonucleoprotein complexes supporting base editing, prime editing and in vivo gene modification. *Nucleic Acids Res.* **51**, 10059–10074 (2023).
29. Banskota, S. *et al.* Engineered virus-like particles for efficient in vivo delivery of therapeutic proteins. *Cell* **185**, 250–265.e16 (2022).
30. An, M. *et al.* Engineered virus-like particles for transient delivery of prime editor ribonucleoprotein complexes in vivo. *Nat. Biotechnol.* 1–12 (2024).
31. Adler, B. A. *et al.* CasPEDIA Database: a functional classification system for class 2 CRISPR-Cas enzymes. *Nucleic Acids Res.* **52**, D590–D596 (2024).
32. Anzalone, A. V., Koblan, L. W. & Liu, D. R. Genome editing with CRISPR-Cas nucleases, base editors, transposases and prime editors. *Nat. Biotechnol.* **38**, 824–844 (2020).
33. Chowell, D. *et al.* TCR contact residue hydrophobicity is a hallmark of immunogenic CD8+ T cell epitopes. *Proc. Natl. Acad. Sci. U. S. A.* **112**, E1754–62 (2015).
34. Simhadri, V. L. *et al.* Cas9-derived peptides presented by MHC Class II that elicit proliferation of CD4+ T-cells. *Nat. Commun.* **12**, 5090 (2021).
35. Chen, J. *et al.* Engineered Cas9 variants bypass Keap1-mediated degradation in human cells and enhance epigenome editing efficiency. *Nucleic Acids Res.* gkae761 (2024).
36. Hung, V. *et al.* Spatially resolved proteomic mapping in living cells with the engineered peroxidase APEX2. *Nat. Protoc.* **11**, 456–475 (2016).
37. Qin, W., Myers, S. A., Carey, D. K., Carr, S. A. & Ting, A. Y. Spatiotemporally-resolved mapping of RNA binding proteins via functional proximity labeling reveals a mitochondrial mRNA anchor promoting stress recovery. *Nat. Commun.* **12**, 4980 (2021).
38. Dumrongprechachan, V. *et al.* Cell-type and subcellular compartment-specific APEX2 proximity labeling reveals activity-dependent nuclear proteome dynamics in the striatum. *Nat. Commun.* **12**, 4855 (2021).
39. Gao, X. D. *et al.* C-BERST: defining subnuclear proteomic landscapes at genomic elements with dCas9-APEX2. *Nat. Methods* **15**, 433–436 (2018).
40. Myers, S. A. *et al.* Discovery of proteins associated with a predefined genomic locus via dCas9-APEX-mediated proximity labeling. *Nat. Methods* **15**, 437–439 (2018).
41. Tyagi, M., Rusnati, M., Presta, M. & Giacca, M. Internalization of HIV-1 tat requires cell surface heparan sulfate proteoglycans. *J. Biol. Chem.* **276**, 3254–3261 (2001).
42. Karp, H. *et al.* Packaged delivery of CRISPR-Cas9 ribonucleoproteins accelerates genome editing. *bioRxivorg* 2024.10.18.619117 (2024) doi:10.1101/2024.10.18.619117.
43. Hamilton, J. R. *et al.* In vivo human T cell engineering with enveloped delivery vehicles. *Nat. Biotechnol.* (2024) doi:10.1038/s41587-023-02085-z.
44. Lambert, G. S., Rice, B. L., Maldonado, R. J. K., Chang, J. & Parent, L. J. Comparative analysis of retroviral Gag-host cell interactions: focus on the nuclear interactome. *Retrovirology* **21**, 13 (2024).

45. Letoha, T. *et al.* Cell-penetrating peptide exploited syndecans. *Biochim. Biophys. Acta* **1798**, 2258–2265 (2010).
46. Gautier, V. W. *et al.* In vitro nuclear interactome of the HIV-1 Tat protein. *Retrovirology* **6**, 47 (2009).
47. Ci, Y., Yang, Y., Xu, C. & Shi, L. Vesicular stomatitis virus G protein transmembrane region is crucial for the hemi-fusion to full fusion transition. *Sci. Rep.* **8**, 10669 (2018).
48. Hossain, M. S., Kerkvliet, J. G. & Hoppe, A. D. Whole genome CRISPR screening strategy to identify genes contributing to SARS-CoV-2 spike and VSV-G mediated entry. *J. Med. Virol.* **95**, e29087 (2023).
49. Ngo, W. *et al.* Mechanism-guided engineering of a minimal biological particle for genome editing. *bioRxivorg* (2024) doi:10.1101/2024.07.23.604809.
50. The Human Protein Atlas. https://www.proteinatlas.org/.
51. Liao, Y., Wang, J., Jaehnig, E. J., Shi, Z. & Zhang, B. WebGestalt 2019: gene set analysis toolkit with revamped UIs and APIs. *Nucleic Acids Res.* **47**, W199–W205 (2019).
52. Elizarraras, J. M. *et al.* WebGestalt 2024: faster gene set analysis and new support for metabolomics and multi-omics. *Nucleic Acids Res.* **52**, W415–W421 (2024).
53. Caudron-Herger, M., Jansen, R. E., Wassmer, E. & Diederichs, S. RBP2GO: a comprehensive pan-species database on RNA-binding proteins, their interactions and functions. *Nucleic Acids Res.* **49**, D425–D436 (2021).
54. Yen, H.-C. S., Xu, Q., Chou, D. M., Zhao, Z. & Elledge, S. J. Global protein stability profiling in mammalian cells. *Science* **322**, 918–923 (2008).
55. Papandreou, M.-E. & Tavernarakis, N. Nucleophagy: from homeostasis to disease. *Cell Death Differ.* **26**, 630–639 (2019).
56. Petrillo, C. *et al.* Cyclosporine H overcomes innate immune restrictions to improve Lentiviral transduction and gene editing in human hematopoietic stem cells. *Cell Stem Cell* **23**, 820–832.e9 (2018).
57. Petrillo, C. *et al.* Cyclosporin a and rapamycin relieve distinct lentiviral restriction blocks in hematopoietic stem and progenitor cells. *Mol. Ther.* **23**, 352–362 (2015).
58. Wang, C. X. *et al.* Rapamycin relieves lentiviral vector transduction resistance in human and mouse hematopoietic stem cells. *Blood* **124**, 913–923 (2014).
59. Santoni de Sio, F. R. *et al.* Lentiviral vector gene transfer is limited by the proteasome at postentry steps in various types of stem cells. *Stem Cells* **26**, 2142–2152 (2008).
60. Cheng, Q. *et al.* Selective organ targeting (SORT) nanoparticles for tissue-specific mRNA delivery and CRISPR-Cas gene editing. *Nat. Nanotechnol.* **15**, 313–320 (2020).
61. Tan, Y. *et al.* Rationally engineered Staphylococcus aureus Cas9 nucleases with high genome-wide specificity. *Proc. Natl. Acad. Sci. U. S. A.* **116**, 20969–20976 (2019).

62. Xie, H. *et al.* High-fidelity SaCas9 identified by directional screening in human cells. *PLoS Biol.* **18**, e3000747 (2020).
63. Yuen, C. T. L. *et al.* High-fidelity KKH variant of Staphylococcus aureus Cas9 nucleases with improved base mismatch discrimination. *Nucleic Acids Res.* **50**, 1650–1660 (2022).
64. Schellekens, H. How to predict and prevent the immunogenicity of therapeutic proteins. *Biotechnol. Annu. Rev.* **14**, 191–202 (2008).
65. Gillmore, J. D. *et al.* CRISPR-Cas9 In Vivo Gene Editing for Transthyretin Amyloidosis. *N. Engl. J. Med.* **385**, 493–502 (2021).
66. King, E. A. *et al.* Chemoproteomics-enabled discovery of a covalent molecular glue degrader targeting NF-κB. *Cell Chem Biol* **30**, 394–402.e9 (2023).

CHAPTER FOUR

Conclusions and Outlook

Discovery of CRISPR genome editors[1], and consequent demonstration of their mammalian genome editing[2–4], has enabled a revolution in both fundamental research and therapeutic development. In nature, CRISPR-cas editors are a critical component of bacterial and archeal adaptive immunity systems[5–7]. However, the evolved characteristics of these immune systems are distinct from the desirable features of a precise mammalian genome engineering tool. Critical limitations of native CRISPR editors include their lack of specificity[4,8], limited targeting scope[9] and compatibility with *in vivo* delivery strategies[10,11].

Chapter One summarizes the extensive engineering efforts towards addressing these challenges by characterizing and engineering improved CRISPR effectors and tools for mammalian genome engineering[12,13]. CRISPR gene therapies have made remarkable progress towards curing diseases with underlying genetic etiologies. In 2023, Casgevy, a treatment for sickle cell disease developed by Vertex and CRISPR therapeutics, was the first CRISPR based gene therapy approved by the FDA[14]. With more than 100 other on-going CRISPR clinical trials it is looking to be the first of many. In 2024, a mere 12 years since SpyCas9 was first demonstrated as a RNA-guided endonuclease[1], there are now hundreds of characterized orthologs and engineered Cas proteins demonstrated to work in mammalian cells, and thousands more characterized *in silico*[15,16]. These variants seek to address the critical limitations of native CRISPR editors including their lack of specificity[4,8], limited targeting scope[9] and compatibility with *in vivo* delivery strategies[10,11].

Importantly, mode of delivery has a dramatic impact on the safety and efficacy of CRISPR[17–19]. Therefore, there is extensive interplay between the engineering goals of delivery strategies and next-generation CRISPR editors. For example, reducing the period that CRISPR editors remain active in the cell can be accomplished either by delivering them as RNPs[18], or by engineering editors with substantially improved specificity[8]. Despite this, almost all CRISPR variants have been primarily studied in extended expression systems, such as lentiviral and plasmid-based expression[20], in HEK293T or derivative cell lines. It is therefore, unsurprising that many of these variants fail to work robustly in more demanding contexts, and with some notable exceptions, such as AsCas12a-ultra[21], have generally failed to be utilized outside of the early stage research. Therefore, it is critical that future engineering develops or validates its variants in the context of transient delivery, which better represents the dosage limited context of therapeutic delivery.

The biggest hurdle for CRISPR-based gene therapies is the safe and effective delivery of genome editors into clinically relevant cells[22,23]. Extensive engineering efforts have generated multiple promising *ex vivo* and *in vivo* Cas9 RNP delivery strategies [22,23]. Broadly speaking, genome editors can be delivered either as a nucleic acid, to be transcribed and/or translated in the target cell, or as an intact RNP [22]. There are distinct advantages to delivering genome editors as RNPs, including shorter intracellular lifetimes that minimize off-target edits [17–19] and reduce immunogenicity [24–26]. Compared to mRNA delivery, RNP delivery may result in lower

levels of toll-like receptor activation [24,27], and enable higher *in vivo* editing efficacy by bypassing *in situ* translation of mRNA [28] and protecting the guide RNA (gRNA) integrity due to Cas9 protein binding [19]. RNP delivery also avoids risks of random DNA integration posed by viral vectors, including lentivirus and adeno-associated virus (AAV)[29,30].

In **Chapter Two**, we compared electroporation and EDVs for the delivery of S. *pyogenes* Cas9 RNPs to edit various human cell types. We determined the impact of delivery modality on the rate of DNA cleavage and repair. Using fluorescence correlation spectroscopy (FCS), we found that >1300 Cas9 RNPs per nucleus are required for editing in human cell lines. At comparable Cas9 RNP doses, EDVs are 30- to 50-fold more effective at editing, across multiple human cell types and target genome sequences. Furthermore, EDV delivery generates genome edits twice as fast as electroporation. We hypothesize that the observed differences in editing efficacy and rate result in part from differences in RNP versus EDV trafficking to the cell nucleus. Our results suggest that the Cas9 RNP dosage used for current *ex vivo* research and clinical genome editing could be substantially reduced by switching from electroporation to a packaged delivery strategy such as EDVs. We show that understanding the impact of delivery modality on RNP intracellular trafficking, localization and genome editing efficacy can identify delivery bottlenecks that could be the focus of future engineering of improved RNP-based gene therapies. Our study examined the dosage requirements of nuclease active SpyCas9 in human cell lines.

These findings also reveal the importance of delivery modality for genome editing efficacy and pave the way for engineering optimal delivery methods to ensure maximal genome editing with minimal side effects. In **Chapter Three**, to identify prominent delivery bottlenecks and commonalities, we utilized spatiotemporally resolved proteomics to compare RNP delivery by electroporation, EDVs, and PERC, in HEK293T and T-cells. *Ex vivo* electroporation disrupts the cell membrane offering direct access to the cytosol, enabling efficient nuclear entry but also triggering significant cell damage and death. Alternative delivery strategies, including enveloped delivery vehicles (EDVs) and cell-penetrating peptides delivered *in trans* (PERC), trigger endocytosis which can safeguard cell integrity but requires subsequent endosomal escape prior to nuclear localization. This workflow uncovered cell-type differences in uptake for EDVs and PERC. Regardless of delivery strategy, Cas9 associates with endogenous RNA binding proteins and localizes to the nucleoli prior to degradation. This method enables flexible comparison of Cas9 RNP delivery strategies, and the impact of cell-type on uptake mechanism.

These projects quantified, for the first time in absolute terms, Cas9 dosage requirements for genome editing and developed novel tools for cell-type specific quantitative profiling of RNP delivery and degradation. Small molecule therapeutics typically need to reside consistently in the window between lowest effective concentration and below the toxicity threshold. CRISPR genome engineering would be more accurately modeled as dependent on the integrated sum of functional RNP within the nucleus during the duration of RNP residence in the cell. This can be conceptualized as the area under the curve of the RNP nuclear concentration for different delivery strategies. Future work should investigate the editor dosage requirements for other clinically-relevant cell types, as well as whether or how these

requirements differ for other editing tools used for base, prime, and epigenome editing, to best preserve genomic and cellular integrity while efficiently achieving the desired genomic alterations.

Enormous progress has been made towards safe and effective intracellular delivery of CRISPR gene editors, but many of these engineering studies use editing as their primary or only readout of delivery. Though extremely useful, editing is an endpoint measurement and only works if every delivery step, from initial uptake into the cell to successful edit at the genomic target, works as intended. However, all current intracellular protein and RNA delivery strategies are extremely inefficient[22,27,31]. Elucidating the impact of delivery modality on intracellular trafficking and localization will enable engineering of improved next-generation protein biologics. Determining the temporal relationship between RNP delivery modality and editing outcomes will foster the design of protein-based gene therapies that introduce sufficient RNP to mediate therapeutic genome modification while minimizing or eliminating unintended clinical consequences.

References

1. Jinek, M. *et al.* A programmable dual-RNA-guided DNA endonuclease in adaptive bacterial immunity. *Science* **337**, 816–821 (2012).
2. Jinek, M. *et al.* RNA-programmed genome editing in human cells. *Elife* **2**, e00471 (2013).
3. Mali, P. *et al.* RNA-guided human genome engineering via Cas9. *Science* **339**, 823–826 (2013).
4. Hsu, P. D. *et al.* DNA targeting specificity of RNA-guided Cas9 nucleases. *Nat. Biotechnol.* **31**, 827–832 (2013).
5. Wiedenheft, B., Sternberg, S. H. & Doudna, J. A. RNA-guided genetic silencing systems in bacteria and archaea. *Nature* **482**, 331–338 (2012).
6. Terns, M. P. & Terns, R. M. CRISPR-based adaptive immune systems. *Curr. Opin. Microbiol.* **14**, 321–327 (2011).
7. Bhaya, D., Davison, M. & Barrangou, R. CRISPR-Cas systems in bacteria and archaea: versatile small RNAs for adaptive defense and regulation. *Annu. Rev. Genet.* **45**, 273–297 (2011).
8. Schmid-Burgk, J. L. *et al.* Highly Parallel Profiling of Cas9 Variant Specificity. *Mol. Cell* **78**, 794–800.e8 (2020).
9. Walton, R. T., Christie, K. A., Whittaker, M. N. & Kleinstiver, B. P. Unconstrained genome targeting with near-PAMless engineered CRISPR-Cas9 variants. *Science* **368**, 290–296 (2020).
10. Ran, F. A. *et al.* In vivo genome editing using Staphylococcus aureus Cas9. *Nature* **520**, 186–191 (2015).
11. Pausch, P. *et al.* CRISPR-CasΦ from huge phages is a hypercompact genome editor. *Science* **369**, 333–337 (2020).
12. Anzalone, A. V., Koblan, L. W. & Liu, D. R. Genome editing with CRISPR-Cas nucleases, base editors, transposases and prime editors. *Nat. Biotechnol.* **38**, 824–844 (2020).
13. Adler, B. A. *et al.* CasPEDIA Database: a functional classification system for class 2 CRISPR-Cas enzymes. *Nucleic Acids Res.* **52**, D590–D596 (2024).
14. Philippidis, A. CASGEVY makes history as FDA approves first CRISPR/Cas9 genome edited therapy. *Hum. Gene Ther.* **35**, 1–4 (2024).
15. Koonin, E. V. & Makarova, K. S. Origins and evolution of CRISPR-Cas systems. *Philos. Trans. R. Soc. Lond. B Biol. Sci.* **374**, 20180087 (2019).
16. Koonin, E. V., Gootenberg, J. S. & Abudayyeh, O. O. Discovery of diverse CRISPR-Cas systems and expansion of the genome engineering toolbox. *Biochemistry* **62**, 3465–3487 (2023).
17. Cameron, P. *et al.* Mapping the genomic landscape of CRISPR-Cas9 cleavage. *Nat. Methods* **14**, 600–606 (2017).
18. Jang, H.-K. *et al.* High-purity production and precise editing of DNA base editing ribonucleoproteins. *Sci Adv* **7**, (2021).

19. Hendel, A. *et al.* Chemically modified guide RNAs enhance CRISPR-Cas genome editing in human primary cells. *Nat. Biotechnol.* **33**, 985–989 (2015).
20. Vakulskas, C. A. *et al.* A high-fidelity Cas9 mutant delivered as a ribonucleoprotein complex enables efficient gene editing in human hematopoietic stem and progenitor cells. *Nat. Med.* **24**, 1216–1224 (2018).
21. Zhang, L. *et al.* AsCas12a ultra nuclease facilitates the rapid generation of therapeutic cell medicines. *Nat. Commun.* **12**, 3908 (2021).
22. Raguram, A., Banskota, S. & Liu, D. R. Therapeutic in vivo delivery of gene editing agents. *Cell* **185**, 2806–2827 (2022).
23. Sinclair, F., Begum, A. A., Dai, C. C., Toth, I. & Moyle, P. M. Recent advances in the delivery and applications of nonviral CRISPR/Cas9 gene editing. *Drug Deliv. Transl. Res.* **13**, 1500–1519 (2023).
24. Wienert, B., Shin, J., Zelin, E., Pestal, K. & Corn, J. E. In vitro-transcribed guide RNAs trigger an innate immune response via the RIG-I pathway. *PLoS Biol.* **16**, e2005840 (2018).
25. Kim, S. *et al.* CRISPR RNAs trigger innate immune responses in human cells. *Genome Res.* **28**, 367–373 (2018).
26. Charlesworth, C. T. *et al.* Identification of preexisting adaptive immunity to Cas9 proteins in humans. *Nat. Med.* **25**, 249–254 (2019).
27. van Haasteren, J., Li, J., Scheideler, O. J., Murthy, N. & Schaffer, D. V. The delivery challenge: fulfilling the promise of therapeutic genome editing. *Nat. Biotechnol.* **38**, 845–855 (2020).
28. Hou, X., Zaks, T., Langer, R. & Dong, Y. Lipid nanoparticles for mRNA delivery. *Nat. Rev. Mater.* **6**, 1078–1094 (2021).
29. Hanlon, K. S. *et al.* High levels of AAV vector integration into CRISPR-induced DNA breaks. *Nat. Commun.* **10**, 4439 (2019).
30. Espinoza, D. A. *et al.* Aberrant Clonal Hematopoiesis following Lentiviral Vector Transduction of HSPCs in a Rhesus Macaque. *Mol. Ther.* **27**, 1074–1086 (2019).
31. Bruce, V. J. & McNaughton, B. R. Inside Job: Methods for Delivering Proteins to the Interior of Mammalian Cells. *Cell Chem Biol* **24**, 924–934 (2017).